UNIVERSITY OF SOUTHAMPTON

FACULTY OF ENGINEERING, SCIENCE & MATHEMATICS

Optoelectronics Research Centre

Development, characterisation and analysis of narrow linewidth, single-frequency DFB fibre lasers in the 1.5 μm - 2 μm region

by

Nyuk Yoong Voo

Thesis submitted for the Degree of Doctor of Philosophy

November 2006

UNIVERSITY OF SOUTHAMPTON

ABSTRACT

FACULTY OF ENGINEERING, SCIENCE & MATHEMATICS
OPTOELECTRONICS RESEARCH CENTRE

Doctor of Philosophy

DEVELOPMENT, CHARACTERISATION AND ANALYSIS OF NARROW LINEWIDTH, SINGLE-FREQUENCY DFB FIBRE LASERS IN THE 1.5 μm – 2 μm REGION

by Nyuk Yoong Voo

The main aim of this study was to investigate the anomalous linewidth behaviour of the DFB fibre lasers, as the observed linewidths of these lasers remain far above their predicted theoretical limit based on the Schawlow-Townes linewidth formula. Narrow linewidth, single-frequency fibre lasers are attractive sources for optical coherent communication, wavelength division multiplexing, optical sensors and spectroscopy, as they have kilohertz linewidths, direct compatibility with the fibre network, wavelength tunability and are simple to fabricate. Another aim of the study was to extend the operating wavelength of the fibre DFB lasers around 2 μm, this research was driven by the number of possible applications in areas such as remote gas sensing, laser imaging detection and ranging (LIDAR) and medicine.

Er^{3+}-Yb^{3+} DFB fibre lasers showed that not only does the laser linewidth deviate from the Schawlow-Townes linewidth formula, by increasing with pump and laser power, but it also varies with the pump configuration. It was found that the backward pumping scheme has the lowest threshold and highest efficiency, while the dual-pumping scheme was the worst in these aspects. The lowest linewidth operation was actually obtained with the dual-pumping configuration. The variations in laser linewidth were 25-40 kHz. Then, the anomalous linewidth was found to be caused by the fundamental thermal noise at low pump power levels and by temperature fluctuations, induced by pump intensity, at higher powers, which in turn leads to refractive index fluctuations and, thus, to the laser frequency jitter. Some of the potential techniques to overcome the linewidth limitations were experimentally investigated and good agreement was observed. The double phase shifts DFB laser showed a reduction in lasing wavelength shift, as compared with the single phase shift design, for similar laser efficiencies. This suggests that the wavelength shift was not only due to the absorbed pump power but was also affected by the signal intensity distribution in the cavity. A 10% decrease in the laser linewidth with the 5 mm apart phase shifts laser was observed in the backward pumping configuration.

A Tm^{3+} co-doped DFB fibre laser operated at 1836 nm, the longest reported operating wavelength, was in-band pumped at 1565 nm and gave an output power of 5 mW with a slope efficiency of 1%. With the MOPA configuration, the laser output was amplified, with 1 m of amplifier fibre, to 345 mW. A Ho^{3+}-doped DFB fibre laser was designed to operate at 2140 nm. However, neither the pump wavelength at 1119 nm nor at 1836 nm managed to make it lase. The reasons could be due to concentration quenching resulting from a high concentration of the Ho^{3+} in the fibre, a nonradiative transition in the 2 μm region and also the large intrinsic losses of the silica fibre associated with the 2.1 μm wavelength.

List of Contents

List of Figures

List of Tables

Author's Declaration

I, **Nyuk Yoong Voo**, declare that this thesis entitled *Development, characterisation and analysis of narrow linewidth, single-frequencyDFB fibre lasers in the 1.5 μm - 2 μm region* and the work presented in it are my own. I confirm that:

- this work was done wholly or mainly while in candidature for a research degree at the University of Southampton;
- where any part of this thesis has previously been submitted for a degree or any other qualification at this University or any other institution, this has been clearly stated;
- where I have consulted the published work of others, this is always clearly attributed;
- where I have quoted from the work of others, the source is always given. With the exception of such quotations, this thesis is entirely my own work;
- I have acknowledged all main sources of help;
- where the thesis is based on work done by myself jointly with others, I have made clear exactly what was done by others and what I have contributed myself;
- parts of this work have been published (see list of publications).

Signed:

Date: November 2006

Acknowledgements

I acknowledge the support of Brunei Darussalam Government studentship.

I would like to thank my supervisor, Dr. Morten Ibsen, for his supervision and guidance.

Thanks to Dr. Wei H. Loh for initializing the study of anomalous linewidth in the DFB fibre lasers. A very special thank you to Dr. Peter Horak for his theoretical support with the analytical model of the DFB lasers linewidth. Thank you Peter for many rewarding technical discussions and proofreading some of the thesis chapters. Thanks to Dr J. K. Sahu and his group for technical discussions and providing the fibres: Er-Yb, Tm and Ho fibres.

I thank the High Power Fibre Lasers group with whom I have the pleasure of discussing ideas, borrowing equipment and who generally helped things along: Christophe, Carl and Pascal. I thank the Advanced Solid State Sources group and Planar Waveguide Lasers group for borrowing equipment. Thanks also go to my office-mates for all the fun times we have had! Thanks to Jing and Jingtao for such an uplifting friendship. Special thanks to Francesca for helping to print, soft bound and submit the thesis ~ *Thank you!* Thanks also go to Sue and Clive for providing a pleasant accommodation and nice meals during my stay there for the viva.

A very special thank you to our postgraduate student mentor, Dr. Eleanor Tarbox, for kindly allocating her valuable time to correct my countless mistakes in my writing. I thank Professor Rob Eason and Mrs. Eveline Smith for being so energetic in their support of the ORC PhD students. Thank also go to Professor J. P. Dakin and his group for starting my journey in sensors and fibre lasers.

Big thanks to my family and friends for their patience and support throughout my studies.

Symbols and Abbreviations

B/Ge	Boron/germanium
C_{cr}	Cross relaxation coefficient
C_{up}	Upconversion coefficient
c_v	Specific heat capacity of silica
CW	Continuous-wave
D	Penetration depth
DBR	Distributed Bragg reflector
DFB	Distributed feedback
Er	Erbium
Er-Yb	Erbium-Ytterbium
FBG	Fibre Bragg grating
g	Small signal gain
Ho	Holmium
hv_P, hv_S	Pump and signal photon energies respectively
I_P, I_S	Pump and signal photon intensities respectively
k_B	Boltzmann constant
L	Length of grating
L_{eff}	Effective cavity length
LIDAR	Laser imaging detection and ranging
MOPA	Master oscillator power amplifier
NA	Numerical aperture
Nd	Neodymium
n	Refractive index
n_{eff}	Effective index of the mode
N_{Er}, N_{Yb}	Concentrations of Er^{3+} and Yb^{3+} respectively
N_1, N_2 *and* N_3	Population density of laser level 1, 2 and 3 respectively
P	Laser power

P_{avg}	Average optical power
P_{elec}	Power-spectral density of photocurrent
$P_{avg(elec)}$	Average power of photocurrent
PZT	Piezoelectric transducer
r	Reflection coefficient
R	Reflection coefficient energy
RIN	Relative intensity noise
ROF	Relaxation oscillation frequency
Sb	Antimony
$S(f)$	Laser spectrum
$S_F(f)$	Laser frequency jitter spectrum
T	Temperature
$T(f)$	Frequency response of the DFB laser to pump fluctuations
Tm	Thulium
UV	Ultra-violet
V	Effective mode volume
W_{ij}	Stimulated transition rates between the i and j levels
WDM	Wavelength division multiplexing
Yb	Ytterbium
σ_P^a , σ_P^e	Absorption and emission cross-section of the pump respectively
σ_S^a, σ_S^e	Absorption and emission cross-section of the signal respectively
λ_B	Bragg wavelength
κ	Coupling coefficient
ρ	Density of silica
α	Field gain
Δf	Laser linewidth
Δn	Index modulation change
ΔP	Amplitude of the pump fluctuations
ΔP^2	Mean square optical intensity fluctuation
Δv	Laser frequency
Δv_{cav}	Grating linewidth
β	Propagation constant

Γ	Phase matching
Λ	Spatial period of the grating
τ_{Er}, τ_{Yb}	Spontaneous emission lifetimes of erbium and ytterbium respectively
τ_2, τ_3	Spontaneous emission lifetime of level 2 and 3 respectively
η	Transverse overlap integral of the modal distribution

To my family

“The beginning of knowledge is the discovery of something we do not understand.”

Frank Herbert

Chapter 1

Introduction

Narrow-linewidth, single-frequency lasers are attractive sources for optical coherent communications, wavelength division multiplexing, optical fibre sensors and high-resolution spectroscopy. Single-frequency fibre lasers are promising alternatives to semiconductor lasers as they have kHz linewidths, direct compatibility with the fibre network, wavelength tunability and are simple to fabricate. The single frequency operation of fibre lasers has been demonstrated in: fibre ring lasers [1], linear cavity fibre lasers with a narrow filter [2], distributed Bragg reflector (DBR) fibre lasers [3, 4] and distributed feedback (DFB) fibre lasers [5] and also in the Fabry-Perot type lasers by making the cavity extremely short <1 mm [6]. The research described here aims to develop compact sources, with a narrow linewidth, low noise and good wavelength stability, suitable for high-end applications.

Laser linewidths of ≤ 10 kHz have been reported in the Er^{3+}-doped fibre ring-lasers [1, 7]. In [1] the single-frequency of the laser was obtained by maintaining the polarisation of the mode. Single-mode operation in the fibre ring cavity can be achieved with the Fabry-Perot filter [7]. Lasing is easy to obtain in the fibre ring-laser with a low Er^{3+} concentration fibre in which the gain medium must be very long (typically longer than 10 m) to produce enough gain. Owing to the long cavity length, this also gives narrow linewidths. However, the long cavity length results in

closely spaced multiple longitudinal modes. This can severely limit their applications due to multimode oscillation and mode hopping. In addition, the length of the cavity is susceptible to thermal drift and this will cause long-term mode hopping, even with a combination of filters inside the ring-cavity to suppress the mode hopping [8]. Mode hopping can be eliminated by actively stabilising the laser through dithering of the cavity length using a piezoelectric transducer (PZT) fibre stretcher controlled by feedback from the output of the laser [9]. However, this solution makes the laser design become more complex.

Recently, a single-frequency ytterbium (Yb^{3+}) fibre laser was demonstrated based on a linear cavity in which a narrow bandwidth filter is used to select the single longitudinal mode and the dual-cascaded fibre Bragg gratings act as an output coupler [2]. Single-mode operation of this laser was achieved by using a saturable absorber, a section of unpumped gain fibre, in which counter-propagating waves formed an interference pattern that generated a dynamic Bragg grating at 1064 nm. The cavity length of this laser was about 1 m and an output power of 18 mW was obtained with a pump power of 107 mW at 976 nm. The mode stability of this laser was limited at high pump power due to the spatial hole burning caused by the high intensity in the cavity.

One can also obtain single-frequency operation in Fabry-Perot-type lasers by making the cavity extremely short < 1mm. Single-longitudinal mode operation is obtained, with the mode spacing in the resonator relatively larger than the gain bandwidth, so that only one mode acquires sufficient gain to reach lasing threshold. A 100-μm long erbium-ytterbium (Er^{3+}-Yb^{3+}) phosphate-glass fibre Fabry-Perot laser, operating at 1535 nm was demonstrated with a two-mirror laser resonator design [6]. Due to a short cavity length, the output power of this laser was very low (~ 20 μW).

Robust single-longitudinal mode operation without mode hopping has been demonstrated in the DBR [3, 4, 10-13] and DFB [5, 14, 15] fibre lasers. Very narrow laser linewidth of a few tens of kilohertz and a low relative intensity noise of < -140 dB/Hz in the megahertz region have been reported for both cavity designs [3, 13, 14]. The construction and operation of these lasers is much simpler than the fibre ring

lasers and linear cavity design. Unlike the ring fibre lasers and linear cavity, in which the laser wavelength was defined by a filter such as an interference filter [1], a fibre Fabry-Perot filter [7] or auto-tracking filter [2]. In the DBR and DFB fibre lasers, the laser wavelength is determined by the ultraviolet (UV) written Bragg gratings and it can be accurately set to ≤ 0.1 nm during manufacture and has a low sensitivity to temperature (~10 pm/K). DBR fibre lasers are only robustly single-frequency provided that the grating bandwidth is kept below ~0.2 nm and the laser length is reduced to a few centimetres to increase the axial mode spacing.

DFB fibre lasers integrate a single grating over the entire cavity for feedback and wavelength determination. The advantage of the geometry of the DFB design, as compared with the DBR design in which the two Bragg gratings are separated by a gain section, is that it can be made shorter to provide robust single-mode operation. In addition, the DFB fibre lasers are more environmentally stable than the DBR fibre lasers as the thermal response of the Bragg wavelength of the two reflectors of the DBR varied slightly and also the wavelength of the reflectors varied slightly as a function of grating exposure. Hence it is this type of DFB fibre laser source that we consider here and also because the fibre DFB lasers have shown flexibility in the pumping conditions and pump redundancy by configuring them in a parallel array [16].

To date, the observed linewidths of these fibre lasers remain far above their theoretical limit predicted, based on the Schawlow-Townes linewidth formula, to be just 60 Hz or less [12]. One common suggestion for this excess phase noise is due to the environmental perturbations, such as external vibration and acoustic noise, to which the fibre laser may be more susceptible. Experimental investigation of the linewidth characteristics of the Er^{3+}-Yb^{3+} DFB fibre lasers is conducted to find the main cause of the excess phase noise. Also, most of the work has been concentrated in developing the single-frequency fibre lasers at the 1.5 μm wavelength region for applications related to optical communications, to gas sensors and to high resolution spectroscopy. The development of laser sources operating around the 2 μm 'eye-safe' region has also started to gather pace, mainly driven by a number of possible applications in areas such as remote gas sensing, laser imaging detection and ranging

(LIDAR) and medicine. The single-frequency DFB fibre laser in the 2 μm region is still under development. Therefore, we also aimed to extend the operating wavelength of the DFB fibre lasers around 2 μm using thulium (Tm) and holmium (Ho) as the gain medium.

1.1 Developments of the single-frequency fibre lasers with Bragg gratings

This section gives a brief history of the development of the single-frequency fibre lasers with Bragg gratings. Short-cavity single-frequency fibre lasers have been a topic of continued interest since the early work of Ball *et al.* on erbium-doped distributed Bragg reflector fibre lasers [3]. Currently, the single-frequency fibre Bragg grating lasers operating in the spectral region of 1 μm have been demonstrated with ytterbium (Yb^{3+}) and neodymium (Nd^{3+}) as the gain medium. In the 1.5 μm region, the gain medium used was erbium (Er^{3+}). The single-frequency DFB fibre lasers operating at ~2 μm based on thulium (Tm^{3+}) dopant have been demonstrated. The advances in the laser cavity designs of the DFB fibre lasers are also included in this chapter.

Most of the research activities in single-frequency fibre lasers has been concentrated in the wavelength region around 1.5 μm, as it is the key component of the optical communication systems such as wavelength division multiplexed (WDM) networks. The first Er^{3+}-doped DBR silica fibre laser was demonstrated by Ball *et al.* in 1991 [3]. It consisted of a 50-cm long Er^{3+}-doped fibre with two discrete Bragg grating reflectors on opposite ends of the fibre. For a robust single-mode operation, the cavity needs to be sufficiently short so that the mode spacing is comparable to the grating bandwidth. For a grating bandwidth below ~0.2 nm, it is desired to have a mode spacing of the order of 10 GHz, i.e. cavity length of the order of 1 cm. The concentration of the Er^{3+} is limited by the germanosilicate glass host, so it is necessary to keep the Er^{3+} concentration below 100 ppm to reduce ion-pair quenching. Combining these practical limits meant that pump absorption in the

cavity length was low and as a result the output power, for a cavity length of only a few centimetres long, was limited to about 200 μW [10, 11, 14]. This power can be boosted using the residual pump in the master oscillator power amplifier (MOPA) configuration [11, 14]. An output power of 60 mW was obtained with a fibre length of 19-m in a Er^{3+}-doped fibre amplifier [11]. However, the amplified spontaneous emission from the amplifier increased the output noise. This fundamental problem was then solved by, Kringlebotn *et al.*, co-doping the Er^{3+} -doped fibre with Yb^{3+} [17]. This increases the pump absorption at 980 nm by more than two orders of magnitude and thus enhances the laser efficiency operation of centimetre long lasers with relatively low Er^{3+} concentration [4, 17]. The pump excites the Yb^{3+} ions which then transfer their energy to the Er^{3+} ions by resonant coupling. An output power of 19 mW for 100 mW pump power was achieved with a 2-cm long Er^{3+}-Yb^{3+} -doped fibre [4]. However, for efficient Er^{3+}-Yb^{3+} -doped devices, fibres require a phosphosilicate host glass, which is not photosensitive. Therefore, the UV written Bragg gratings are unable to be directly written into the fibre. For these lasers, the Bragg grating reflectors were written into a photosensitive fibre which was then spliced to the doped fibre, and as a result intra-cavity splice loss was introduced. A heavily co-doped Er^{3+}-Yb^{3+} fibre laser has also been reported with an output power of 200 mW, with a pump power of ~850 mW [13]. The laser cavity was based on two passive fibre Bragg gratings (FBGs) that are fusion spliced to a 2-cm long doped fibre.

The photosensitivity of the Er^{3+}-Yb^{3+} -doped fibre can be enhanced by loading the fibre with hydrogen and nearly 100% reflectivity in the grating was observed by Kringlebotn *et al.* and was followed by the first demonstration of DFB fibre laser in 1994 [5]. The feedback grating at 1.5 μm was directly written into a length of 2-cm Er^{3+}-Yb^{3+} -doped fibre. The output power of this laser was 3.2 mW, with a slope efficiency of 5.4%. Then, a DFB fibre laser based on Er^{3+}-Yb^{3+} co-doped with tin, (rather than using the hydrogenation technique which increased the fibre losses), to improve the fibre photosensitivity has been demonstrated [18]. The slope efficiency of this laser was 11%. A further improvement in the photosensitivity of the Er^{3+}-Yb^{3+} co-doped fibre has been demonstrated, by L. Dong *at el.*, using a highly photosensitive boron/germanium (B/Ge)-doped ring to surround the Er^{3+}-Yb^{3+} core

[19]. Both DBR and DFB lasers have been realised with this fibre and have shown slope efficiencies of 25%. Before the photosensitivity of the Er^{3+}-Yb^{3+} -doped fibre was enhanced by using the B/Ge cladding, developments were carried out to improve the laser efficiency in the Er^{3+}-doped fibre by using an intra-cavity pumping scheme [20] and also by pumping into the 520 nm absorption band [21]. For the intra-cavity pumping, the DFB laser was placed inside an Yb^{3+} fibre laser, which was used as the pump source for the DFB laser. A three-fold increase in the output power was observed as compared with direct 980 nm pumping [20]. Pumping in the 520 nm absorption band has shown an increase in the slope efficiency of 10% which was an order of magnitude improvement over that attainable by 980 nm pumping [21].

Research was not only conducted in improving the fibre material for high pump absorption of Er^{3+}, but also in the designs of the feedback cavity of the DFB fibre lasers to maximise the laser output. A DFB laser with a uniform grating, i.e. without a phase shift and with no end reflectors, will operate in two longitudinal modes at different wavelengths, corresponding to the edges of the grating bandgap and gives equal output power from both ends [22]. However, single wavelength operation is required in real practice. In [5] the single-frequency operation of the DFB fibre lasers has been achieved by using an end reflector to change the round-trip phase shift in the cavity or by locally heating the grating to slightly increase its refractive index around that point in order to create the optical phase shift of $\pi/2$ such that the round-trip phase condition is satisfied at the Bragg wavelength. The permanently induced phase shift in the centre of the grating has been achieved by locally elevating the background refractive index in the fibre core with additional exposure of UV light around the centre of the uniform grating [14]. The other techniques to introduce the phase-shifted gratings were with the moving fibre-scanning beam technique and with phase masks in which the phase shifts can be incorporated into the grating during the writing process by simply moving the fibre by an appropriate distance at the desired time while the UV beam is scanning [23]. The output powers of these lasers are equally divided at both ends; this is because of the symmetry of the cavity. The laser wavelength coincided with the Bragg wavelength. For a high performance laser, unidirectional output is desirable. This can be obtained by placing the phase shift asymmetrically with respect to the grating centre and a large output was obtained

from the shorter end [24, 25]. A further improvement in the laser efficiency has been demonstrated with a step-apodised design in which the position and length of the effective cavity can be enhanced without impacting the cavity asymmetry, cavity Q-factor, or the overall laser length [26]. Basically, the step-apodised DFB laser has employed a step change in the coupling coefficient on either side of the phase shift to restore the optimum optical feedback. It has shown an increase in the pump-to-signal conversion of 40% in the Er^{3+}-Yb^{3+} co-doped fibre. The different types of DFB laser cavity mentioned are shown in Figure 1.1, P_{left} and P_{right} refer to output powers of the laser.

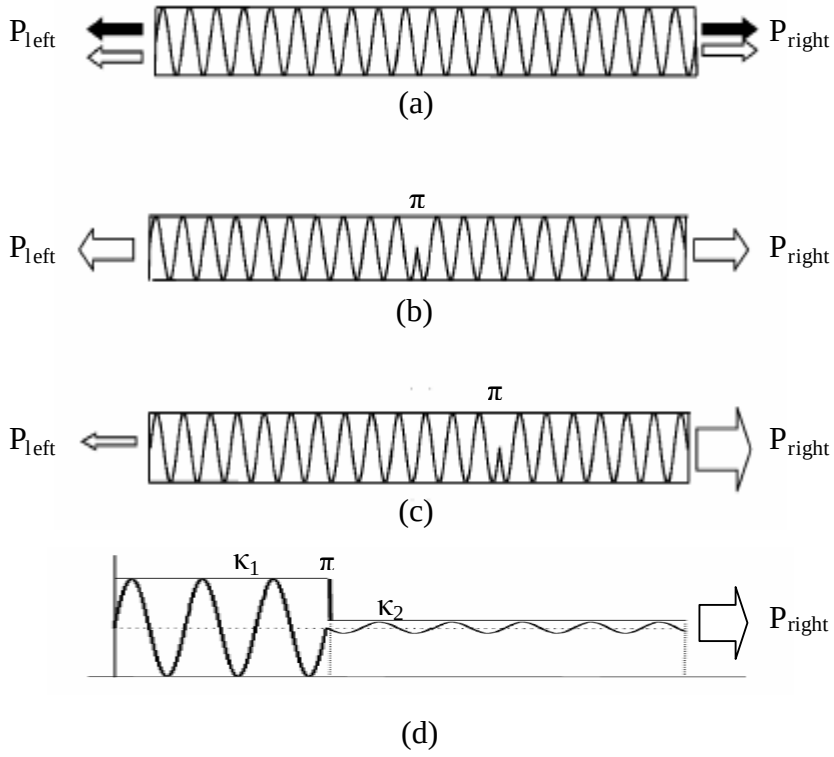

Figure 1.1: *DFB laser cavity designs (a) uniform non phase shifted, (b) symmetric single π-phase shifted, (c) asymmetric single π-phase shifted and (d) asymmetric single π-phase shifted step-apodised [26].*

Other laser wavelengths operating in the 1 μm region have been demonstrated with Nd^{3+}-doped [27] and Yb^{3+}-doped [28] fibre. The cavity feedback of the Nd^{3+}-doped fibre laser was based on the intra-core Bragg reflectors on the opposite ends of a 4-m long doped fibre. The output power was ~12 mW with a pump power of 265 mW. In [28] the DFB fibre laser was a 10-cm long grating, with a UV-induced π phase shift

in the centre of the grating, written throughout the whole length of the Yb^{3+}-doped fibre. The maximum power achieved was ~8 mW with a pump power of ~20 mW. The sources operating around 2 μm also began to develop, driven by a number of applications such as in LIDAR, sensing applications and medicine. The single frequency DFB fibre laser operating in the 2 μm region was demonstrated with Tm^{3+}-doped fibre by S. Agger *at el.* two years ago [29]. The laser cavity was 5-cm long and had an output power of 1 mW with a slope efficiency of 0.2%.

Some applications, as in the wavelength-division multiplexing and sensor systems, required a continuously tunable wavelength. The single-frequency DBR and DFB fibre lasers are not restricted by their Bragg grating wavelength, they are capable of being continuously wavelength tuned, without mode hopping [30-32]. The laser wavelength tuning techniques used are uniformly stretching [30], compression [31] and a combination of extension and compression [32]. In the stretching or compression technique, the change in reflected wavelength from the Bragg reflector tracks the change in cavity resonance wavelength so that mode hopping is avoided. The fibre laser was mounted, at both ends, onto a PZT and a maximum wavelength tuning of 0.72 nm was obtained for maximum stretching. This technique is mechanically simple to implement but its tuning range is limited by the maximum range of the PZT as well as the fibre strength. The compression technique has shown a wavelength tuning of over 32 nm in a DBR fibre laser [31]. In this compression technique, the fibre laser was fixed by epoxy between two ferrules, one mounted to a fixed stage and the other to the stepper motor for compression. Three floating ferrules were placed between the two fixed ferrules and attached to the stepper motor. The other technique that has been demonstrated was using a combination of the extension and compression [32]. The DFB fibre laser was embedded in a firm bendable material and a wavelength tuning range of 27 nm was demonstrated.

1.2 Applications

Fibre distributed Bragg reflector and distributed feedback lasers are attractive devices for optical communication systems, sensing applications and spectroscopy

because of their narrow linewidth, robust single-mode operation, compact in-fibre design, flexible and accurate wavelength selection in production, as well as easy tuning of the wavelength. A number of the applications have been illustrated with these sources.

(a) Optical communication systems

The first data transmission experiment has been demonstrated using an Er^{3+}-doped DBR fibre laser transmitter [33]. The available laser power was 91 μW and externally modulated at 2.5 Gbit/s. This permitted data transmission over 654 km, with Er^{3+}-doped fibre amplifiers to boost the signal power. Even at higher transmission rates of 5 Gbit/s this has also been demonstrated with an Er^{3+}-doped DBR fibre laser with a similar output power as in Ref. [33] and the bit-error-rate (BER) at the 10^{-15} level has been observed over a distance of 86-km with non-dispersion shifted transmission fibre [34].

Both DBR and DFB fibre lasers have also been demonstrated in wavelength-division multiplexing (WDM) systems, in which multiple optical signals are carried on a single optical fibre for a multiplication in capacity [35-37]. The Er^{3+}-doped DBR fibre laser with MOPA has been modulated at 2.5 Gbit/s and signals transmitted over a 475 km long WDM transmission line [35]. Multiplexing of four DFB fibre lasers, separated in frequency by 100GHz (0.8 nm), on a 10 Gbit/s WDM link has been demonstrated over a 200 km standard single-mode fibre [36]. A further increase in channel capacity has been demonstrated by multiplexing eight and sixteen DFB fibre lasers together to form an 8- and 16-channel WDM transmitter array respectively [37]. In this setup, the DFB fibre lasers were pumped using a pump redundancy scheme in which the powers from the pumps are split equally between the fibre lasers. It will always remain in operation even if one or more pump failures occur.

(b) Acoustic sensors

Optical fibre acoustic sensors have been demonstrated both in air [38] and for underwater pressure measurement [39]. The acoustic sensor in air consisted of an

uncoated fibre DFB laser to sense the acoustic-wave motion and the fibre laser's frequency shifts induced by it were measured by using a Mach-Zehnder interferometer. The acoustically induced frequency shifts measured in [38] ranged from 0.61 MHz/Pa at 100-Hz to 0.34 kHz/Pa at 15 kHz. The use of DBR and DFB fibre lasers as a hydrophone has been demonstrated [39]. The principle of operation of the hydrophone is similar to the acoustic air sensor, in which the pressure induced wavelength shift of the laser is then measured with the interferometer. The fibre lasers gave a minimum detectable acoustic signal of -69 dB re Pa/√ Hz at 1 kHz [39]. Then, three DFB fibre lasers were spliced together on a single fibre to form a hydrophone array and no optical cross-talk was observed [39].

(c) Spectroscopic application

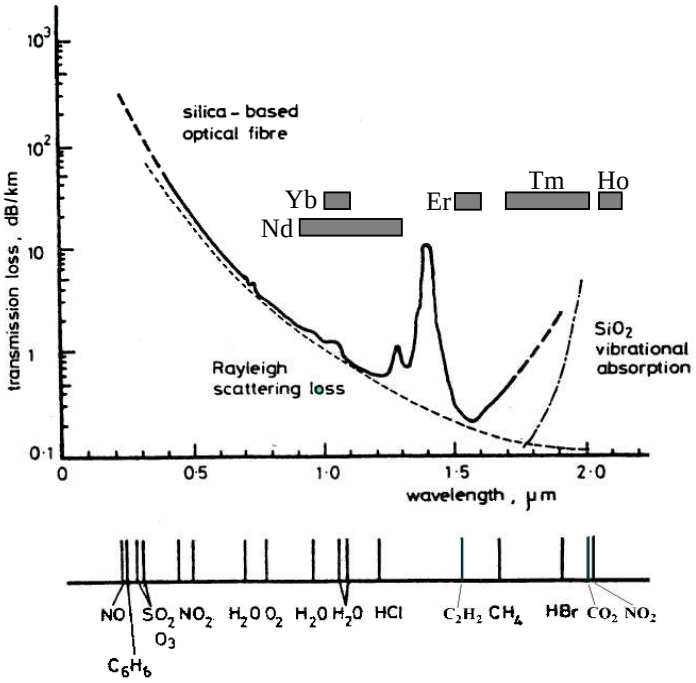

Figure 1.2: *Absorption wavelength of various molecular species present in the atmosphere and environment within the transmission loss of typical fibres and the gain bandwidth of the rare-earth materials* [40].

Figure 1.2 shows absorption wavelengths of various common gases in the atmosphere and environment, together with the transmission loss of typical fibres in

the visible and near infrared regions, in which the associated wavelength can be covered by the rare-earth doped fibre lasers. The possibility of using a grating-based fibre laser for the spectroscopic detection of gaseous species has been demonstrated in [41]. The fibre laser realised was used for the detection of atmospheric water. The laser cavity was formed by two UV written Bragg gratings at both ends of the Nd^{3+}-doped fibre. The laser operating wavelength was at 1117.96 nm and tuned around an absorption line of water molecules at 1118.06 nm.

1.3 Fabrication of gratings inside the fibre

Currently, fibre grating fabrication techniques used for the feedback gratings in the lasers are holographic [42] and by using the phase mask approaches [43, 44]. In the holographic method, the gratings are formed, usually in the core of the fibres which is photosensitive, by irradiating the fibre from the side, with a coherent two-beam UV interference pattern. The 244-nm UV radiation is split into two equal-intensity beams and then recombined to produce a periodic interference pattern that writes a corresponding periodic index grating in the core. The period of the grating depends on the angle between the two interfering coherent beams. For the phase mask technique, it allows fibre gratings to be written with a lower coherence UV laser beam and with better repeatability. The phase mask is a surface relief grating etched, by a photolithographic technique, in fused silica. In this technique, a phase mask grating is placed in contact, or nearly in contact, with the fibre. When the UV laser beam is incident on the mask, it diffracts into the 0, +1 and -1 orders, as seen in Figure 1.3, where the zero-order is suppressed by the depth of the corrugations in the phase mask. The +1 and -1 order diffracted beams interfere to produce a periodic pattern that photoimprints a corresponding grating in the fibre. The period of the photoimprinted index grating is half of the phase mask grating. For the fabrication of a phase shifted DFB fibre laser, the uniform phase mask method based on the moving fibre-scanning beam technique allows the insertion of the phase shift into the fibre grating [45]. The fibre is mounted on a computer-controlled PZT stage, and it can move slowly relative to the phase mask, permitting the phase shift to be incorporated into the grating during the writing scan.

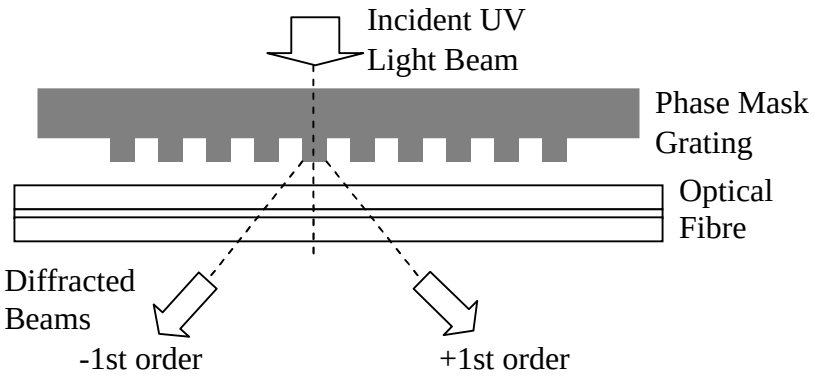

Figure 1.3: *Phase mask technique with the zero order being suppressed.*

1.4 Outline of thesis

Following this introduction chapter, Chapter 2 begins with the basic principles of fibre DFB lasers with a phase shift.

Chapter 3 studies the linewidth characteristics of the Er^{3+}-Yb^{3+} DFB fibre laser as they were found to contradict the Schawlow-Townes linewidth prediction. A few experiments were conducted to investigate this anomalous laser linewidth. Lastly, an analytical model was developed to explain the main cause of the excess phase noise that was due to the temperature fluctuation resulting from the intensity noise of the pump source. This was followed by the possible techniques that could be used to avoid this limitation.

The non-standard DFB fibre laser designs were investigated in Chapter 4. Some of the suggested techniques for the linewidth limitation were experimentally investigated in this chapter. The laser was operated in the narrow linewidth regime with low output power and subsequently, operated in the MOPA regime to show that the characteristics of the laser were still maintained. The other methods were to investigate the laser linewidth due to different effective cavity lengths by using coupling coefficients of 100 m^{-1}, 150 m^{-1} and 200 m^{-1}. Its linewidth was configuration dependent. We also observed that the laser wavelength shift was decreased as the coupling coefficient was reduced. Then, a step-apodised design was

fabricated to increase the effective cavity length of the laser and its performance was compared with the standard design. The discrete double phase shift lasers were implemented to modify the intra-cavity intensity and this showed a reduction in linewidth as well as the lasing wavelength shifting with DFB power or pump power.

From the success in realising the Er^{3+}-Yb^{3+} DFB fibre lasers, with the same phase mask technique and DFB structure, it was feasible for us to realise even longer wavelengths to open a new window for the possible applications of this source. In Chapter 5, an improved efficiency of the DFB laser at 1.8 μm was demonstrated with the thulium, co-doped with antimony, fibre. The laser output was about 5 mW with a pump power of 1.4 W at 1565nm. Then, the output was amplified with the MOPA for high power and a gain of 15 dB was achieved.

In Chapter 6, we aimed to push the laser wavelength even further into the 2.1 μm region with the holmium doped fibre. The laser has been pumped with a Raman fibre laser at 1119 nm and also the thulium DFB fibre laser. However, no lasing was observed for either pump source. Then, the DBR fibre laser was set-up and still no lasing was observed. Some of the reasons causing failure to lase have been discussed.

The final chapter summarises the key results and recommendations for further work.

1.5 References

[1] K. Iwatsuki, H. Okamura, and M. Saruwatari, "Wavelength-tunable single-frequency and single-polarisation Er-doped fibre ring-laser with 1.4 kHz linewidth," *Electronics Letters*, vol. 26, pp. 2033-2035, 1990.

[2] S. Huang, G. Qin, Y. Feng, A. Shirakawa, M. Musha, and K.-I. Ueda, "Single-frequency fiber laser from linear cavity with loop mirror filter and dual-cascaded FBGs," *IEEE Photonics Technology Letters*, vol. 17, pp. 1169-1171, 2005.

[3] G. A. Ball, W. W. Morey, and W. H. Glenn, "Standing-wave monomode erbium fiber laser," *IEEE Photonics Technology Letters*, vol. 3, pp. 613-615, 1991.

[4] J. T. Kringlebotn, J.-L. Archambault, L. Reekie, J. E. Townsend, G. G. Vienne, and D. N. Payne, "Highly-efficient, low-noise grating-feedback Er^{3+}:Yb^{3+} codoped fibre laser," *Electronics Letters*, vol. 30, pp. 972-973, 1994.

[5] J. T. Kringlebotn, J.-L. Archambault, L. Reekie, and D. N. Payne, "Er^{3+}:Yb^{3+} codoped fiber distributed-feedback laser," *Optics Letters*, vol. 19, pp. 2101-2103, 1994.

[6] K. Hsu, C.M. Miller, J.T. Kringlebotn, E.M. Taylor, J. Townsend, and D. N. Payne, "Single-mode tunable erbium:ytterbium fiber Fabry-Perot microlaser," *Optics Letters*, vol. 19, pp. 886-888, 1994.

[7] J. L. Zyskind, J. W. Sulhoff, Y. Sun, J. Stone, L. W. Stulz, G. T. Harvey, D. J. Digiovanni, H. M. Presby, A. Piccirilli, U. Koren, and R. M. Jopson, "Singlemode diode-pumped tunable erbium-doped fibre laser with linewidth less than 5.5 kHz," *Electronics Letters*, vol. 27, pp. 2148-2149, 1991.

[8] N. Park, J. W. Dawson, K. J. Vahala, and C. Miller, "All fiber, low threshold, widely tunable single-frequency, erbium-doped fiber ring laser with a tandem fiber Fabry--Perot filter," *Applied Physics Letters*, vol. 59, pp. 2369-2371, 1991.

[9] C.Y. Yue, G.W. Schinn, J.W.Y. Lit, and J. Zhang, "Single-mode EFL using an all-fiber subresonator," OFC-1994, pp. 129-131.

[10] J. L. Zyskind, V. Mizrahi, D. J. DiGiovanni, and J. W. Sulhoff, "Short single frequency erbium-doped fibre laser," *Electronics Letters*, vol. 28, pp. 1385-1387, 1992.

[11] G. A. Ball, C. E. Holton, G. Hull-Allen, and W. W. Morey, "60 mW 1.5 μm single-frequency low-noise fiber laser MOPA," *IEEE Photonics Technology Letters*, vol. 6, pp. 192-194, 1994.

[12] G. A. Ball, C. G. Hull-Allen, and J. Livas, "Frequency noise of a Bragg grating fibre laser," *Electronics Letters*, vol. 30, pp. 1229-1230, 1994.

[13] C. Spiegelberg, J. Geng, Y. Hu, Y. Kaneda, S. Jiang, and N. Peyghambarian, "Low-noise narrow-linewidth fiber laser at 1550 nm (June 2003)," *Journal of Lightwave Technology*, vol. 22, pp. 57-62, 2004.

[14] M. Sejka, P. Varming, J. Hubner, and M. Kristensen, "Distributed feedback Er^{3+}-doped fibre laser," *Electronics Letters*, vol. 31, pp. 1445-1446, 1995.

[15] W. H. Loh, B. N. Samson, L. Dong, G. J. Cowle, and K. Hsu, "High performance single frequency fiber grating-based erbium/ytterbium-codoped fiber lasers," *Journal of Lightwave Technology*, vol. 16, pp. 114-118, 1998.

[16] L. B. Fu, R. Selvas, M. Ibsen, J. K. Sahu, J. N. Jang, S.-U. Alam, J. Nilsson, D. J. Richardson, D. N. Payne, C. Codemard, S. Goncharov, I. Zalevsky, and A. B. Grudinin, "Fiber-DFB laser array pumped with a single 1-W CW Yb-fiber laser," *IEEE Photonics Technology Letters*, vol. 15, pp. 655-657, 2003.

[17] J. T. Kringlebotn, P. R. Morkel, L. Reekie, J.-L. Archambault, and D. N. Payne, "Efficient diode-pumped single-frequency erbium:ytterbium fiber laser," *IEEE Photonics Technology Letters*, vol. 5, pp. 1162-1164, 1993.

[18] W. H. Loh, L. Dong, and J. E. Caplen, "Single-sided output Sn/Er/Yb distributed feedback fiber laser," *Applied Physics Letters*, vol. 69, pp. 2151-2153, 1996.

[19] L. Dong, W. H. Loh, J. E. Caplen, J. D. Minelly, K. Hsu, and L. Reekie, "Efficient single-frequency fiber lasers with novel photosensitive ErYb optical fibers," *Optics Letters*, vol. 22, pp. 694-696, 1997.

[20] W. H. Loh, B. N. Samson, Z. E. Harutjunian, and R. I. Laming, "Intracavity pumping for increased output power from a distributed feedback erbium fibre laser," *Electronics Letters*, vol. 32, pp. 1204-1205, 1996.

[21] W. H. Loh, S. D. Butterworth, and W. A. Clarkson, "Efficient distributed feedback erbium-doped germanosilicate fibre laser pumped in 520 nm band," *Electronics Letters*, vol. 32, pp. 2088-2089, 1996.

[22] H. Kogelnik and C. V. Shank, "Coupled-wave theory of distributed feedback lasers," *Journal of Applied Physics*, vol. 43, pp. 2327-2335, 1972.

[23] W. H. Loh and R. I. Laming, "1.55 μm phase-shifted distributed feedback fibre laser," *Electronics Letters*, vol. 31, pp. 1440-1442, 1995.

[24] V. C. Lauridsen, J. H. Povlsen, and P. Varming, "Design of DFB fibre lasers," *Electronics Letters*, vol. 34, pp. 2028-2030, 1998.

[25] M. Ibsen, E. Ronnekleiv, G.J. Cowle, M.O. Berendt, O. Hadeler, M.N. Zervas, and R. I. Laming, "Robust high power (>20 mW) all-fibre DFB lasers with unidirectional and truly single polarisation outputs," in *CLEO*, 1999, pp. CWE4.

[26] K. Yelen, L. M. B. Hickey, and M. N. Zervas, "A new design approach for fiber DFB lasers with improved efficiency," *IEEE Journal of Quantum Electronics*, vol. 40, pp. 711-720, 2004.

[27] G. A. Ball, W. W. Morey, and J. P. Waters, "Nd^{3+} fibre laser utilising intra-core Bragg reflectors," *Electronics Letters*, vol. 26, pp. 1829-1830, 1990.

[28] A. Asseh, H. Storoy, J. T. Kringlebotn, W. Margulis, B. Sahlgren, S. Sandgren, R. Stubbe, and G. Edwall, "10 cm Yb^{3+} DFB fibre laser with permanent phase shifted grating," *Electronics Letters*, vol. 31, pp. 969-970, 1995.

[29] S. Agger, J. H. Povlsen, and P. Varming, "Single-frequency thulium-doped distributed-feedback fiber laser," *Optics Letters*, vol. 29, pp. 1503-1505, 2004.

[30] G. A. Ball and W. W. Morey, "Continuously tunable single-mode erbium fiber laser," *Optics Letters*, vol. 17, pp. 420-422, 1992.

[31] G. A. Ball and W. W. Morey, "Compression tuned single frequency Bragg grating fiber laser," *Optics Letters*, vol. 19, pp. 1979-1981, 1994.

[32] M. Ibsen, S. Y. Set, G. S. Goh, and K. Kikuchi, "Broad-band continuously tunable all-fiber DFB lasers," *IEEE Photonics Technology Letters*, vol. 14, pp. 21-23, 2002.

[33] J. L. Zyskind, J. W. Sulhoff, P. D. Magill, K. C. Reichmann, V. Mizrahi, and D. J. DiGiovanni, "Transmission at 2.5 Gbit/s over 654 km using an erbium-doped fibre grating laser source," *Electronics Letters*, vol. 29, pp. 1105-1106, 1993.

[34] V. Mizrahi, D. J. DiGiovanni, R. M. Atkins, S. G. Grubb, Y.-K. Park, and J.-M. P. Delavaux, "Stable single-mode erbium fiber-grating laser for digital communication," *Journal of Lightwave Technology*, vol. 11, pp. 2021-2025, 1993.

[35] G. Bonfrate, F. Vaninetti, and F. Negrisolo, "Single-frequency MOPA Er^{3+} DBR fiber laser for WDM digital telecommunication systems," *IEEE Photonics Technology Letters*, vol. 10, pp. 1109-1111, 1998.

[36] M. Ibsen, A. Fu, H. Geiger, and R. I. Laming, "All-fibre 4 x10 Gbit/s WDM link with DFB fibre laser transmitters and single sinc-sampled fibre grating dispersion compensator," *Electronics Letters*, vol. 35, pp. 982-983, 1999.

[37] M. Ibsen, S.-u. Alam, M. N. Zervas, A. B. Grudinin, and D. N. Payne, "8- and 16-channel all-fiber DFB laser WDM transmitters with integrated pump redundancy," *IEEE Photonics Technology Letters*, vol. 11, pp. 1114-1116, 1999.

[38] S. W. Løvseth, J. T. Kringlebotn, E. Rønnekleiv, and K. Bløtekjr, "Fiber distributed-feedback lasers used as acoustic sensors in air," *Applied Optics*, vol. 38, pp. 4821-4830, 1999.

[39] D. J. Hill, P. J. Nash, D. A. Jackson, D. J. Webb, S. F. O'Neill, I. Bennion, and L. Zhang, "A fiber laser hydrophone array," in *SPIE*. Boston, MA, USA, 1999, pp. 55-66.

[40] H. Inaba, T. Kobayasi, M. Hirama, and M. Hamza, "Optical-fibre network system for air-pollution monitoring over a wide area by optical absorption method," *Electronics Letters*, vol. 15, pp. 242-244, 1979.

[41] G. Martinelli, M. Douay, D. Pureur, P. Bernage, P. Niay, J. F. Henninot, C. Li, P. Carette, J. F. Bayon, and S. Boj, "Design of a photowritten cavity neodymium-doped fiber laser tunable around an absorption molecular line," *Applied Optics*, vol. 34, pp. 5338-5342, 1995.

[42] G. Meltz, W.W. Morey, and W. H. Glenn, "Formation of Bragg gratings in optical fibers by a transverse holographic method," *Optics Letters*, vol. 14, pp. 823-825, 1989.

[43] K. O. Hill, B. Malo, F. Bilodeau, D. C. Johnson, and J. Albert, "Bragg gratings fabricated in monomode photosensitive optical fiber by UV exposure through a phase mask," *Applied Physics Letters*, vol. 62, pp. 1035-1037, 1993.

[44] D. Z. Anderson, V. Mizrahi, T. Erdogan, and A. E. White, "Production of in-fibre gratings using a diffractive optical element," *Electronics Letters*, vol. 29, pp. 566-568, 1993.

[45] M. J. Cole, W. H. Loh, R. I. Laming, M. N. Zervas, and S. Barcelos, "Moving fibre/phase mask-scanning beam technique for enhanced flexibility in producing fibre gratings with uniform phase mask," *Electronics Letters*, vol. 31, pp. 1488-1490, 1995.

Chapter 2

Background Theory of Fibre DFB Lasers

The lasing action in a DFB laser occurs as a result of the signal generation by the gain medium and the feedback by the gratings. The objective of this chapter is to elucidate the physical phenomena involved in the operation of DFB lasers with a qualitative discussion. The optical feedback of the fibre DFB lasers is performed with the FBGs that are formed by exposure of the fibre core to an optical interference pattern. The parameters for optimum feedback of the gratings are described in the following section. For the gain in the fibre, it may be obtained by solving the appropriate atomic rate equations. First, the general rate equations of the two- and three-level lasers are described and this is followed by a set of rate equations that describes the gain medium of our fibre DFB lasers, i.e. Er^{3+}-Yb^{3+}, Tm^{3+} and Ho^{3+} -doped fibre. A number of gain models have been developed for the numerical analysis of Er^{3+}-Yb^{3+} co-doped fibre lasers pumped at 980 nm [1-4]. The different pump schemes for Tm^{3+} have been numerically modelled by Jackson and King [5]. Numerical analysis and experimental data of Er^{3+}-Yb^{3+} co-doped DFB fibre lasers has also been reported [6]. The model of the fibre lasers comprised the pump source, the active medium and the grating.

2.1 Operation of DFB lasers

The theoretical analysis for the operation of lasers with a distributed feedback structure was first proposed in the semiconductor field, by Kogelnik and Shank [7], this analysis can also be used to describe the operation of the fibre DFB lasers. The analysis is based on two counter-propagating waves coupled via backward Bragg scattering from the periodic perturbations of the refractive index [7]. Figure 2.1 shows a simplified illustration of the operation of a distributed feedback structure with the two counter-propagating waves represented with arrows, where λ is the wavelength of light in the medium. As each wave travels in the periodic structure, it receives light at each point along its path by Bragg scattering from the oppositely travelling wave. In this way, the feedback mechanism is distributed throughout the length of the periodic structure, entirely within the gain medium. Because of the gain, these waves grow and their energy is coupled into each other due to Bragg scattering.

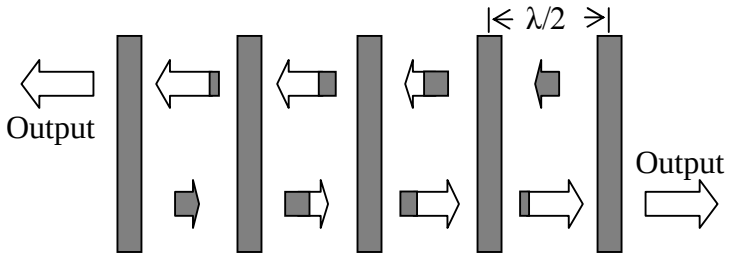

Figure 2.1: *Illustration of the laser oscillation in a periodic structure [7].*

The forward and the backward propagating waves can get strongly coupled provided the Bragg condition is satisfied, in which the difference in the propagation constants of the waves is equal to the spatial frequency of the grating [8].

$$\overrightarrow{\beta_1} + \overrightarrow{\beta_2} = \overrightarrow{K} = \frac{2\pi}{\Lambda} \qquad \textbf{(2.1)}$$

Where β_1 is the wave vector of the forward propagating guided mode, β_2 is the backward propagating guide mode, and Λ is the spatial period of the grating. Since the propagation constants for the forward and backward direction are the same,

then $|\beta_1| = |\beta_2| = \frac{2\pi}{\lambda} n_{eff}$, where n_{eff} is the effective index of the mode. Then, Equation (2.1) can be written as

$$\Lambda = \left(\frac{\lambda_B}{2 n_{eff}} \right) \quad \textbf{(2.2)}$$

where λ_B is the Bragg wavelength that satisfied the Bragg condition.

2.2 Optimisation of fibre Bragg gratings

This section introduces the definition of the reflectivity of the fibre grating and the effective cavity length (L_{eff}) which is used to optimise the gratings design for the DFB lasers. The coupled-mode theory has been used to model the optical properties of the fibre gratings [9, 10]. In this section, we leave out the derivation of coupled-mode theory as it has been detailed in numerous articles and texts [7, 8]. In the Bragg gratings, the light is coupled from a forward propagating mode to the same mode propagating in the backward direction. To consider this coupling let β_1 and β_2 be the propagation constant of the mode travelling in the +z and –z directions, respectively. Assuming that the power gets coupled only among these two modes, then the total electric field at any z is given as [8],

$$E(x,z,t) = \left[A(z) E_1(x) e^{-i\beta_1 z} + B(z) E_2(x) e^{i\beta_2 z} \right] e^{i\omega t} \quad \textbf{(2.3)}$$

where E_1(x) and E_2(x) represent the transverse mode profiles and A(z) and B(z) are the z-dependent amplitudes of the two modes. The coupling between the two modes is described by the following coupled-mode equations,

$$\frac{dA}{dz} = \kappa B e^{i\Gamma z} \quad \textbf{(2.4)}$$

$$\frac{dB}{dz} = \kappa A e^{-i\Gamma z} \quad \textbf{(2.5)}$$

where $\Gamma = \beta_1 + \beta_2 + \kappa = 0$ is the phase matching condition and κ is the coupling coefficient among the modes. The solution of the equations is given as follows:-

$$A(z) = b_1 e^{\kappa z} - b_2 e^{-\kappa z} \quad \textbf{(2.6)}$$

$$B(z) = b_1 e^{\kappa z} + b_2 e^{-\kappa z} \quad \textbf{(2.7)}$$

The reflection coefficient (r) of a periodic structure of length (L) is found by assuming a forward-going wave incident from z = 0, i.e. A (z = 0) = 1 and requiring that no backward-going wave exists beyond z = L, then

$$r = \frac{B(z=0)}{A(z=0)} = -\tanh \kappa L \quad \textbf{(2.8)}$$

The energy reflection coefficient is given by

$$R = |r|^2 = \tanh^2 \kappa L \quad \textbf{(2.9)}$$

For a medium of refractive index n having a periodic refractive index grating given by

$$n(z) = n_{ave} + \Delta n \sin\left(\frac{2\pi}{\Lambda}\right) z \quad \textbf{(2.10)}$$

where n_{ave} is the index change averaged over a grating period, the coupling coefficient is given as

$$\kappa = \frac{\pi \Delta n}{\lambda_B} \quad \textbf{(2.11)}$$

where Δn is the index modulation. The coupling coefficient (κ) depends on the photo-induced refractive index change in the fibre which depends on the irradiation conditions (wavelength, intensity, and total dosage of irradiating light), the compositions of glassy material forming the core and any processing of the fibre prior to irradiation.

In an optical fibre with a refractive index in the core given by the equation (2.10), then the reflectivity of a fibre grating of length L is

$$R = \tanh^2 \left(\frac{\pi \Delta n L}{\lambda_B}\right) \quad \textbf{(2.12)}$$

The reflectivity of a grating with constant gain at the Bragg wavelength is approximately equal to the reflectivity of a passive grating, with no gain, provided that the coupling coefficient is very much larger than the gain [11]. With the definition of the reflectivity, it implies that we can vary the reflectivity of our laser cavity with the coupling coefficient and length of the gratings. In the phase shift lasers, the laser cavity comprises two grating segments separated by the phase shift and each grating segment is considered as a separate reflector, i.e. a high reflector (R_1) and an output coupler (R_2). For a constant κ case, i.e. a uniform refractive index profile, by moving the phase shift, we change the length of the segments and this leads to a change in reflectivity of both grating segments. The other approach, to vary the reflectivity of the laser cavity, is to change the coupling coefficient and keep the length of the segments constant.

Now, we look at the definition of the effective length (L_{eff}) of the laser cavity, as demonstrated in [11] that increased the effective cavity length of the laser in which more of the gain medium can be used for signal generation, and hence increased the optical efficiency. The total effective cavity length of the phase shift DFB laser is the sum of the penetration depth into the grating segments on the left- and on the right-hand side of the phase shift. The penetration depth (D) is defined as the effective distance in which the incident wave penetrates into the grating, as a result of the distributed nature of the reflection process, before re-emerging at the front end. It is defined as follows, with constant gain at the Bragg wavelength, by [11]

$$D = \frac{1}{2}\frac{\alpha L\left(\frac{\tanh(\gamma L)}{\gamma L} - \frac{1}{\cosh^2(\gamma L)}\right) + \tanh^2(\gamma L)}{\alpha \tanh^2(\gamma L) + \gamma \tanh(\gamma L)} \qquad \textbf{(2.13)}$$

where α is the field gain and $\gamma = \sqrt{\kappa^2 + \alpha^2}$. If $\alpha << \kappa$, then D can be approximated by its passive cavity value

$$D \approx \frac{\tanh(\kappa L)}{2\kappa} = \frac{|r|}{2\kappa} \qquad \textbf{(2.14)}$$

For a π phase shifted DFB laser, the total length of the effective cavity (L_{eff}) in which the fields are circulating is given as follows by

$$L_{eff} = D_1 + D_2 \approx (\frac{|r_1|}{2\kappa_1} + \frac{|r_2|}{2\kappa_2}) \quad \textbf{(2.15)}$$

where D_1 and D_2 are the penetration depths into the grating segments on the left- and on the right-hand side of the phase shift, respectively. In the case of a uniform refractive index profile, $\kappa_1 = \kappa_2 = \kappa$.

The penetration depth can be increased by reducing the coupling coefficient and, therefore, decreasing the reflectivity of the grating results in a decrease in the optical feedback, and also a deviation from the optimum confinement condition. For a stronger grating, the round-trip reflectivity is close to unity, showing a much stronger cavity confinement. The reduction in the reflectivity, due to smaller κ, can be compensated by increasing the segment length. When the length of one segment is increased, the other segment length needs to be reduced so that the total device length is unchanged. In this case, the reduction in the other segment can be compensated by increasing its coupling coefficient so that the optimum reflectivity is restored. This has been shown with a step-apodised design in which a step change in the coupling coefficient on either side of the phase shift can be realised [11]. The effective cavity length of the step-apodised design is given by

$$L_{eff}(z_\pi) = \left[\frac{|r_2|L}{2c_2} + (\frac{|r_1|}{2c_1} - \frac{|r_2|}{2c_2}) z_\pi \right] \quad \textbf{(2.16)}$$

where z_π is the phase shift location, $\kappa_1 L_1 = c_1$, $\kappa_2 L_2 = c_2$ and the total cavity length $L = L_1 + L_2$.

The effective length of the cavity is increased towards the left-hand side of the phase shift, and this means that its coupling coefficient has to increase and this is limited by the photosensitivity of the fibre.

Based on the above definitions of the reflectivity and the effective cavity length, the feedback gratings of our DFB lasers are designed and optimised. For instance, the effective laser cavity length of the DFB lasers is varied with different coupling coefficients.

2.3 General rate equations of laser

The atomic rate equations are used to analyse the performance and efficiency of a laser. This system of equations relates the total number of atoms undergoing a transition and the total number of photons being created or annihilated. First, the general three-level laser system is shown in Figure 2.2, with the ground state denoted by 1, an intermediate state labelled 3 which is the pump level, and state 2 as the metastable level which has a long lifetime. In the lasing process, pump ground-state absorption excites the ions from level 1 to level 3 and this is followed by a rapid decay to level 2, the upper laser level. In level 2 the ions may decay to the ground level through either spontaneous emission or stimulated emission, at the signal wavelength. This three-level system is intended to represent that part of the energy level structure of Er^{3+} and Ho^{3+} that is relevant to the pump scheme used for our fibre DFB lasers. To obtain lasing, a population inversion is required between state 1 and state 2, and since state 1 is the ground state, at least half of the population of ions is required to be excited to level 2 to achieve population inversion. The populations of the levels are labelled N_1, N_2 and N_3. The rate equations for the population changes are [1, 12]:-

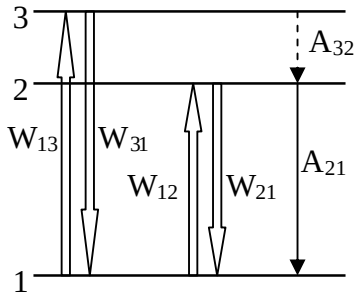

Figure 2.2: *Three-level laser scheme [12].*

$$\frac{\partial N_1}{\partial t} = -W_{13}N_1 + W_{31}N_3 - W_{12}N_1 + W_{21}N_2 + A_{21}N_2 \qquad \textbf{(2.17)}$$

$$\frac{\partial N_2}{\partial t} = W_{12}N_1 - W_{21}N_2 - A_{21}N_2 + A_{32}N_3 \qquad \textbf{(2.18)}$$

$$\frac{\partial N_3}{\partial t} = W_{13}N_1 - W_{31}N_3 - A_{32}N_3 \qquad \textbf{(2.19)}$$

In a steady-state situation,

$$\frac{\partial N_1}{\partial t} = \frac{\partial N_2}{\partial t} = \frac{\partial N_3}{\partial t} = 0 \quad \textbf{(2.20)}$$

By the conservation relation, the total population N is given by

$$N = N_1 + N_2 + N_3 \quad \textbf{(2.21)}$$

where W_{ij} terms represent the stimulated transition rates between the i and j levels, A_{21} is the spontaneous transition rate and A_{32}, the nonradiative relaxation rate.

Using equation (2.19), the population of level 3 is

$$N_3 = \frac{W_{13}}{W_{31} + A_{32}} N_1 \quad \textbf{(2.22)}$$

The decay rate from level 3 to level 2 is fast as compared to the pump rate into level 3, so the population is mostly in level 1 and level 2, and level 3 is assumed empty, i.e. $N_3 \simeq 0$. Using equation (2.22) to substitute for N_3 in equation (2.18), then

$$N_2 = \frac{W_{12}W_{31} + W_{12}A_{32} + A_{32}W_{13}}{W_{31}W_{21} + W_{31}A_{21} + A_{32}A_{21} + W_{12}W_{31} + W_{12}A_{32} + A_{32}W_{13}} N \quad \textbf{(2.23)}$$

$$N_1 = \frac{W_{31}W_{21} + W_{31}A_{21} + A_{32}W_{21} + A_{32}A_{21}}{W_{31}W_{21} + W_{31}A_{21} + A_{32}W_{21} + A_{32}A_{21} + W_{12}W_{31} + W_{12}A_{32} + A_{32}W_{13}} N \quad \textbf{(2.24)}$$

Population inversion is as follows

$$\Delta N = N_2 - N_1 \quad \textbf{(2.25)}$$

The individual definitions of these terms are as follows:

$$W_{13} = \frac{I_P}{h\nu_P} \sigma_P^a \quad \textbf{(2.26)}$$

$$W_{31} = \frac{I_P}{h\nu_P} \sigma_P^e \quad \textbf{(2.27)}$$

$$W_{12} = \frac{I_S}{h\nu_S} \sigma_S^a \quad \textbf{(2.28)}$$

$$W_{21} = \frac{I_S}{h\nu_S}\sigma_S^e \tag{2.29}$$

$$A_{21} = \frac{1}{\tau_2} \tag{2.30}$$

$$A_{32} = \frac{1}{\tau_3} \tag{2.31}$$

I_P, I_S are the pump and signal photon intensities and their photon energies are $h\nu_P, h\nu_S$, respectively. The absorption and emission cross-section of the pump and signal are denoted by σ_P^a , σ_P^e, σ_S^a and σ_S^e. The spontaneous lifetime of level 2 and 3 are represented by τ_2, τ_3.

Now, we consider the two-level laser system in which the upper pump level and the upper laser level belong to the same multiplet, i.e. broadened individual levels due to interaction of the ions and the crystalline host, as shown in Figure 2.3. Our lasers were also configured to operate in the two-level system as the theoretical quantum efficiency limit of the lasers is much higher. The entire system can be represented through the absorption and emission cross sections that interact with the pump and signal fields. The rate equations of the two-level system involve only the total population densities of multiplets 1 and 2 [12].

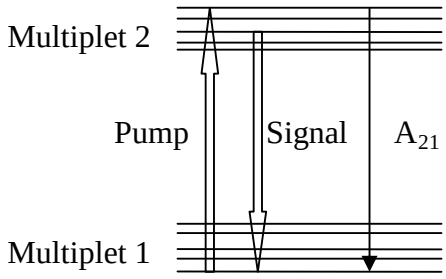

Figure 2.3: *Energy level of a two-level system where the two levels comprise many sublevels [12].*

$$\frac{\partial N_1}{\partial t} = A_{21}N_2 + (N_2\sigma_s^e - N_1\sigma_s^a)\frac{I_S}{h\nu_S} - (N_1\sigma_p^a - N_2\sigma_p^e)\frac{I_P}{h\nu_P} \tag{2.32}$$

$$\frac{\partial N_2}{\partial t} = -A_{21}N_2 + (N_1\sigma_s^a - N_2\sigma_s^e)\frac{I_S}{h\nu_S} - (N_2\sigma_p^e - N_1\sigma_p^a)\frac{I_P}{h\nu_P} \tag{2.33}$$

The total population density N is given by

$$N = N_1 + N_2 \tag{2.34}$$

We have

$$\frac{\partial N_1}{\partial t} = -\frac{\partial N_2}{\partial t} \tag{2.35}$$

and only one of the equations from equation (2.32) and (2.33) is an independent equation. N_2 is calculated in terms of signal and pump intensities. N_1 is then simply given by $N - N_2$.

After introducing the general rate equations, the following sections describe the gain media of our lasers with detail rate equations, particular for the Er^{3+}-Yb^{3+} case.

(a) Er^{3+}-Yb^{3+} co-doped system

Depending on the pump wavelength, pump energy can be absorbed by both the Er^{3+} ions in the $^4I_{15/2}$ and by the Yb^{3+} ions in the $^2F_{7/2}$ ground levels. The excited Yb^{3+} ions in the $^2F_{5/2}$ level transfer their energy to neighbouring Er^{3+} ions in the $^4I_{15/2}$ ground level, then these ions are excited to the $^4I_{11/2}$ pump level from where they rapidly relax to the metastable $^4I_{13/2}$ level. The radiative and nonradiative transitions of the Er^{3+}-Yb^{3+} co-doped system is shown in Figure 2.4. These transitions include pump absorption, spontaneous emission, forward and backward energy transfer, and the upcoversion among Er^{3+} ions. The system is described in the steady-state by the following rate equations [1] :-

$$\frac{\partial N_1}{\partial t} = -W_{12}N_1 - W_{13}N_1 + W_{21}N_2 + \frac{N_2}{\tau_{Er}} + C_{up}N_2^2 - C_{14}N_1N_4 + C_{up}N_3^2 - C_{cr}N_1N_6 = 0 \tag{2.36}$$

$$\frac{\partial N_2}{\partial t} = W_{12}N_1 - W_{21}N_2 - \frac{N_2}{\tau_{Er}} + A_{32}N_3 - 2C_{up}N_2^2 + 2C_{14}N_1N_4 = 0 \tag{2.37}$$

$$\frac{\partial N_3}{\partial t} = W_{13}N_1 - A_{32}N_3 + A_{43}N_4 - 2C_{up}N_3^2 + C_{cr}N_1N_6 = 0 \tag{2.38}$$

$$\frac{\partial N_4}{\partial t} = C_{up}N_2^2 - C_{14}N_1N_4 - A_{43}N_4 + C_{up}N_3^2 = 0 \tag{2.39}$$

$$\frac{\partial N_6}{\partial t} = W_{56} N_5 - \frac{N_6}{\tau_{Yb}} - W_{65} N_6 - C_{cr} N_1 N_6 = 0 \quad \textbf{(2.40)}$$

$$N_1 + N_2 + N_3 + N_4 = N_{Er} \quad \textbf{(2.41)}$$

$$N_5 + N_6 = N_{Yb} \quad \textbf{(2.42)}$$

N_1, N_2, N_3, N_4 are the populations of Er^{3+} levels $^4I_{15/2}$, $^4I_{13/2}$, $^4I_{11/2}$, $^4I_{9/2}$ and N_5, N_6 the populations of Yb^{3+} levels $^2F_{7/2}$, $^2F_{5/2}$. The τ_{Er} and τ_{Yb} are the spontaneous emission lifetimes for $^4I_{13/2}$ and $^2F_{5/2}$ levels, respectively. A_{32} and A_{43} are the nonradiative transition rates and C_{up}, C_{14} and C_{cr} are the upconversion and cross-relaxation coefficients, respectively. N_{Er}, N_{Yb} are the Er^{3+} and Yb^{3+} concentrations. The W_{56}, W_{65} represent $\frac{I_P}{h\nu_P}\sigma_s^a$ and $\frac{I_P}{h\nu_P}\sigma_P^e$ in which the cross-sectional absorption and emission are of the Yb^{3+}.

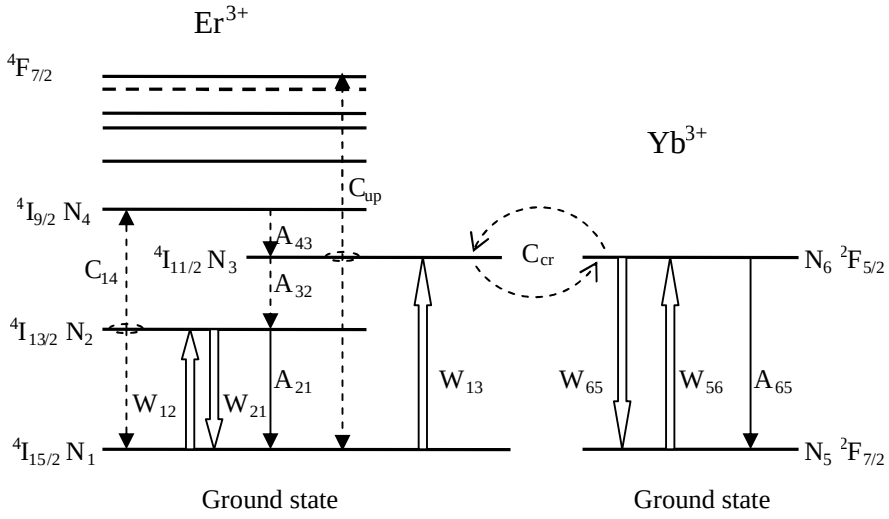

Figure 2.4: *Energy-level diagram for the Er^{3+}-Yb^{3+} co-doped system [1].*

For the case when the $^4I_{13/2}$ upper laser level is pumped directly, the system rate equations involve (2.36) and (2.37) with the cross relaxation process neglected. Equation (2.36) contains the term $-W_{12} + W_{21}$ (with W_{13} omitted) and also the spontaneous transition from level 2 to level 1, A_{21}. Equation (2.37) contains the term $W_{12} - W_{21}$ and A_{21}. The rate equations are the same as in Equation (2.32) and (2.33).

(b) Thulium (Tm^{3+}) system

A simplified energy diagram of Tm^{3+} is shown in Figure 2.5. The $^3H_6 \rightarrow {}^3H_4$ pump scheme was used in our Tm^{3+} fibre DFB laser, this corresponded to a two-level laser and the system rate equations can be described as in Equation (2.32) and (2.33). The lasing transition of the laser occurs between the $^3H_4$ and $^3H_6$.

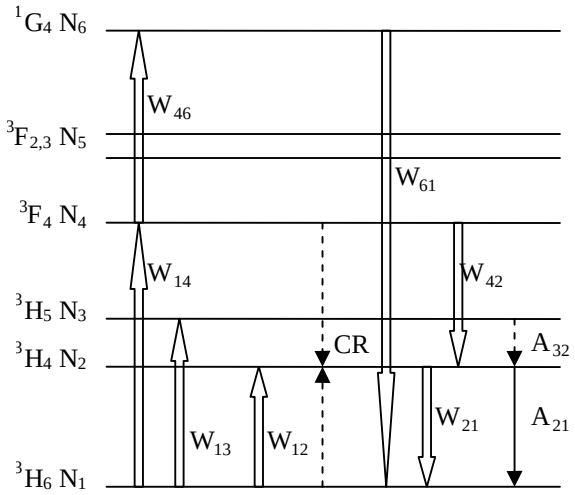

Figure 2.5: *Simplified energy-level diagram of Tm^{3+} system.*

(c) Holmium (Ho^{3+}) system

Figure 2.6 is the energy diagram of Ho^{3+} showing the pump absorption band that our DFB fibre laser is pumped by, i.e. $^5I_8 \rightarrow {}^5I_6$, and laser emission. The Ho ions absorbed the pump energy and were excited from the $^5I_8$ ground state to the $^5I_6$ level. The ions are then rapidly decayed to the upper laser level, $^5I_7$. Laser action occurs between the $^5I_7$ and the ground state. The rate equations of the system are the same as in Equation (2.17-2.19). We also pumped the laser in the $^5I_8 \rightarrow {}^5I_7$ scheme which is an in-band pumping scheme. The system rate equations of this scheme are the same as in Equation (2.32) and (2.33).

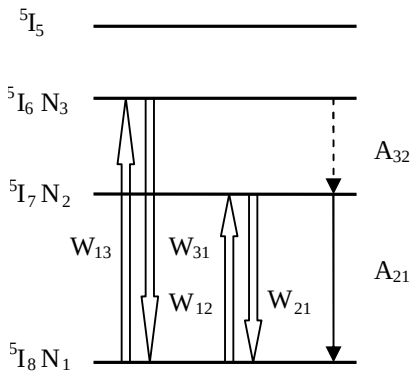

Figure 2.6: *Simplified energy level diagram of Ho^{3+} system.*

In the Er^{3+}-Yb^{3+} co-doped system, the laser efficiency is diminished due to the cooperative upconversion in which the neighbouring Er^{3+} ions, which are excited to the $^4I_{13/2}$ laser level, transfer energy among the ions and the result is that one decays to the ground $^4I_{15/2}$ level, while the other is promoted to the $^4I_{9/2}$ level. From this level, it decays rapidly back to the $^4I_{13/2}$ level by multiphonon decay. The consequence of the upconversion is that one excited Er^{3+} in the $^4I_{13/2}$ level is quenched to the ground level so the population of that level is reduced by 50%. The other cause of a reduction in the efficiency of the laser is due the lifetime quenching of a portion of Yb^{3+} in which the pump energy is lost [6]. The short lifetime causes the excited Yb ions to return to the ground state through some nonradiative relaxation.

The upconversion and the cross relaxation process are eliminated in the two-level laser system. In fact, this is an advantage in operating the laser in a two-level system as it avoids the pump energy being lost through these processes.

2.4 Summary

This chapter described the parameters for the feedback gratings and the effective laser cavity length of the lasers. The effective laser cavity length of the uniform apodised and step-apodised design are discussed. In the case of the step-apodised

design, its effective cavity length can be increased while maintaining the optimum reflectivity of the grating, so that more of the gain medium can be utilised for signal generation. The rate equations are used to describe the gain media of the laser in which the ions' population for inversion and the losses in the system, such as the upconversion, cross-relaxation and the ion quenching, can be predicted, which in-turn predicts the laser efficiency.

2.5 References

[1] F. Di Pasquale, "Modeling of highly-efficient grating-feedback and Fabry-Perot Er^{3+}-Yb^{3+} co-doped fiber lasers," *IEEE Journal of Quantum Electronics*, vol. 32, pp. 326-332, 1996.

[2] M. Karasek, "Optimum design of Er^{3+}-Yb^{3+} codoped fibers for large-signal high-pump-power applications," *IEEE Journal of Quantum Electronics*, vol. 33, pp. 1699-1705, 1997.

[3] E. Yahel and A. Hardy, "Modeling high-power Er^{3+}-Yb^{3+} codoped fiber lasers," *Journal of Lightwave Technology*, vol. 21, pp. 2044-2052, 2003.

[4] C. Jiang, W. Hu, and Q. Zeng, "Improved gain performance of high concentration Er^{3+} -Yb^{3+} -codoped phosphate fiber amplifier," *IEEE Journal of Quantum Electronics*, vol. 41, pp. 704-708, 2005.

[5] S. D. Jackson and T. A. King, "Theoretical modeling of Tm-doped silica fiber lasers," *Journal of Lightwave Technology*, vol. 17, pp. 948-956, 1999.

[6] K. Yelen, L. M. B. Hickey, and M. N. Zervas, "Experimentally verified modeling of erbium-ytterbium co-doped DFB fiber lasers," *Journal of Lightwave Technology*, vol. 23, pp. 1380-1392, 2005.

[7] H. Kogelnik and C. V. Shank, "Coupled-wave theory of distributed feedback lasers," *Journal of Applied Physics*, vol. 43, pp. 2327-2335, 1972.

[8] A. Ghatak and K. Thyagarajan, *Introduction of fibre optics*: The University of Cambridge Press, 1998.

[9] G. A. Ball and W. H. Glenn, "Design of a single-mode linear-cavity erbium fiber laser utilizing Bragg reflectors," Journal of Lightwave Technology, vol. 10, pp. 1338-1343, 1992.

[10] T. Erdogan, "Fiber grating spectra," Journal of Lightwave Technology, vol. 15, pp. 1277-1294, 1997.

[11] K. Yelen, L. M. B. Hickey, and M. N. Zervas, "A new design approach for fiber DFB lasers with improved efficiency," IEEE Journal of Quantum Electronics, vol. 40, pp. 711-720, 2004.

[12] P. C. Becker, N.A. Olsson, and J. R. Simpson, Erbium-doped fiber amplifiers fundamentals and technology. San Diego: Academic Press, 1999.

Chapter 3

Erbium-Ytterbium Co-doped Fibre DFB Laser

Short-cavity single frequency fibre lasers have been a topic of continued interest since the early work of Ball *et al*. on Er^{3+} -doped DBR fibre lasers [1]. Their size, simplicity, ease of fabrication, compatibility to transmission fibre and their optical emission characteristics make them attractive for a number of applications, particularly in the sensing area. However, there have been few detailed experimental investigations on the linewidth or phase noise characteristics of these lasers, with much of the work being focused on improving the efficiency and output power through fibre, cavity, or grating design [2-4]. With the widespread adoption of Er^{3+}-Yb^{3+} fibres, laser efficiencies in the tens of percent are now easily achievable [5]. An implicit assumption, however, in many of these designs is that the attainable laser frequency noise characteristics will not be substantively compromised by the proposed modifications. This is clearly an important assumption as it is usually the single frequency characteristics of these kinds of fibre lasers that make them so attractive. To our knowledge, however, there has been very little evidence given to verify the extent to which this assumption is true.

To date, the phase noise properties of these fibre lasers continues to fail to measure up to that achievable in bulk solid state lasers. This is perhaps surprising, considering that predictions of the intrinsic linewidths of fibre lasers, based on the well-know Schawlow-Townes formula, indicate linewidths of just 60 Hz or less [6]. A common suggestion as to why the observed linewidths remain far above their theoretical limit is that the increased noise is caused by environmental perturbations, such as external vibration and acoustic noise, to which the fibre laser may be more susceptible. The inference then is that this issue is primarily a packaging problem, which could be solved by better mechanical designs in holding the fibre, vibration isolation and stabilisation.

The purpose of this work is to present experimental data which strongly suggests that the anomalously large linewidths of these fibre lasers should be more accurately viewed as an intrinsic aspect of these lasers, and show that designs for maximizing output power and efficiency may need to take into account potential trade-offs in their single frequency characteristics [7, 8]. Later, an analytical model is used to explain the observed anomalous linewidth. We found good agreement between the analytical model and the observations [9, 10]. The excess noise is significantly elevated due to the temperature fluctuations induced by pump intensity noise. The various possibilities to overcome these linewidth limitations are also discussed in this chapter. Some of the possibilities for reducing the linewidth are experimentally analysed in the next chapter.

I would like to acknowledge that this work was carried out in collaboration with Dr P. Horak, a senior research fellow in the ORC, who did the simulation and modelling.

3.1 Review of linewidth of DBR/DFB fibre lasers

This section reviews some of the linewidths of the DBR and DFB fibre lasers, operating around 1.5 μm, that have been demonstrated in Er^{3+} and Er^{3+}-Yb^{3+} doped fibres. Linewidth variations of 47 kHz to 6 MHz, depending on the cavity designs,

have been reported for the Er^{3+}-doped DBR fibre lasers [1, 11]. Two grating reflectors of 12.5 mm long were written on opposite ends of a 0.5 m long Er^{3+}-doped fibre. The laser had a linewidth of $\leq$ 47 kHz, with an output of 5 mW for the maximum pump power of 50 mW at 980 nm [1]. Another DBR fibre laser, with a 2 cm resonator, having an output power of 181 μW for a maximum pump of 61 mW at 980 nm has been demonstrated. The output of this laser exhibited self-pulsation possibly associated with clustering of erbium in the high concentration (2500 ppm) and this could be the reason that the linewidth was larger. The linewidth of this laser was 6 MHz [11]. For the Er^{3+}-doped DFB designs, linewidths of 13 kHz to 300 kHz were observed [12-14]. A 10-cm long DFB fibre laser, with a permanent phase shift incorporated into the fibre grating during writing, was pumped at 980 nm and an output power of 1 mW was measured for the maximum pump power of 120 mW. The optical linewidth of 13 kHz was observed [12].

A MOPA DFB laser configuration, having a linewidth of 15 kHz, based on a 36 mm long Bragg grating with a $\pi/2$ phase shift, was pumped with a 50 mW semiconductor laser at 1480 nm and an output power of 5.4 mW was demonstrated [14]. Pumping into the large absorption cross-section of Er^{3+} in the 520 nm band, a laser with an output power of 17 mW for 190 mW pump power, was demonstrated [13]. The linewidth was broader at high output power. A linewidth of 260 kHz was observed at an output power of 17 mW and was 40 kHz at 2 mW. Due to the low pump absorption of Er^{3+}, the fibre was then co-doped with ytterbium (Yb^{3+}), to enhance the pump absorption by energy transfer from Yb^{3+} to Er^{3+}. Both DBR [4, 15] and DFB [4] designs have been demonstrated with this fibre. Using Er^{3+}-Yb^{3+} co-doped phosphosilicate fibre, with relatively high Er^{3+} doping concentrations (1000 ppm [2]), DBR lasers have shown output powers of up to 60 mW [4], and 166 mW in a MOPA configuration [15]. Unfortunately, these lasers have shown a much broader linewidth of 200 to 500 kHz.

In [4] a laser linewidth of 500 kHz was observed. The cavity of this laser was based on a highly reflecting mirror butt-coupled onto one end of the fibre and the other end was a centimetre long Bragg grating written directly into the fibre. The entire laser was shorter than 1.5 cm. A 5-cm long DFB laser made from the same material, has

shown a much better performance with a 18 kHz linewidth [4]. The laser cavity of Ref. [15] exploited the advantages of low noise and stable-single-mode operation of phase-shifted DFB fibre laser, and combined this with a DBR laser to boost the fibre laser output power. The laser cavity consisted of a fibre grating with a $\pi/2$-phase shift and with two fibre gratings of different reflectivity at both ends, it was 48 mm long with the gratings written directly into the fibre. The laser linewidth of 200 kHz was observed. A tin co-doped Er^{3+}-Yb^{3+} DFB fibre laser with an output power of 10 mW, pumped at 980 nm, having a linewidth of 25 kHz, was demonstrated [16]. The laser cavity was formed by using a strong reflectivity grating, having a length of 1.5 cm, spliced to a 8.5-cm long active grating. Recently, a DBR fibre laser, based on heavily Er^{3+}-Yb^{3+} co-doped phosphate glass, with a linewidth as low as 2 kHz was demonstrated [17]. The laser cavity was formed by two spectrally narrow passive fibre Bragg gratings that were fusion spliced to a 2-cm long Er^{3+}-Yb^{3+} fibre. The output power of 200 mW was achieved with a maximum pump power of ~850 mW at 980 nm.

3.2 Er^{3+}-Yb^{3+} co-doped phosphosilicate fibre

This section gives the details of the fibre that we used to construct the DFB laser, covering the function of Er^{3+} co-doping with Yb^{3+}, the structure of the fibre, the concentration of the dopants and the small signal loss at the pump wavelength. In a singly doped Er^{3+} fibre, the amount of Er^{3+} doping concentration is limited to 100 ppm by the germanosilicate glass host, in order to avoid clustering problems, and the pump absorption is low in a short laser length, which leads to poor laser efficiencies of <1%. It has been demonstrated that by co-doping Er^{3+} fibre with Yb^{3+}, the absorption of 980-nm pump energy can be increased by more than 2 orders of magnitude due to energy transfer to the Er^{3+} [2, 18]. This allows the realisation of highly efficient short cavity lasers. However, a phosphosilicate glass host, which is not photosensitive, is required to ensure efficient energy transfer between Er^{3+} and Yb^{3+} ions. Nevertheless, Ref. [19] has shown that the photosensitivity of the fibre can be achieved by surrounding the core with a highly photosensitive boron/germanium (B/Ge) doped silica cladding, as seen in Figure 3.1. The structure

of our fibre used for constructing the DFB lasers is similar to that reported in [19]. The same refractive index as of the pure silica can be achieved by the cladding, as Ge doping increases the refractive index of silica and B doping lowers it. In addition, UV-exposure of the gain medium during grating fabrication induced loss that can cause degradation of the gain medium and thus a lowering of the laser efficiency [20]. The concentration of Er^{3+} in our fibre was $1x10^{25}$ m^{-3}. The concentration ratio of Er^{3+} to Yb^{3+} in the fibre was 1:19. The maximum small signal absorption of the fibre was 850dB/m at 975 nm, and was 45dB/m at 1530 nm, as measured in the next section.

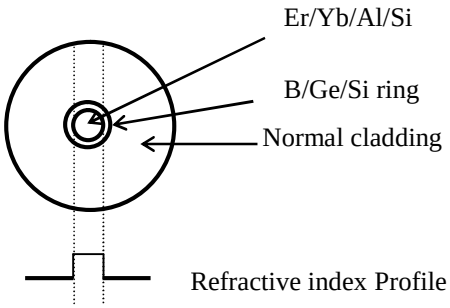

Figure 3.1: *Structure of the photosensitive Er^{3+}-Yb^{3+} with an index matching B/Ge/Si cladding [19].*

3.2.1 Absorption of the fibre used

The absorption of the Er^{3+}-Yb^{3+} co-doped fibre was measured to ensure that the operating wavelength of the pump diode was within the absorption band of the Er^{3+}-Yb^{3+} co-doped fibre. The absorption loss of a ~13 cm long doped fibre was measured, by the cut-back technique, with a white light source, launched into one end of the fibre, with the use of an objective lens, and the other end was measured with an OSA (Advantest Q8384 optical spectrum analyser). The measured absorption loss in the spectral regions of 970 – 980 nm and 1400 – 1600 nm is shown in Figure 3.2. The majority of this work was conducted with the 977 nm pump laser diode, as Yb^{3+} has high pump absorption around this wavelength region, so by energy transfer from Yb^{3+} to Er^{3+}, it can provide an efficient indirect pumping mechanism for Er^{3+}, as mentioned earlier. The use of 1480 nm as the pumping wavelength, directly pumping into the upper laser level of Er^{3+}, was also performed

for the investigation of the laser linewidth. The associated self-heating, due to the non-radiative phonon decay, is eliminated with this pumping wavelength. Later, we used a diode laser operated at 975 nm for the validation of the analytical model which explained the main cause of the laser linewidth behaviour in the later part of this chapter.

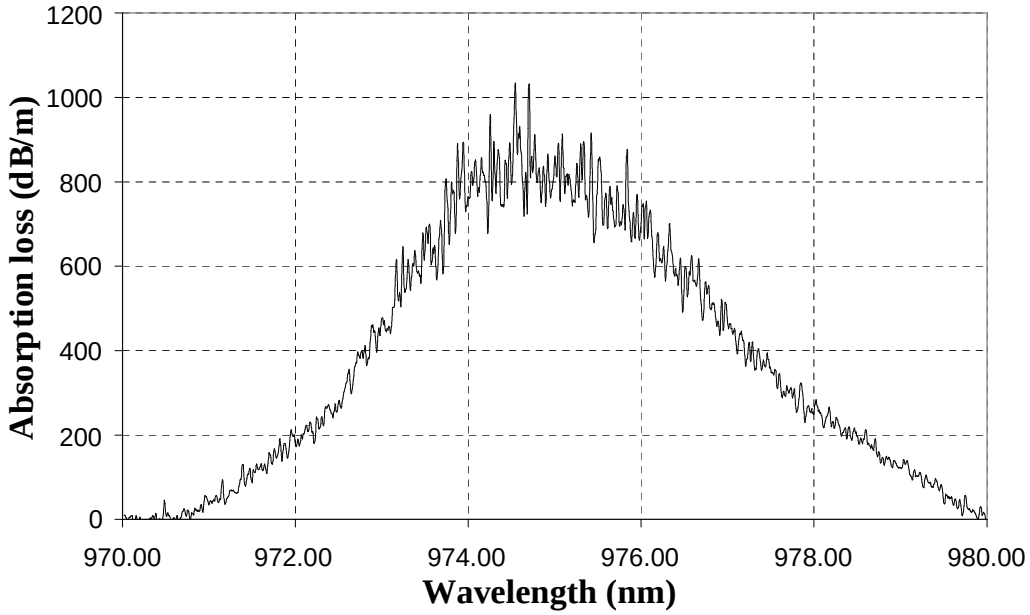

(a)

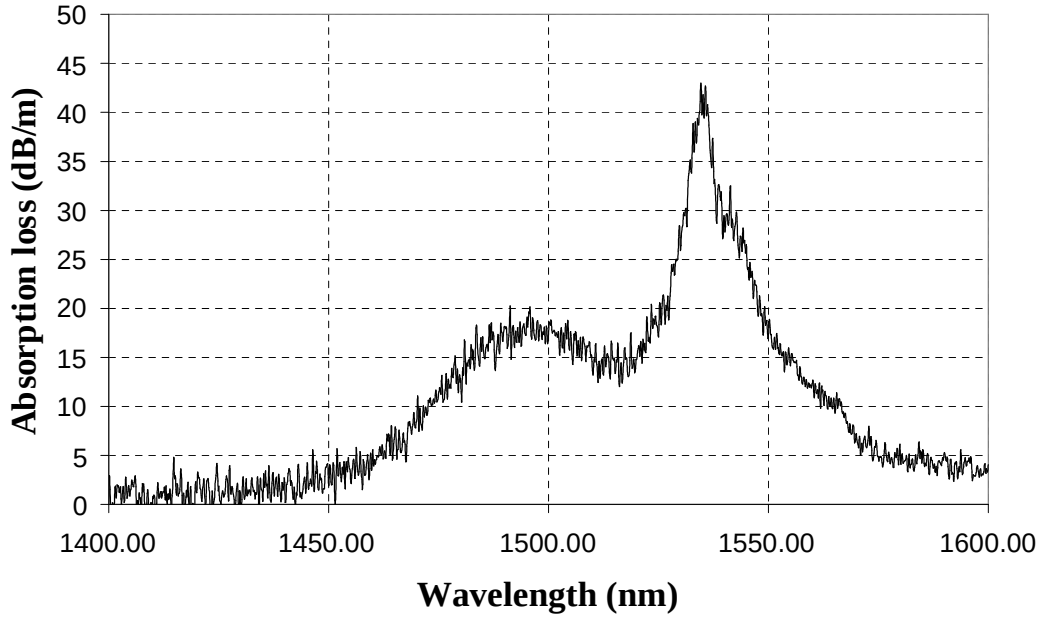

(b)

Figure 3.2: *The measured absorption loss of the Er^{3+}-Yb^{3+} co-doped fibre in spectral regions (a) 970 - 980 nm and (b) 1400 - 1600 nm.*

As observed in the absorption loss of this fibre in the 980 nm region, the slope of the absorption is very steep at this absorption band. A wavelength variation of just 5 nm, from 970 nm to 975 nm, has an absorption loss increase from 0dB/m to ~ 850dB/m. The absorptions measured at pump wavelengths of 977 nm and 975 nm are ~450dB/m and ~850dB/m, respectively. The absorption of Er^{3+} at 1480 nm is ~14dB/m which is very much lower as compared with that of 977 nm.

3.3 The structure of the DFB fibre laser

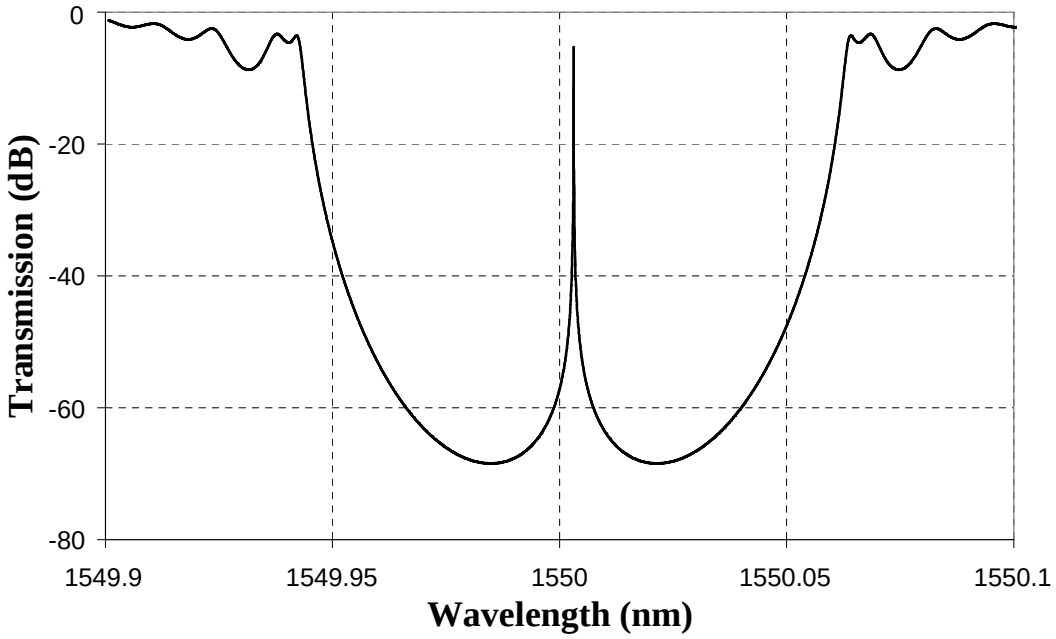

Figure 3.3: *A typical transmission spectrum of the feedback grating with grating strength of 10 of a DFB laser.*

This section describes the structure of the DFB laser, which is constructed from a 125 μm diameter, Er^{3+}-Yb^{3+} co-doped phosphosilicate fibre with a B/Ge ring surrounding the core, as described in Section 3.2. The laser cavity, based on UV written Bragg gratings that were written with the phase-mask technique [21], was 5 cm in length with a π-phase shift located slightly off centre, 3mm from the mid-point of the gratings. This asymmetry enables the output power to be emitted predominantly from one end of the laser [22, 23]. The DFB gratings, with a resulting

period (Λ) of 539 nm, are written into the B/Ge ring surrounding the core. After writing, the gratings were annealed for 24 hours at 100 ºC to stabilise the index modulation. The final grating strength (κL) was estimated to be ~10 with a transmission of ~ -80 dB. Figure 3.3 shows a typical transmission of the feedback grating with grating strength of 10 is simulated by, my colleague, Zhaowei Zhang. The single polarisation operation of the laser was obtained by writing the phase-shifted gratings with continuous-wave (CW) UV light at 244 nm, polarised perpendicular to the propagation axis of the fibre, as reported in [23], and is shown in Figure 3.4. A relative coupling coefficient change along the y-axis of 2% is adequate to cause the laser to lase in the direction parallel to y-axis.

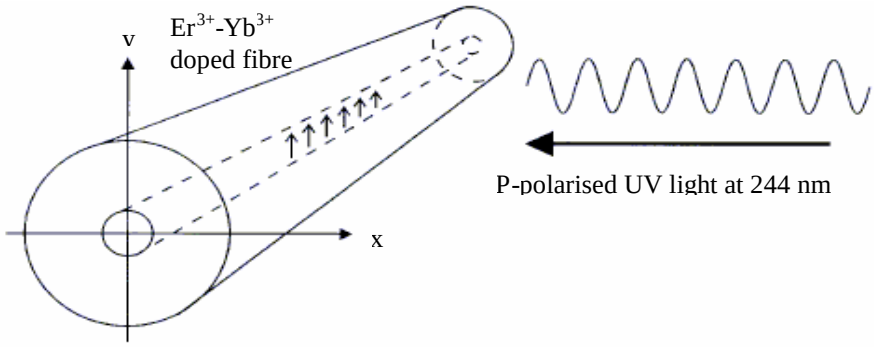

Figure 3.4: *Technique for the formation of polarisation dependent gratings [23].*

3.4 Linewidth and phase noise characteristics of the DFB fibre laser

This section presents the experimentally observed data which suggested that the large linewidths of the laser should be viewed as the intrinsic aspect of the laser, and that designs for maximizing the output power and efficiency in the laser may be required to take into account trade-offs in their single-frequency characteristics. The fibre DFB laser was set-up in three different pumping configurations for this study. The possible sources responsible for this anomalous laser linewidth, such as due to heating of the fibre because of heat dissipation of the absorbed pump power, the cavity intensity noise of the laser and the non-radiative phonon decay from the metastable level ($^4I_{11/2}$) to the upper laser level ($^4I_{13/2}$), were investigated.

3.4.1 Experimental set-up

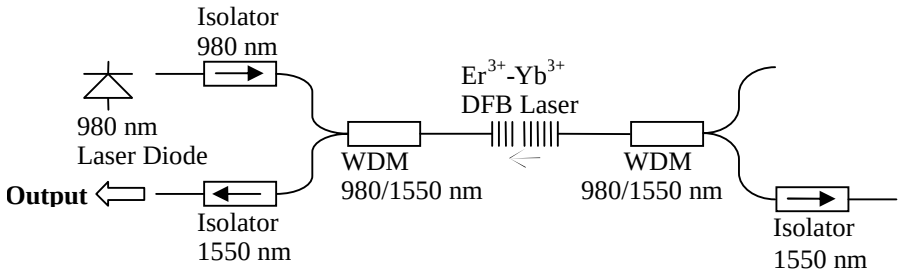

(a)

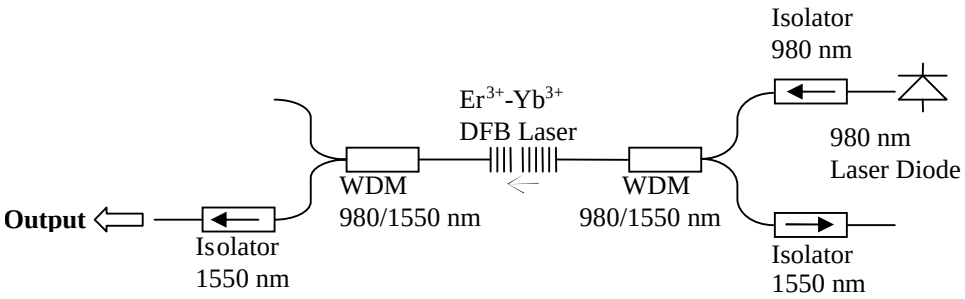

(b)

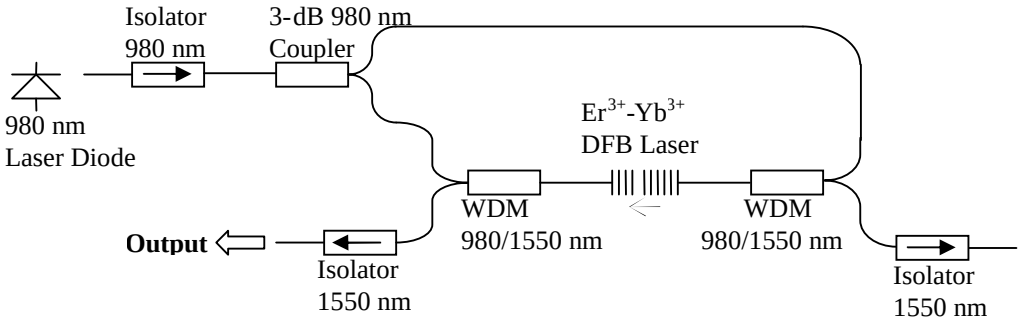

(c)

Figure 3.5: *Schematic of the laser configurations with pump wavelength of 980 nm: (a) backward pumping, (b) forward pumping, and (c) dual pumping configuration.*

The fibre laser was investigated by pumping through three different configurations, as shown in Figure 3.5. The first configuration, backward pumping, consists of the pump power counter-propagating to the main laser output, i.e. the pump is coupled in at the end nearer to the grating phase shift. The second configuration, forward pumping, has the pump coupled in from the opposite end of the grating, i.e. the far end with respect to the phase shift. In the third scheme, dual pumping, the pump is split equally in two and coupled into the fibre laser at both ends. A 980-nm optical isolator is used at the output of the pump laser in all cases to prevent undesired optical feedback from destabilising the pump diode. 1550-nm optical isolators were also placed at both output ends of the fibre laser to ensure that the linewidth behaviour being studied is not compromised by unintended feedback effects into the DFB laser. The fibre laser is placed on a temperature-controlled heat sink, and pumped with a 977-nm, grating stabilised, laser diode. The lasing threshold, output power, and linewidth were all measured for the three pumping configurations.

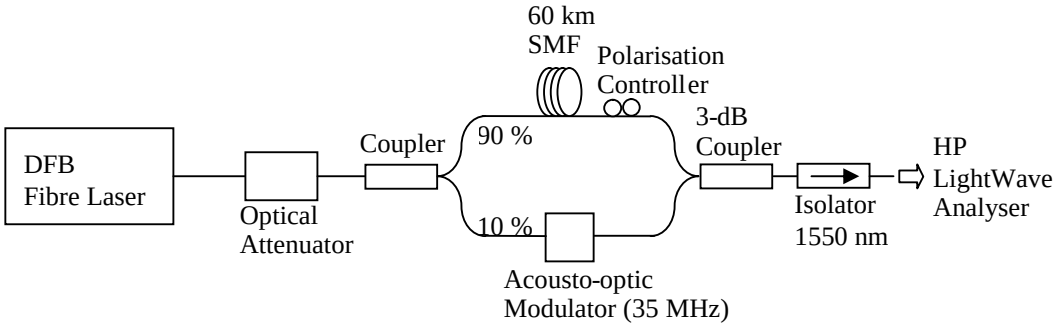

Figure 3.6: *Schematic diagram showing the linewidth measurement set-up.*

The laser linewidth measurement has been demonstrated by using a delayed self-heterodyne technique [24]. Our delayed self-heterodyne setup is shown in Figure 3.6. In this setup, the laser beam is divided into two paths by a 10/90 fibre coupler for the optimal fringe visibility. One beam is sent through a delay line which provides some time delay (τ_d), while the other beam is frequency shifted with respect to the other before both beams are recombined, and the resulting beat response is measured with a HP lightwave signal analyser which consists of an optical detector with a RF analyser. The laser linewidth can be estimated from the width of this beat spectrum. A 35 MHz acousto-optic modulator was used to shift it to a frequency much higher

than the noise spectrum to be measured. For an accurate linewidth measurement of a laser with a white frequency noise spectrum, the delay path needs to be greater than the coherence length of the laser so the two combining beams would be effectively uncorrelated. In this case, a high measurement resolution is achieved with a longer delay line. However, as will be shown later our DFB laser does not exhibit a white frequency noise spectrum. In such a situation [25] the delay time has to be long enough to generate a sufficient number of cycles of $\sin^2(\pi f \tau_d)$ within the frequency noise spectrum to avoid undersampling. On the other hand, a long delay line will introduce high propagation losses. For our setup, a delay line of 60 km long single mode fibre is used which, for a white noise laser, provides a linewidth resolution of 3.5 kHz. The single polarisation status of the laser was confirmed with an Agilent lightwave polarisation analyser.

3.4.2 DFB power characteristics

Figure 3.7 shows the threshold and output power characteristics of the fibre laser under the three pumping configurations. As indicated in the figure, the backward pumping scheme had the lowest threshold and highest efficiency, while the dual pumping scheme was the worst in these aspects. This can be explained by the asymmetry of the grating design and the different pumping configurations. The pump intensity within the grating was strongest at the grating input, saturating the Yb^{3+} absorption there first, and then decayed during propagation as it was strongly absorbed. The resulting unabsorbed pump power was less than 1% of the input pump power. The lasing threshold approximately corresponded to the pump power where the laser light experienced gain on one side of the phase shift and loss on the other. Because of the asymmetry, this was achieved for lower pump powers in the backward pumping configuration than for forward pumping. For dual pumping, on the other hand, where each input port only receives half the pump power, the pump absorption is generally a little larger according to the later onset of the saturation of the Yb^{3+} transition. This results in the highest lasing threshold for this configuration. A pump to signal conversion efficiency of 17 %, with an output power of ~20 mW, was achieved in the backward pumping scheme for a pump power of ~110 mW.

Forward pumping has an output power of ~18 mW with a power conversion efficiency of 14 % for the same pump power. An output power of ~14 mW, with a conversion efficiency of 10 %, was obtained for the dual pumping. If maximizing efficiency and output power is the over-riding criterion, then backward pumping is clearly the configuration to adopt. The laser output was highly asymmetric for all three pumping configurations, which is expected due to the location of the grating phase shift: ~95% of the total laser output was measured to come out of the end nearer to the phase shift.

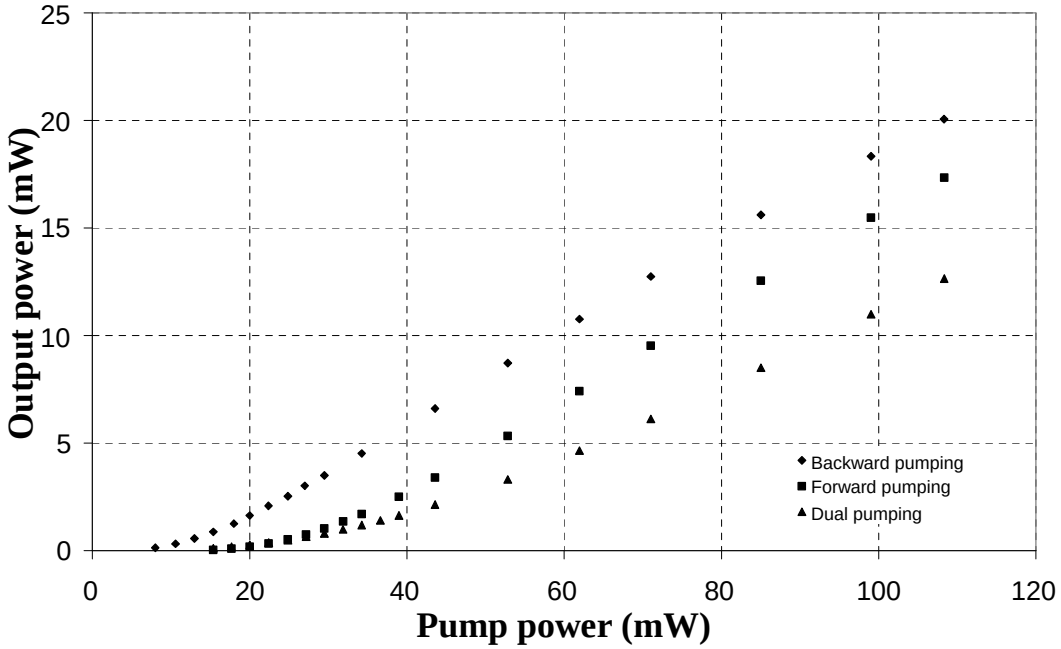

Figure 3.7: *Threshold and laser output characteristics of the DFB fibre laser for the three pumping configurations.*

3.4.3 Laser linewidth characteristic

The measured 3-dB laser linewidth behaviour, as a function of pump power and laser output power, is shown in Figure 3.8 (a) and (b), respectively. The trend lines shown in the figure are presented simply as a guide, rather than as a rigorous fit. As observed the laser linewidth behaviours were different for the three pumping configurations, particularly for the backward pumping in which the linewidth is

nearly constant over the pump power range shown. This behaviour is related to the different response of various configurations to pump intensity fluctuation. At the low pump powers, the backward pumping configuration has the largest wavelength sensitivity to pump power compared to the other pumping configurations. This may be attributed the fact that for the backward pumping configuration, the pump intensity at the grating phase shift is large than for the other configurations, and thus the thermal response to intensity fluctuation is stronger. At high pump powers, this simple picture no longer holds due to saturation effects. This is discussed in more detail in Section 3.5. In direct contrast to the threshold characteristics, the data showed that the lowest linewidth operation was actually obtained with the dual pumping configuration, with linewidths of 15 kHz to 35 kHz over the pump power range of ~110 mW. For the given pump power range, the linewidth of the backward pumping configuration was between 30 kHz and 35 kHz and between 20 kHz to 40 kHz for the forward pumping configuration. In fact, for output powers up to 1 mW, the linewidth of the dual pumping configuration was about half that achievable with a backward pump, although it increases and then levels off at high powers as seen in (b). Even over its entire output power range, the laser linewidth under the dual pumping configuration was lower or comparable to that attainable with the other two pump configurations.

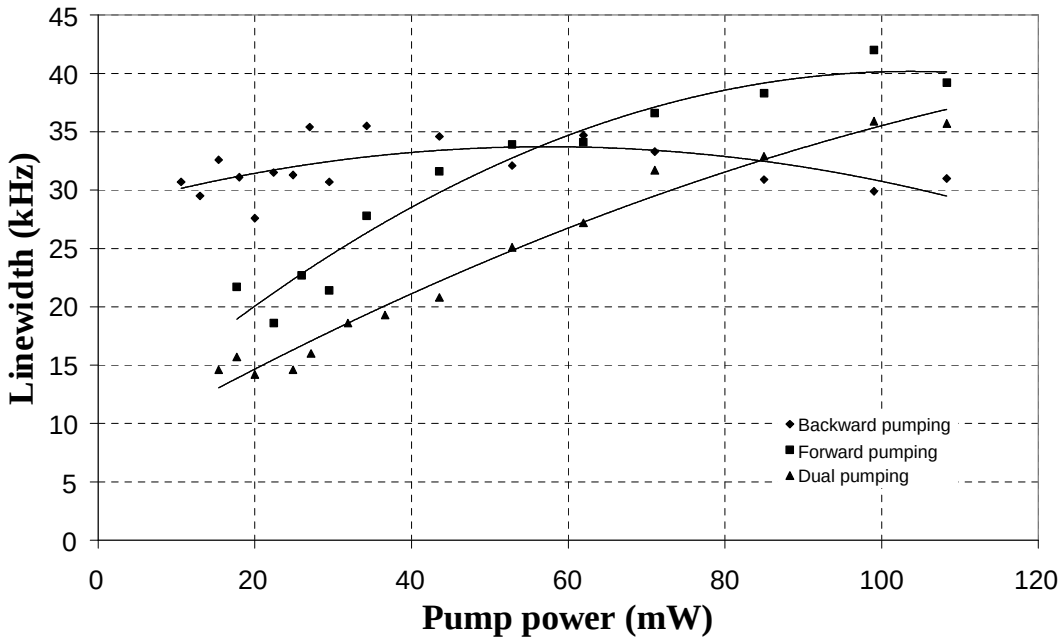

(a)

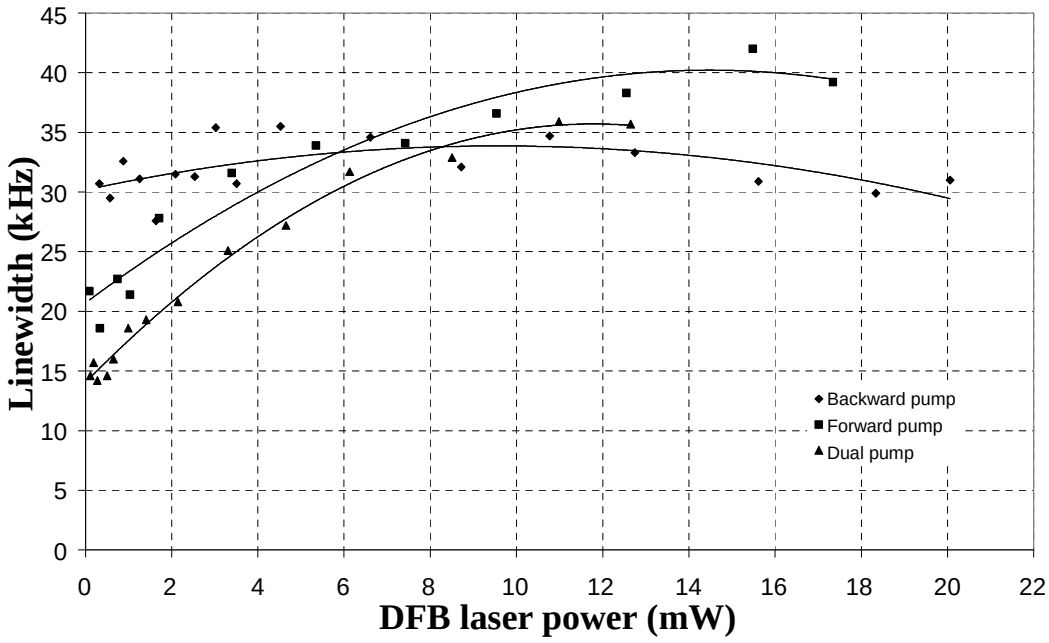

(b)

Figure 3.8: *Laser linewidth with (a) pump power and (b) output power for the three pumping configurations.*

Clearly, there are significant trade-offs between efficiency and power, with linewidth and optical phase noise, when designing and operating these fibre lasers. We showed that the trends displayed are real, given our linewidth uncertainty of 5 kHz. It is also worth pointing out that this anomalous linewidth behaviour is not unique to this laser, but has been seen elsewhere in the other DBR [26] and DFB [13] fibre lasers. The issues raised by this work are, thus, likely to be quite general in nature.

Now, we take a look at the relation of the laser linewidth with DFB power. The behaviour of the laser linewidth with power is somewhat surprising. The well-known Schawlow-Townes linewidth formula [27]

$$\Delta\nu = \frac{2\pi h\nu\left(\Delta\nu_{cav}\right)^2}{P} \qquad \textbf{(3.1)}$$

where ν is the lasing frequency, P is the laser output power, and $\Delta\nu_{cav}$ the (passive) grating linewidth, predicts that the laser linewidth should decrease in inverse proportion to the laser power. It may be instructive to briefly review the physical

picture underlying the above formula. The origin of this linewidth is the perturbation to the laser phase caused by spontaneous emission into the laser cavity. Intuitively, it is clear that each spontaneous emission event, resulting in the emission of a single photon, will have less impact as the total number of photons (laser power) in the cavity gets larger. This is the physical basis for the decrease of the Schawlow-Townes linewidth with increasing laser power. In particular, note that as the DFB power increased from 1 to 10 mW, the linewidth should have decreased tenfold. Instead, we observed the opposite, with the linewidth actually increasing substantially with power, particularly for the forward and dual pumping configurations. As it seems inconceivable that the spontaneous emission rate could have increased by more than ten-fold, the observations here point to a different physical origin for the linewidth.

Although the underlying reason(s) for the anomalous linewidth behaviour is still unclear at this point, the dependence on pump and output power suggests that the variations in linewidths (15 kHz to 40 kHz) are a feature of the laser rather than due to externally induced environmental perturbations. One would expect external perturbations (e.g. mechanical vibration) to contribute to a fixed noise floor that is independent of pump power. As pointed out in [5], a large intensity build-up occurs around the phase shift because field propagation is trapped around it by the two grating segments. Accordingly, the lasing intensity profile of the DFB in the three pumping configurations was modelled by Dr P. Horak. The model of the DFB laser was based on a gain mechanism together with the feedback grating. The gain of the DFB was obtained based on the rate equations given in Ref. [28] and using the transfer matrix equations in Ref. [29] for the feedback mechanism. The numerical model of the lasing profile is shown in Figure 3.9. It shows that the lasing intensity within the fibre laser in the close vicinity of the phase shift is very high, but the peak lasing intensity was very similar (to within 5%) for the three pumping configurations, given the same operating powers. Therefore, one might also expect effects arising directly from strong spatial or polarisation hole burning that could cause gain saturation, i.e. distortion of the gain shape, or fibre nonlinearity (e.g. modification of the propagation of light in the cavity), to be similar for different pumping configurations, in contrast to the different behaviours observed in Figure 3.8. In

addition, with backward pumping, the pump is counter-propagating to the main laser output; nonlinear optical interactions (e.g. cross-phase modulation) between the pump and signal should, thus, have the least impact, at odds with the trends observed. The effect of pump noise on the DFB laser frequency noise has also been analyzed in [30] to be a secondary factor compared to thermal noise. The temperature fluctuations in the optical cavity lead to local strains and refractive index perturbations which in turn result in phase detuning. It is perhaps most surprising that the forward and backward pumping configurations yield significantly different linewidth behaviour with pump and output power, as the grating phase shift is only located a little off-centre, by 3 mm. This suggests that modifying the grating or cavity design solely to optimize for threshold and output power may incur unexpected and undesired penalties in the laser phase noise characteristics.

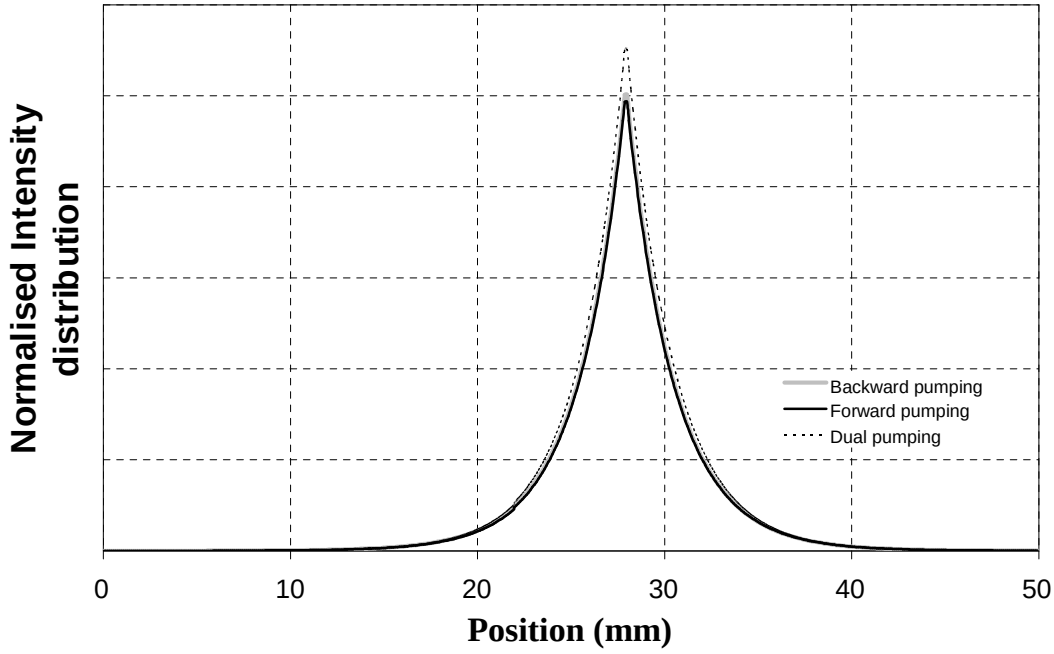

Figure 3.9: *Laser intensity profile build-up around the phase shift of the 5-cm long DFB.*

To investigate further, the laser linewidth was analysed from the measured self-heterodyne rf (radio frequency) spectrum, shown in Figure 3.10. Although the spectral shape is clearly non-Lorentzian, an excellent fit could be obtained, with little

deviation over a range of more than 20 dB, using a convolution of a Gaussian and a Lorentzian function,

$$S(f) \propto \int dw \exp(-w^2 / w_G^2) \frac{1}{1+(f-w)^2 / w_L^2} \qquad \textbf{(3.2)}$$

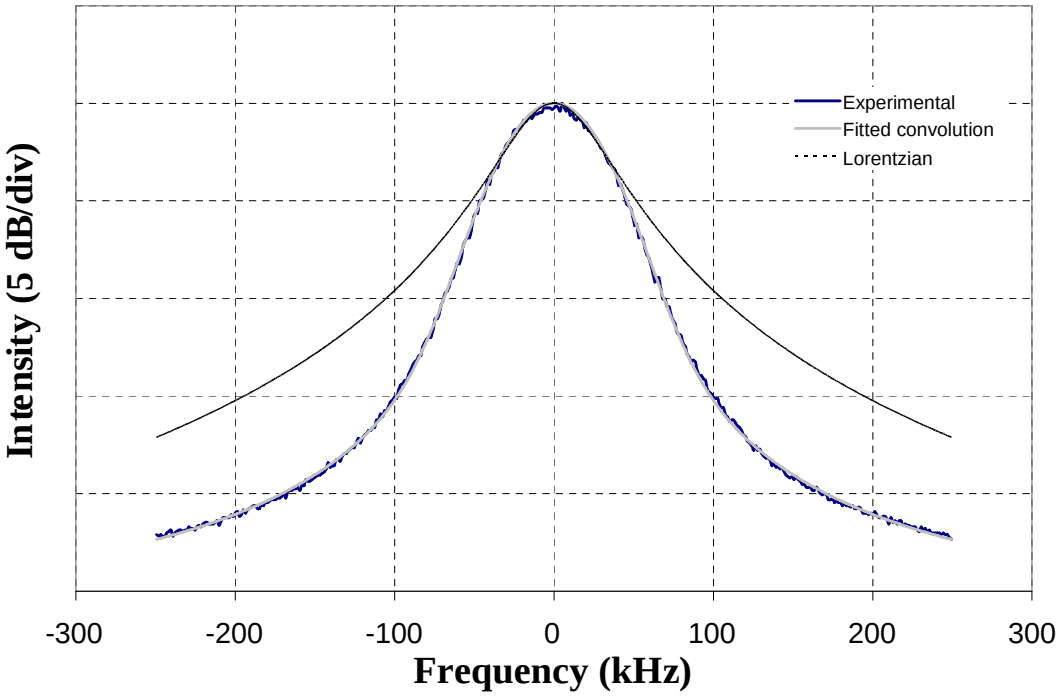

Figure 3.10: *Self-heterodyne rf-spectrum and its theoretical fit using a convolution of a Gaussian and Lorentzian function.*

For the particular spectrum shown, the extracted Gaussian 1/e width was w_G= 36.8 kHz, and the 3-dB width of the Lorentzian component was w_L = 7.9 kHz. It was found that, as the linewidth increases, both these components increase as well. It is often assumed that these components represent two distinct noise contributions. The Lorentzian component is sometimes viewed as more intrinsic by association with the Schawlow-Townes Lorentzian lineshape, and laser linewidths have been reported based on estimates of the Lorentzian component only [17]. Our findings, that the Lorentzian component of the linewidth actually increases with power, contravening the Schawlow-Townes inverse power relation, render the above assumption questionable. That the extracted Lorentzian component of the linewidth might not be uniquely related to spontaneous emission should not be too unexpected. First, these

Lorentzian linewidths are still orders of magnitude larger than that expected from the Schawlow-Townes spontaneous emission-induced values [6]. Secondly, while the white noise spectrum, arising from spontaneous emission, will yield a Lorentzian lineshape, the converse need not be strictly true. As has been pointed out by Lax, it is primarily the noise behaviour in the close vicinity of the laser frequency which dictates the Lorentzian lineshape [31].

In general, the laser spectrum *S(f)* is related to the laser frequency jitter (FM-noise) spectrum $S_F(f)$ by the relationship [32].

$$S(f) \propto F\left\{\exp\left(-4\int_0^\infty d\varpi S_F(\varpi)\frac{\sin^2(\varpi\tau/2)}{\varpi^2}\right)\right\} \qquad \textbf{(3.3)}$$

where $F\{\ldots\}$ denotes the Fourier transform with respect to τ. Depending on the origin and behaviour of $S_F(f)$, various spectral lineshapes, non-Lorentzian or pseudo-Lorentzian, would result. For example, Lorentzian-like lineshapes can also be shown to result from thermally-excited index fluctuations [33], using the derived expression for the associated optical phase noise in fibres [34]. One should therefore be cautious in assuming that any Lorentzian component extracted from the laser lineshape naturally represents a more important contribution to the phase noise than, say, the Gaussian portion.

3.4.4 Thermal effects of the DFB laser

The relatively high pump powers involved here and the strong pump absorption afforded by the Yb^{3+}-Er^{3+} in the fibre core, and also the fibre small signal absorption at 977 nm being 450 dB/m, required us to investigate the possibility of heating/thermal effects occurring in the fibre in accounting for the anomalous laser behaviour. It has been pointed out that the temperature may rise by as much as 30 ºC for every 10 mW/cm of absorbed pump power in doped fibres [35] with an insulating fibre cladding interface. With our pump powers of up to 100 mW and more, virtually all of it absorbed over the 5 cm grating length, it was necessary to check the effectiveness of the heat sink in maintaining the temperature stability of the doped

fibre. For this reason, the lasing wavelength was measured as a function of pump power for three heat sink temperatures. The lasing wavelength was measured with a Burleigh wavemeter WA1500, having a resolution of 0.2 pm. Figure 3.11 shows the lasing wavelength as a function of pump power at a heat sink temperature of 13 ºC, 24 ºC and 80 ºC. It was found that, for a fixed pump power, the lasing wavelength increases with heat sink temperature at the rate of 0.01 nm/ºC, in line with the temperature sensitivity of the fibre grating, i.e. ~8 pm/ºC. For a fixed heat sink temperature, the lasing wavelength increased gradually with pump power, by ~20 pm as pump power increased from 20 mW to 110 mW. This indicated a maximum temperature increase due to the pump of less 3 ºC.

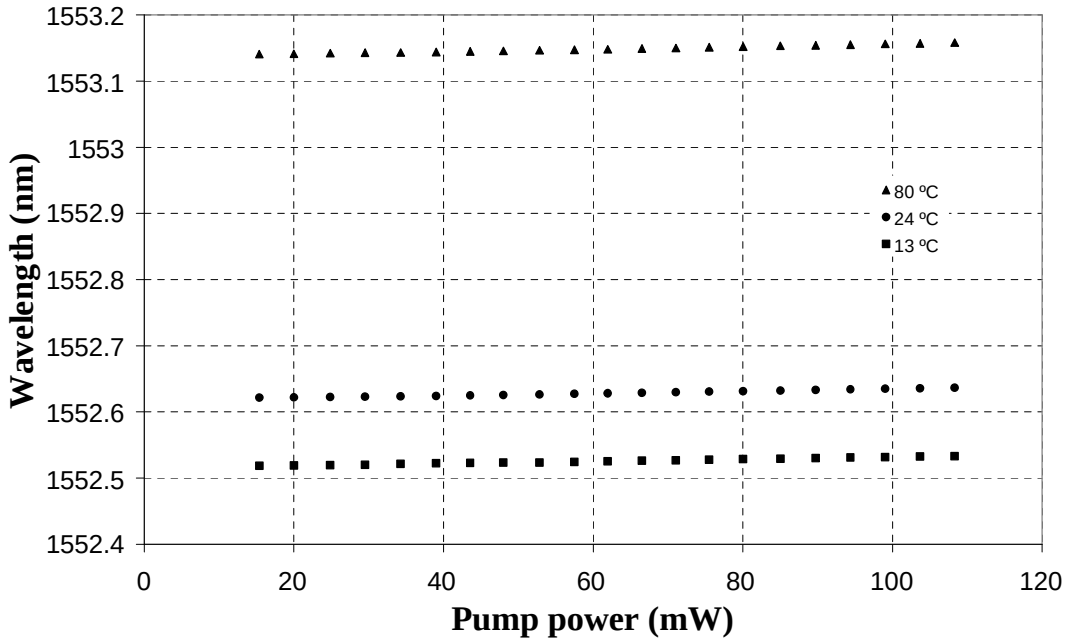

Figure 3.11: *Lasing wavelength with pump power of dual-pumping scheme for different heat sink temperatures.*

To confirm that the temperature increase in the fibre, due to the large absorbed pump, was actually below 3 ºC, the heat diffusion equations for the fibre as given in Ref. [35] were used, by Dr. P. Horak, to simulate the temperature profile in the fibre. In this numerical simulation, only the heat flow out of the sides of the fibre was considered, as the temperature gradient is larger than at the end of the fibre, i.e. heat flow is radial rather than longitudinal. Assuming that a fixed amount of heat is

deposited in the core, due to the pump, for a finite time, then heat is radiated outward so temperature rise is spread towards the sides of the fibre. Figure 3.12 shows the numerical simulation of the radial temperature profile in the fibre with 100 mW pump absorption in the core, assuming that the 125 μm fibre cladding interface is held at 20 ºC, this also showed that the resulting temperature rise in the core would be ~1ºC.

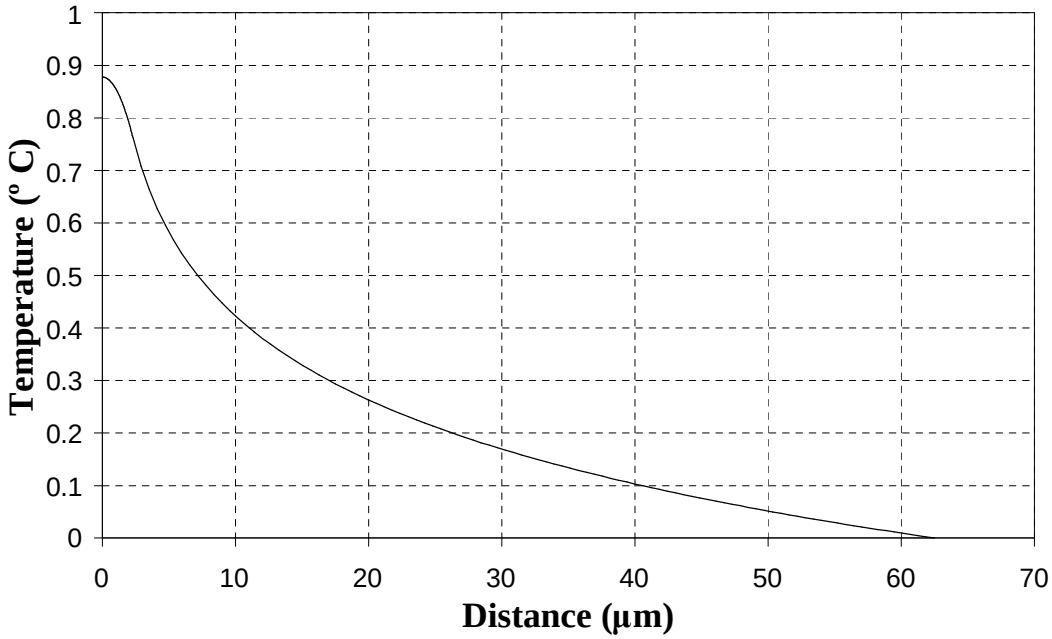

Figure 3.12: *Radial temperature profile in the fibre at 100 mW absorbed pump power.*

As the thermal contribution to optical noise in the fibre [33, 34] is generally accepted to vary as T^2 (T is the temperature in Kelvin), the 3 ºC change incurred in the fibre over the entire laser operating range would seem to be much too small to be able to account for large increases in observed linewidth, so long as the laser is properly placed in the heat sink. Nonetheless, it has been pointed out that the thermal noise contribution to the frequency stability of these fibre lasers is not necessarily negligible [36, 37]. To verify this, the linewidth of the dual pumping scheme was measured for heat sink temperatures between 10 ºC to 80 ºC. The results are shown in Figure 3.13, with just the two extreme temperatures for clarity of presentation. Indeed, for low pump powers, there is a marked broadening of the linewidth by ~50% when the temperature is increased from 13 ºC to 75 ºC, which is roughly in

line with the expected T^2 relation for thermally-induced phase noise. These observations indicate that thermally-excited index fluctuations in the fibre laser do contribute to a substantive portion of the laser phase noise, particularly at low operating powers. However, it was found that at high pump powers, the linewidth proves to be virtually insensitive to temperature over the range that we were able to investigate, indicating that another dominant factor is operating here.

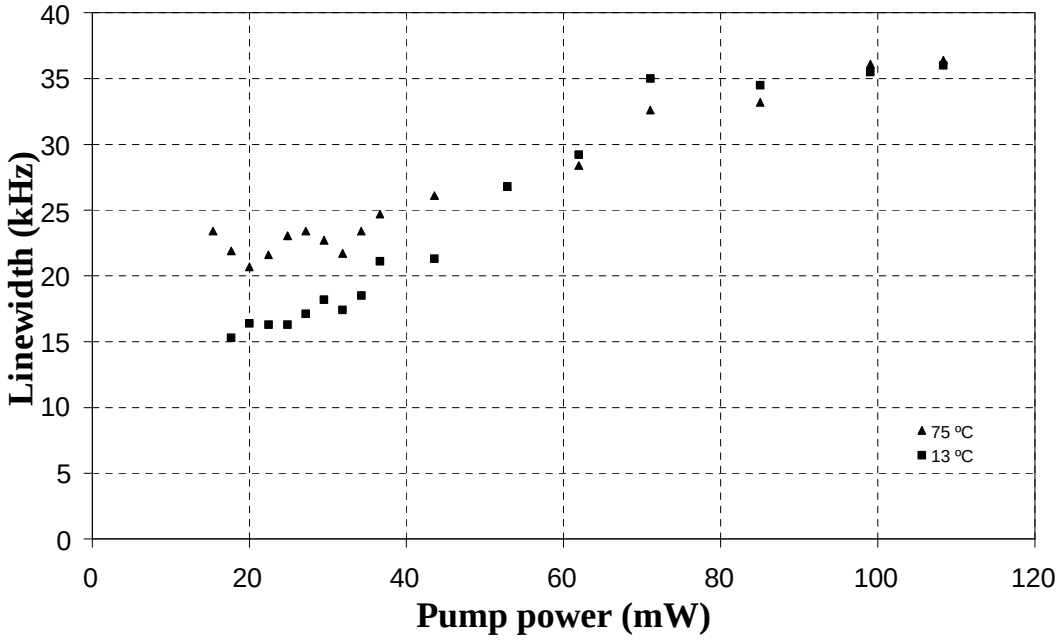

Figure 3.13: *Linewidth behaviour with pump power for two different heat sink temperatures.*

3.4.5 Relative intensity noise of the DFB laser

As indicated in [37], the laser frequency and intensity noise are to some degree correlated, due to thermal effects in the gain medium. It is therefore of interest also to investigate the intensity noise of the laser. The relative intensity noise (RIN) of the laser describes the intensity stability of the laser output. It is defined as the mean square fluctuation of the power, in unit frequency range, divided by the square of the average power. The unit of RIN is dB/Hz.

$$RIN = \left(\frac{\left\langle \Delta P^2 \right\rangle}{P_{avg}^2} \right) Hz^{-1} \quad \textbf{(3.4)}$$

where $\left\langle \Delta P^2 \right\rangle$ is the mean square optical intensity fluctuations (in W^2/Hz) in a 1-Hz bandwidth at a specified frequency, and P_{avg} is the average optical power (in W). The ratio of the optical powers squared is equivalent to the ratio of the detected electrical powers. Thus, RIN can be expressed in terms of detected electrical powers [38]. Equation (3.4) can be written as

$$RIN = \frac{P_{elec}}{P_{avg(elec)}} dB/Hz \quad \textbf{(3.5)}$$

Where P_{elec} is the power-spectral density of the photocurrent at a specified frequency, and $P_{avg(elec)}$ is the average power of the photocurrent.

The RIN of the laser was measured at the relaxation oscillation frequency (ROF), i.e. the oscillation of intensity in the cavity around their steady state values, caused when either the laser is first turned on or when the laser is suddenly perturbed by a small fluctuation in gain or cavity loss. It was performed with the lightwave signal analyser, in which the laser RIN was directly measured as a function of frequency, with the shot noise and thermal noise of the system being removed from the measurement.

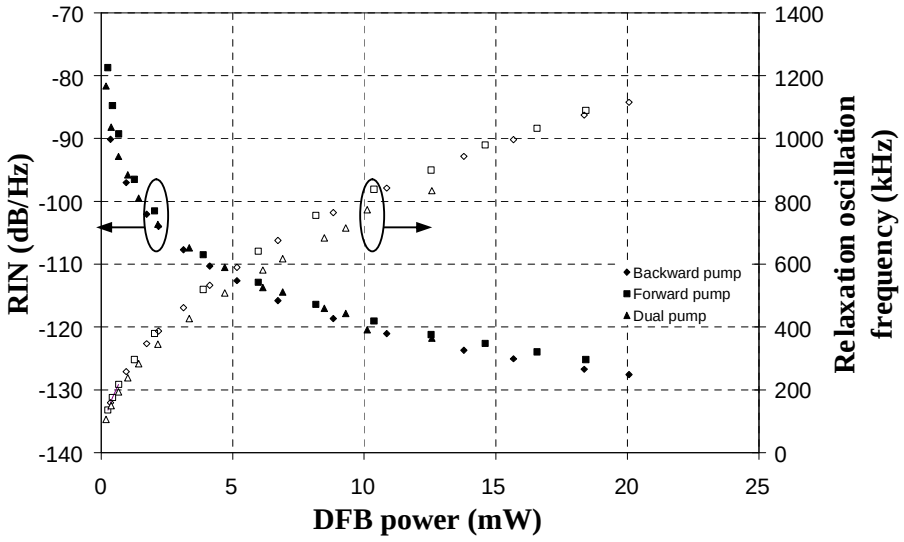

Figure 3.14: *Measured RIN at the relaxation oscillation frequency of the laser for three pumping configurations.*

Figure 3.14 shows the RIN peak at the relaxation oscillation frequency, as a function of the laser power. The ROF of the dual pumping configuration was slightly lower for the given output power, but there was no obvious difference in the RIN for the three pumping configurations. As observed, the RIN peak at 'turn on' was -80 dB/Hz at 100 kHz and this peak reduced to -127 dB/Hz at 1.1 MHz as the laser power increased to 20 mW. This was expected because as the laser began lasing, the intensity in the cavity was unstable so noise due to this fluctuation was a maximum close to the threshold and reduced with increasing output power. The ROF increased as the laser power increased and the curve followed a $\sqrt{g}$ relationship as expected, where g is the small signal gain [39]. Nevertheless, this RIN peak can be suppressed by means of electronic feedback circuits [40] and, by using a semiconductor optical amplifier, operated in the saturated gain regime [41], a noise reduction of -30 dB has been demonstrated.

The observed RIN were similar for the three pumping configurations and yet their linewidths were quite different. This indicated that the RIN and the laser frequency noise was uncorrelated for our DFB laser.

3.4.6 Self-heating effect associated with non-radiative phonon decay

The observed laser linewidth contradicted the Schawlow-Townes linewidth formula, i.e. it broadened as the power increased; self-heating from the non-radiative phonon decay could be the possible noise source. The high absorption cross section of the Yb^{3+} ion enables it to absorb the pump radiation at 980 nm efficiently and then transfer this absorbed energy to Er^{3+}, as the $^2F_{5/2}$ level of Yb^{3+} and the $^4I_{11/2}$ level of Er^{3+} are near-resonant in energy. The excited Er^{3+} ions then drop non-radiatively, by phonon decay, to the upper laser level $^4I_{13/2}$. This non-radiative relaxation process caused some of the absorbed pump power to be turned into heat and this raised the fibre temperature. As for our DFB laser pumped at 980 nm, the laser efficiency was ~20 % which indicated that some of the pump and signal power had turned into heat. Accordingly, the performance of the laser was investigated by pumping, directly into

the upper laser level $^4I_{13/2}$ of Er^{3+}, at 1480 nm to eliminate the heat generated due to the non-radiative phonon decay. The lasing threshold, output power, laser linewidth, wavelength shift with pump power, as well as RIN and relaxation oscillation of the laser, were measured.

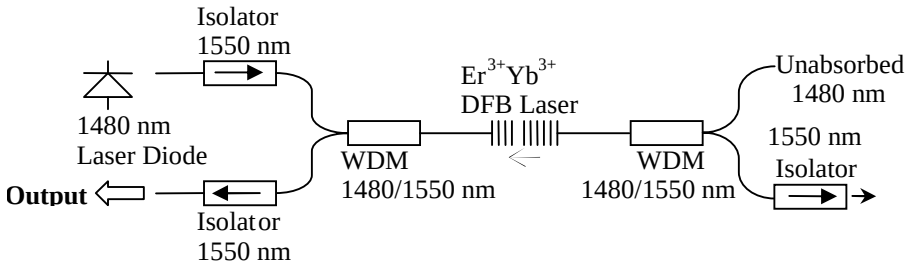

(a)

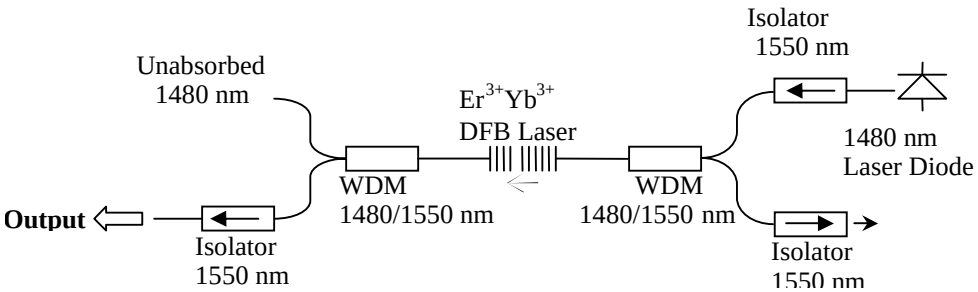

(b)

Figure 3.15: *Schematic of the laser pumping configurations pumped at 1480 nm: (a) backward and (b) forward pumping configuration.*

Figure 3.15 shows the experimental set-up of the DFB laser pumped at 1480 nm in backward and forward pumping configurations. The laser was pumped with a 130 mW, grating-stabilised, laser diode operating at 1480 nm. The pump laser was coupled into the DFB laser via a WDM through a 1550-nm optical isolator which works well at the 1480 nm pump wavelength. 1550-nm isolators were also spliced to the outputs of the laser to prevent feedback effects. The laser is placed on a temperature-controlled heat sink at 24 ºC. Only two pumping configurations, backward and forward, were set-up for this analysis. As it was found that the linewidth in both pumping configurations remained at ~ 14 kHz throughout the absorbed pump power range of ~ 30 mW, this indicated that the linewidth had

reached the thermal noise level of the laser. The same is true for the linewidth of the dual pumping configuration; it is believed to be limited by the noise floor as well.

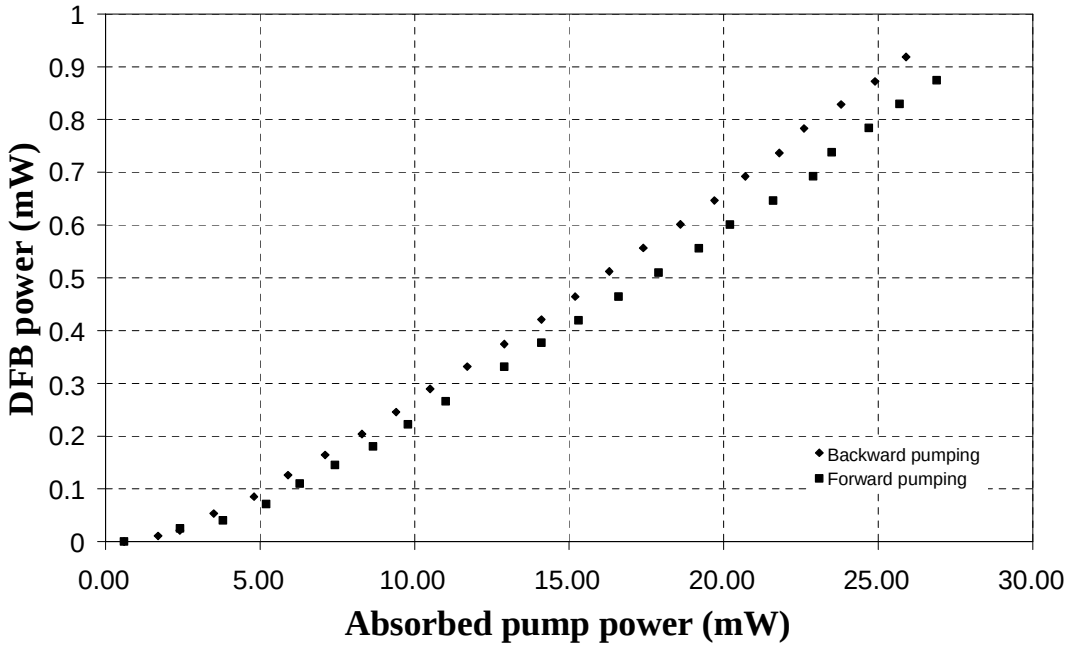

Figure 3.16: *Threshold and laser output characteristics pumped at 1480 nm.*

As observed from the measured absorption spectrum of the fibre, the absorption at 1480 nm was ~14dB/m which was very low as compared with the absorption at 977 nm. According, the unabsorbed pump powers were measured for both pumping configurations. For the backward pumping, the unabsorbed pump was measured at the end opposite to the laser output. The unabsorbed pump of the forward pumping was measured at the end co-propagating with the laser output. The unabsorbed pump powers for both pumping configurations were ~80 % of the launched pump power. The threshold and output power characteristics of the laser for both pumping configurations were measured and plotted, as shown in Figure 3.16, as a function of the absorbed pump power. Threshold values as low as ~3 mW were observed in both pumping schemes. The output power of < 1mW, at an absorbed pump power of ~27 mW, was obtained for both pumping configurations. The quantum limit of the laser pumped at 1480 nm was ~95%. However, the slope efficiencies of the backward pumping and forward pumping configurations were 3.8% and 3.6%, respectively. As observed, the efficiency for 977 nm pumping is higher than for the 1480 nm

pumping, which is because of the higher small signal gain. It was ~6 times more efficient than pumping at 1480 nm. A laser efficiency of less than 1% was observed in [14, 37] for 1480 nm pumping.

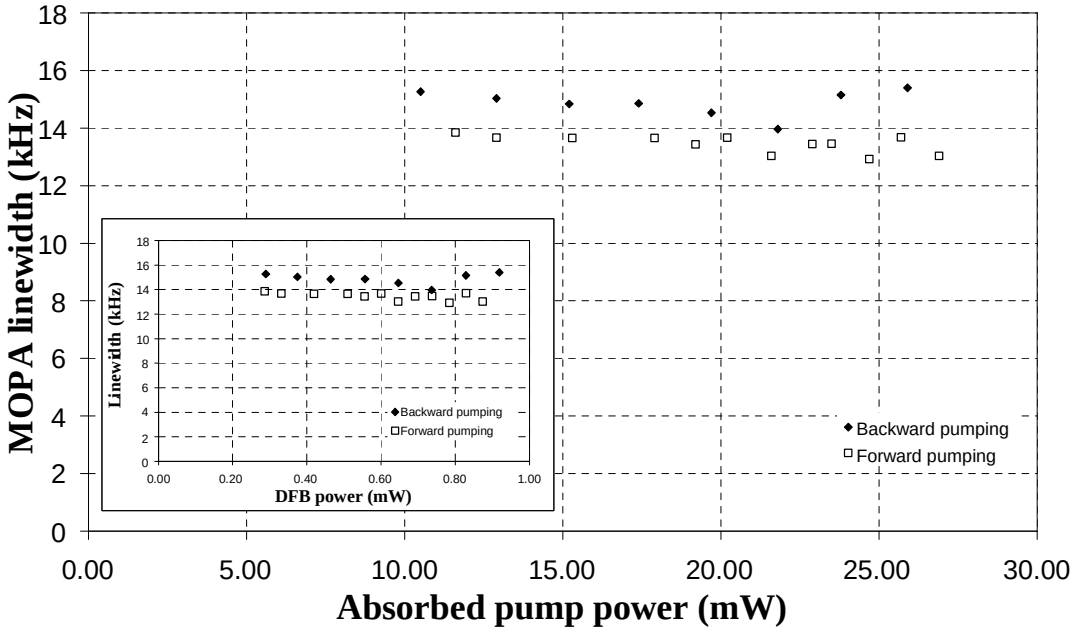

Figure 3.17: *3-dB laser linewidth as a function of absorbed pump power at 1480 nm pump wavelength.*

The 3-dB laser linewidth was measured using the same delayed self-heterodyne setup as before. The laser linewidth behaviour, as a function of the absorbed pump power, was plotted in Figure 3.17. The inset in the figure shows the laser linewidth versus output power. The linewidth of the backward pumping configuration was between 14 kHz and 15.5 kHz. As for the forward pumping configuration, a linewidth of 13-14 kHz was observed. Their linewidth can be considered to be the same, as the resolution of the delayed self-heterodyne setup was ~3.5 kHz. Both pumping configurations have shown a decrease in linewidth as compared with pumping at 977 nm. When the laser was pumped at 977 nm, the linewidth of the backward pumping configuration, in the regime of ~1 mW output power, was ~ 30 kHz. While for the forward pumping configuration, a linewidth of ~20 kHz was observed for the same output power. Hence, this showed that the non-radiative decay has some effect on the laser linewidth. The linewidths of both configurations have decreased to ~ 14 kHz

and remained quite constant at this value. This could suggest that the laser linewidth has reached the thermal noise level which depends on the material properties of silica, the temperature, and the optical mode volume [34]. Pumping at 1480 nm has shown a decrease in the laser linewidth but the laser power was too low, i.e. in the μW regime. Nevertheless, the laser power can be boosted by using a MOPA configuration. In the next chapter, we show how the linewidth limitation of this laser can be improved by operating the laser at a narrower linewidth and subsequently the laser was configured in the MOPA for high power.

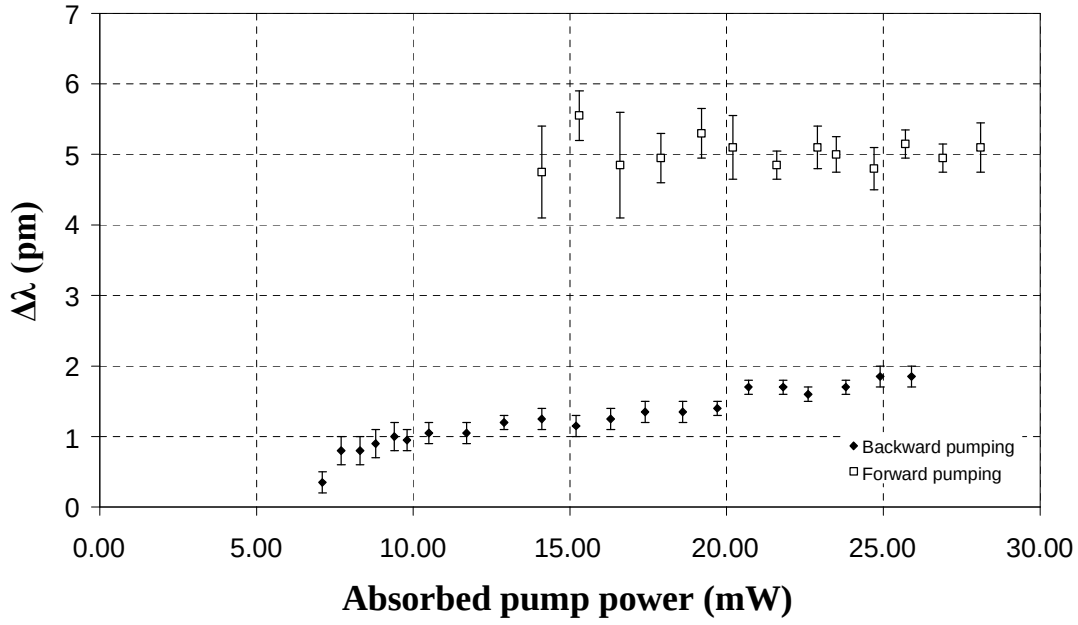

Figure 3.18: *Laser wavelength shift with the absorbed pump power.*

As observed, the linewidth became narrower at the 1480 nm pump wavelength so it is interesting to investigate the thermal effects due to absorbed pump power. Consequently, the lasing wavelength of the fibre laser was measured with the wavemeter. Figure 3.18 shows the change in the lasing wavelength as a function of absorbed pump power for the backward- and forward-pumping scheme. The backward pumping scheme shows that the lasing wavelength increased by ~1.5 pm for ~27 mW absorbed pump power. This indicates a temperature increase of ~0.2 ºC in the fibre due to absorbed pump. There was no clear increase in the lasing wavelength of the forward pumping configuration over the absorbed pump power

range. But, the wavelength was noted to vary by ~0.8 pm, this indicates a temperature variation of ~ 0.1 ºC. The temperature rise in the fibre, due to the absorbed pump power, was ~0.003 ºC/mW. This indicates that the temperature rise in the fibre was 10 times lower than when pumped at 977 nm. This suggests that the fibre heating was mainly due to the non-radiative decay.

The RIN of the laser, for both pumping configurations, was also investigated. The RIN measurement was performed with the lightwave signal analyser. Figure 3.19 shows the RIN peak at the ROF of the laser as a function of DFB power. Both pumping configurations showed a similar ROF at the given DFB power. Similar RIN peak values from ~-58 dB/Hz to ~-90 dB/Hz were observed in the output power ranges of 0.15 to 0.9 mW. The RIN of the laser at this pump wavelength was higher than for the 977 nm pumping wavelength for the given DFB power.

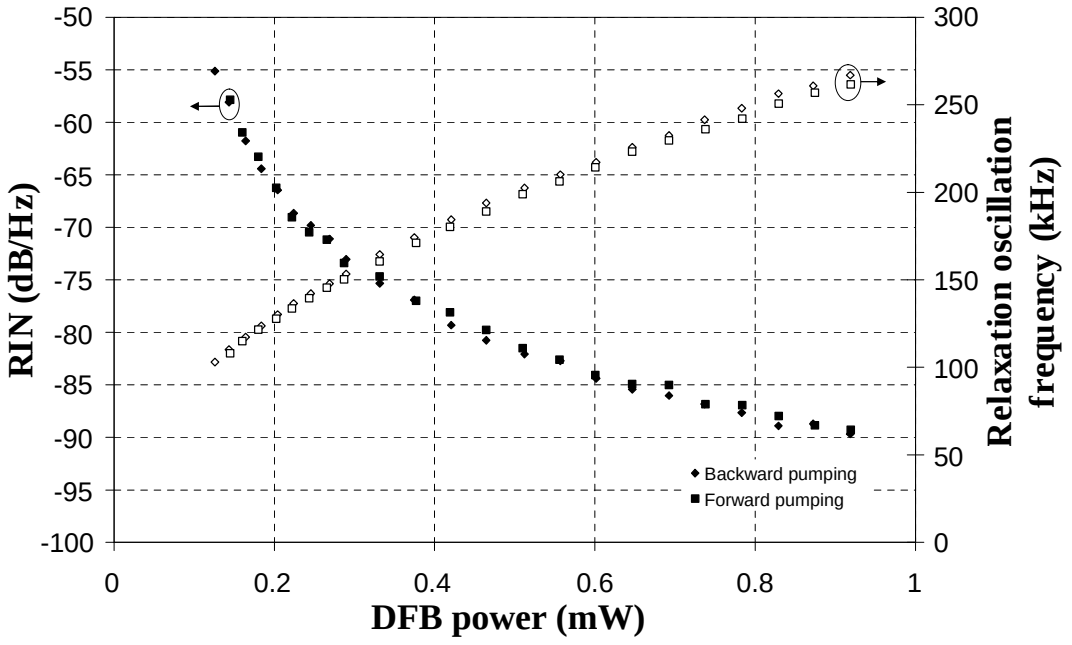

Figure 3.19: *Measured RIN and ROF of the laser in the backward and forward pumping configurations.*

The possible noise source(s) that could cause the anomalous laser linewidth has just been investigated through the possibility of thermal effects in the fibre due to the high pump absorption and the non-radiative phonon decay from the metastable level

to the upper laser level. The fibre temperature rise of 3 ºC in the fibre core was too small to explain the broadening of laser linewidth due to fundamental thermal fluctuations. We observed a thermal noise floor of 15 kHz when the heating due to non-radiative phonon decay was eliminated. Nevertheless, the main cause of laser linewidth broadening, identified by Dr P. Horak, was actually due to the temperature fluctuation induced by the pump noise. The details of this are explained in the following section.

3.5 The main cause of excess noise

This section describes an analytical model used to explain the mechanisms giving rise to the laser linewidth, for the three pumping configurations, and the experimental verification of some of the parameters in the model. Overall, we find good agreement between the analytical model and the observed linewidth of the laser, as reported in [9, 10]. The understanding of these mechanisms allowed optimization of the design of the laser, in order to minimise the linewidth broadening, as has been proposed.

3.5.1 Analytical model of the laser linewidth

The analytical model was developed based on a potential noise source due to dissipated pump power which resulted in heating of the fibre laser [35]. Accordingly, the lasing wavelength of the three pumping schemes was measured and the results are plotted in Figure 3.20(a) as a function of the pump power. The wavelength shift for the three pump configurations was quite different, particularly as the curvature of the backward- and dual- pump configurations results were in opposite directions. The curves in the figure imply that the low-frequency intensity noise of the pump laser leads to fibre temperature fluctuations, which in turn leads to refractive index fluctuation and, thus, to laser frequency jitter. From a close examination of the data, the change of wavelength with pump power is seen to depend on both the power level and the pump configuration. This becomes more readily evident by plotting the slope $d\lambda_{DFB}/dP$ in Figure 3.20(b), obtained by a third-order polynomial fit to the data

points in (a). The backward pumping configuration clearly has the largest wavelength sensitivity to pump power compared to the other pumping configurations, particularly for the low pump power.

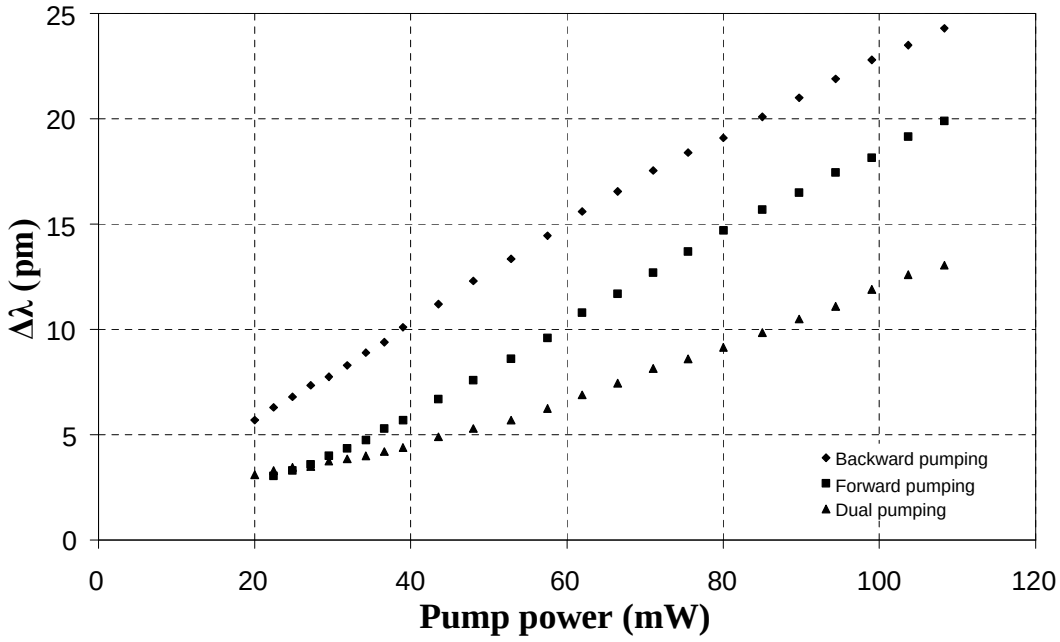

(a)

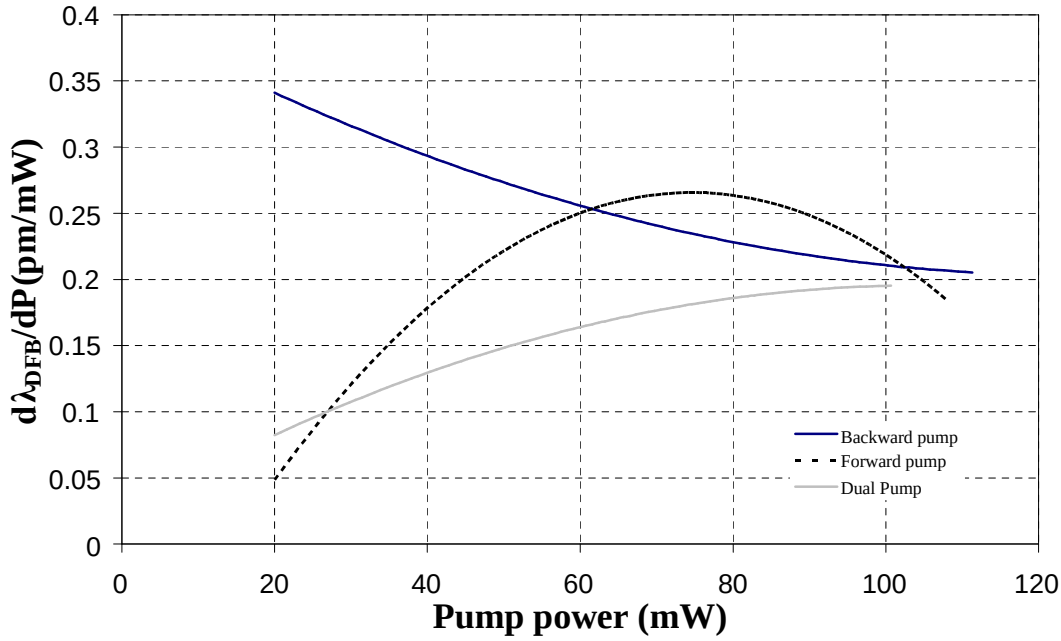

(b)

Figure 3.20: *(a) DFB Laser wavelength λ_{DFB} (b) its derivative of the DFB laser wavelength $d\lambda_{DFB}/dP$ versus pump power for the different pump configurations.*

Hence, Dr P. Horak predicted that the instantaneous laser frequency jitter $\Delta f(t)$ is related to slow pump power fluctuations $\Delta P(t)$ by

$$\Delta f(t) = \frac{c}{\lambda_{DFB}^2}\frac{d\lambda_{DFB}}{dP}\Delta P(t), \tag{3.6}$$

where λ_{DFB} is the laser wavelength, P is the pump power, and ΔP is the rms amplitude of the pump fluctuations. Consequently, the laser frequency spectrum $S_F(f)$ can be expressed in terms of the relative intensity noise, $RIN(f)$, of the pump laser

$$S_F(f) = 2\left(\frac{c}{\lambda_{DFB}^2}\frac{d\lambda_{DFB}}{dP}\right)^2 P^2 RIN(f)T(f)^2. \tag{3.7}$$

The function $T(f)$ represents the frequency response of the DFB laser to pump fluctuations. Because of the large pump absorption, ~99 % of the pump power being absorbed (due to the high concentration of the Yb^{3+}), heat is generated in the DFB laser. This leads to the consideration of the frequency-dependent response of the rare-earth ions as well as the finite response time of the fibre to be the dominating factors. The measurements for the RIN of the pump laser and the filter function $T(f)$ are found in the followings sections.

The contribution of $S_F(f)$ to the laser spectrum, as measured by a self-heterodyne technique, is given rigorously by [32],

$$S(f) = F\left\{\exp\left[-4\int_0^\infty S_F(f)\frac{\sin^2(\pi f\tau)}{f^2}(1-\cos(2\pi f\tau_d))df\right]\right\} \tag{3.8}$$

where F denotes the Fourier transform. For the measured values of $d\lambda_{DFB}/dP$ and RIN, Equation (3.8) is solved to a good approximation for a Gaussian laser lineshape with full-width at half-maximum,

$$\Delta f \approx \left[8\log(2)\int_0^\infty S_F(f)\sin^2(\pi f\tau_d)df\right]^{1/2}. \tag{3.9}$$

Substituting Equation (3.7) into (3.9), the expression for the linewidth in terms of measured quantities was given as

$$\Delta f = \frac{c}{\lambda_{DFB}^2}\frac{d\lambda_{DFB}}{dP}P\sqrt{RIN}\left[16\log(2)\int_0^\infty T(f)^2\sin^2(\pi f\tau_d)df\right]^{1/2}. \tag{3.10}$$

3.5.2 Pump laser RIN measurement

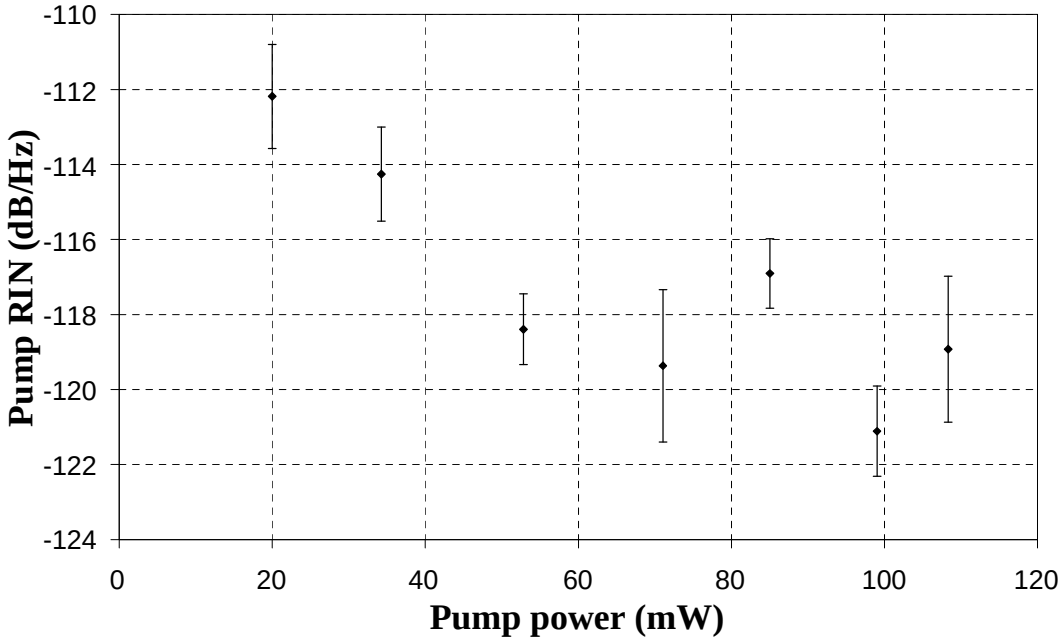

Figure 3.21: *Relative pump intensity noise (RIN) as a function of pump power.*

The RIN of the pump laser was measured with an external detector, as the built-in detector of the lightwave signal analyser is insensitive to the pump wavelength, and then the RIN was calculated using Equation (3.5). The output of the pump laser via the 980 nm isolator was connected to a 1 GHz, New Focus model 1611, detector which consisted of an InGaAs PIN photodetector followed by a transimpedance amplifier. The detector has a DC and AC output port. The DC output of the detector was connected to an oscilloscope for measuring the average voltage, $V_{avg(elec)}$, and the average power of the electrical signal was calculated using $P_{elec} = (0.07V_{avg(elec)})^2/R$. A scaling factor of 0.07 is included in the $V_{avg(elec)}$ for the compensation of the DC and AC transimpedance gain conversion. The AC output of the detector was connected to the lightwave signal analyser to measure the intensity fluctuations, P_{elec}, of the pump laser in a bandwidth of 750 Hz. The intensity fluctuations measured in dBm were then converted into W/Hz using $(10^{dBm/10})/750$. Due to the limitation of the analyser that prevented us from measuring the noise at the relevant lower frequency, the pump RIN was measured over the frequency range of 200 kHz to 1 MHz and was found to be approximately flat in this region, and hence, it can be

assumed to be frequency-independent below 1 MHz. The results are shown in Figure 3.21. The pump RIN was slightly decreased as a function of power from -112 dB/Hz at 20 mW to -119 dB/Hz at 110 mW.

3.5.3 Filter function of the DFB laser measurement

To observe the frequency response of the DFB laser to pump power fluctuation, *T(f)*, experimentally, the spectral broadening of the DFB fibre laser under periodic pump power modulation, using the same delayed self-heterodyne set-up as before, was measured. The pump laser was externally modulated with a sinusoidal wave at a fixed amplitude of ~120 mV, corresponding to ~ 3 mW of power fluctuation, over a frequency range of 200 Hz - 2 MHz. Then, the linewidth of backward and dual pumping configurations, at pump powers of 33 mW and 100 mW, were measured. The measured linewidth broadening per milliwatt pump fluctuation was plotted, for a better observation of the T (*f*), as shown in Figure 3.22. It can be seen that a slowly varying envelope function $\Delta f_{mod}(f)$ appears, modified by the sinusoidal response of the interferometer. In fact, Figure 3.22(a) shows the dependence on the laser configuration and pump power in line with Figure 3.20(b), i.e. Δf_{mod} is proportional to *T(f)*, where the proportionality factor is obtained from the low frequency jitter response in Equation (3.6). The periodic nature of the curves on Figure 3.22(b) is due to the interference of the two combining beams and the period is depending on the length of the delay line [25].

To confirm that the envelope function is independent of the measurement, i.e. that is not an artifact of the interferometer response, the delay line in the self-heterodyne set-up was varied. The delay line of 42 km was used to measure the linewidth of the backward pumping configuration at 100 mW pump power. And yet, it still followed the same envelope function as the 60 km delay line, with a change in the periodic function, as shown in Figure 3.22 (b). Hence, it was confirmed that the function was caused totally by the laser dynamics.

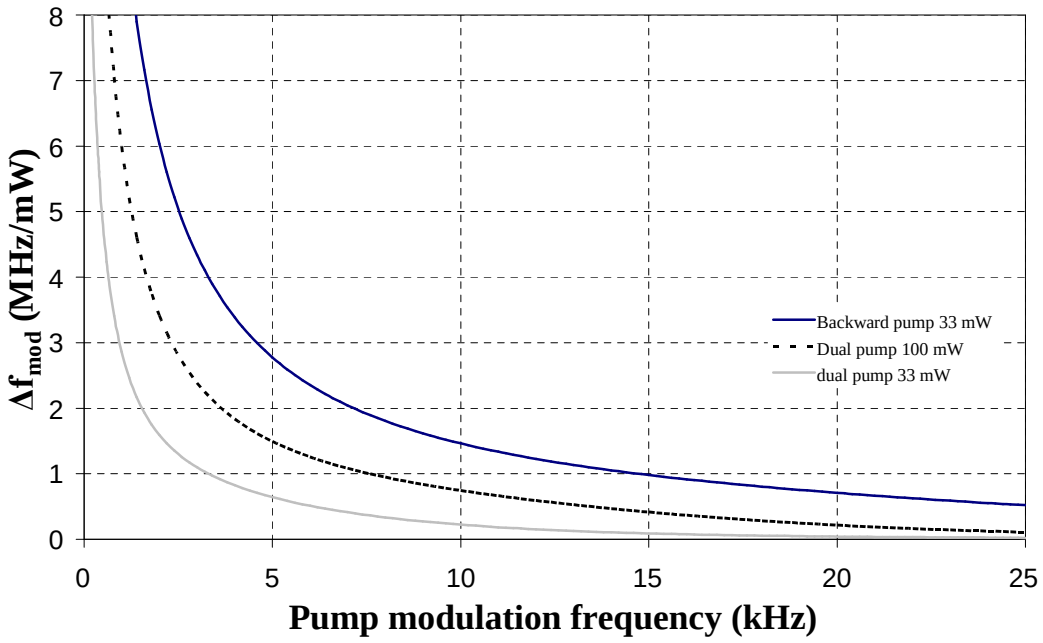

(a)

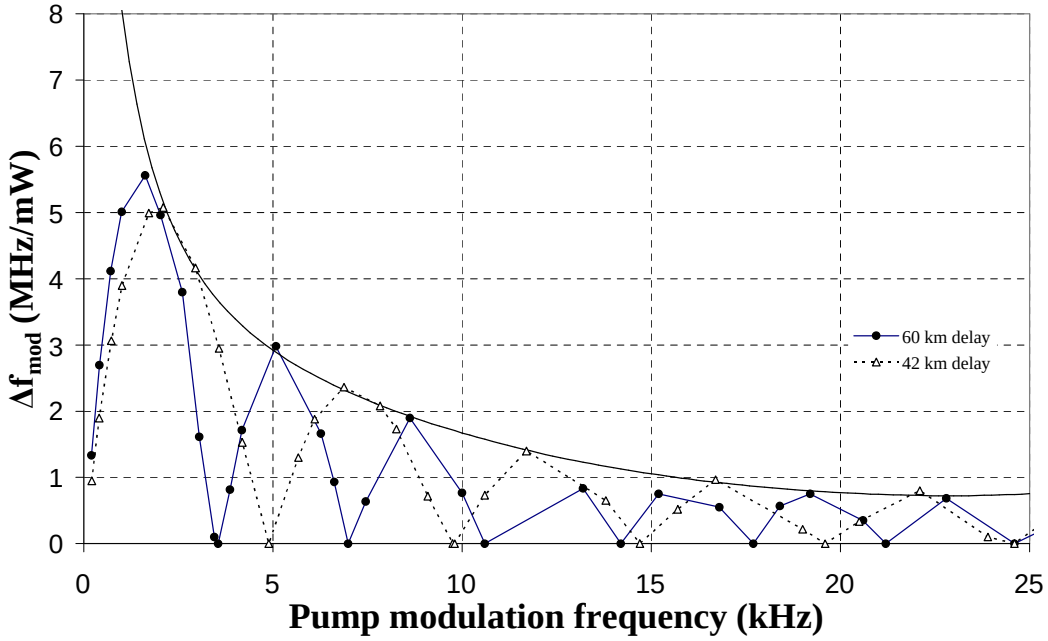

(b)

Figure 3.22: *Spectral broadening Δf_{mod} versus pump modulation frequency (a) dependant on the laser configuration and pump power (b) showing independence on the length of the delay line for the backward pump at 100 mW.*

3.5.4 Model calculation of the laser linewidth

The contribution of pump-noise induced thermal fluctuations to the DFB laser linewidth for the different pumping configurations was calculated using Equation (3.10). The calculated linewidth, plotted as a function of pump power, is shown in Figure 3.23. These curves agree qualitatively with the behaviour of the experimentally observed linewidth as in Figure 3.8. The remaining difference between the model calculations and the experimental results can be explained by other noise sources, in particular a linewidth floor due to the fundamental thermal noise [33, 34] of ~15 kHz as observed in Figure 3.13. Note also that the theoretical expression for fundamental temperature fluctuations [42]

$$\Delta T^2 = \frac{k_B T^2}{\rho c_v V} \qquad \textbf{(3.11)}$$

where ρ is the density (2.2 x 10^3 kg/m^3), c_v is the specific heat capacity of silica (741 J/kg/K), V is the effective mode volume (17.34 x 10^{-12} m^3), k_B is the Boltzmann constant (1.38 x 10^{-23} m^2kgs^{-2} K^{-1}), predicts a linewidth of 9 kHz which agrees quite well with our value of 15 kHz.

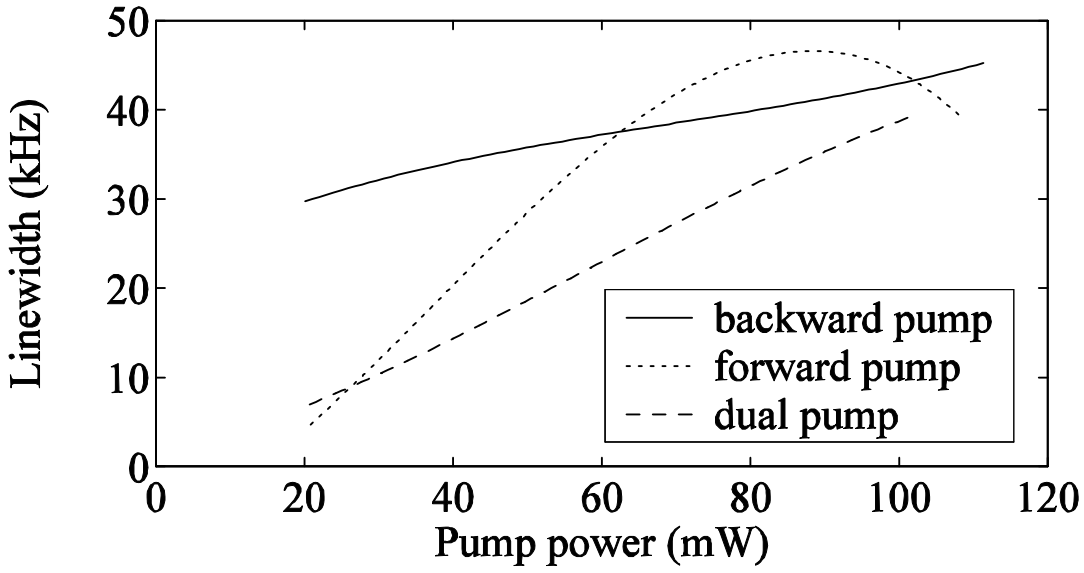

Figure 3.23: *Contribution of pump-noise-induced temperature fluctuations to the DFB laser linewidth for the different pump configurations.*

A previous analysis of pump intensity noise as a potential source of linewidth broadening in single-frequency fibre lasers [30] primarily considered its effect through the laser gain, which led to a negligible impact. Thermal fluctuations due to pump noise were also dismissed as a significant noise source in [37].

3.5.5 Validation of the model

For a rough check on the validation of the analytical model, the change of the DFB laser wavelength due to the pump power fluctuation $(\partial\lambda_{DFB}/\partial P)$, one of the parameters that contributed to the laser linewidth, was measured. A diode laser operating at 975 nm was used to pump the DFB laser and the laser wavelength of the DFB was measured in the three pumping configurations. The threshold and output characteristics of the laser were also measured and plotted in Figure 3.24.

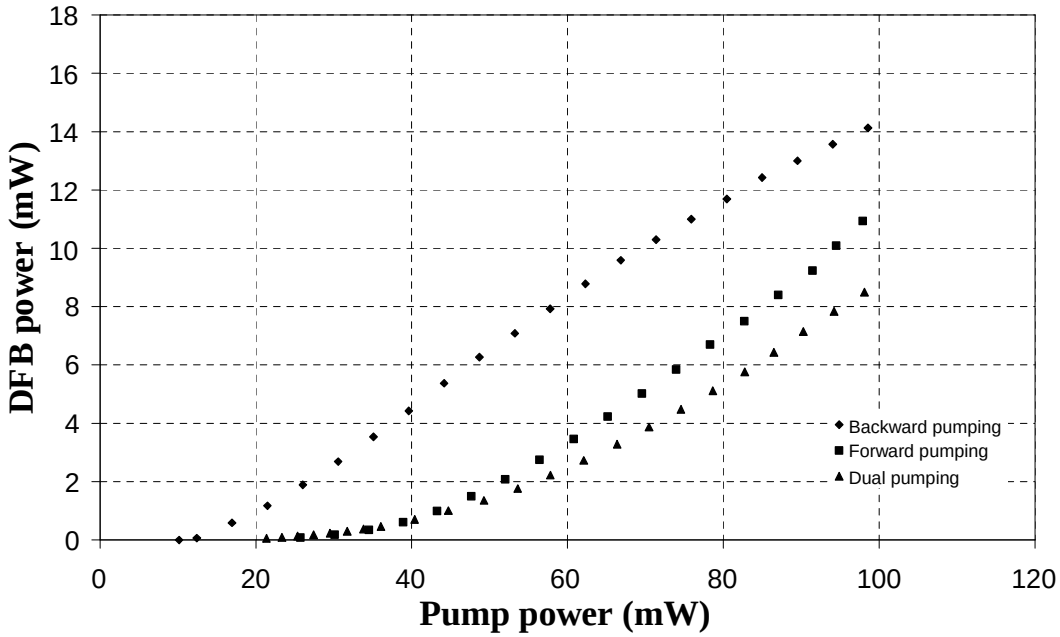

Figure 3.24: *Threshold and output characteristics of the laser for the three pumping configuration pumped at 975 nm.*

The same characteristics resulted as were observed with the 977 nm pump wavelength. The backward pump has the lowest threshold and the highest laser

efficiency as compared with the other two pumping schemes. This can be explained, as for the 977 nm pump wavelength, as being associated with the asymmetry of the grating design and the different pump absorption within the grating for different pumping configurations. The output power of the laser was slightly lower as compared with the 977 nm pump wavelength for the given pump power. The total efficiencies of the laser in the backward, forward and dual pumping configurations were 16 %, 15 % and 11 %, respectively. The efficiency is slightly lower than for the 977 nm pumping wavelength owing to a slightly higher absorption loss (0.85 dB/cm), so the threshold of the laser is increased and hence, a decrease in the laser efficiency will result.

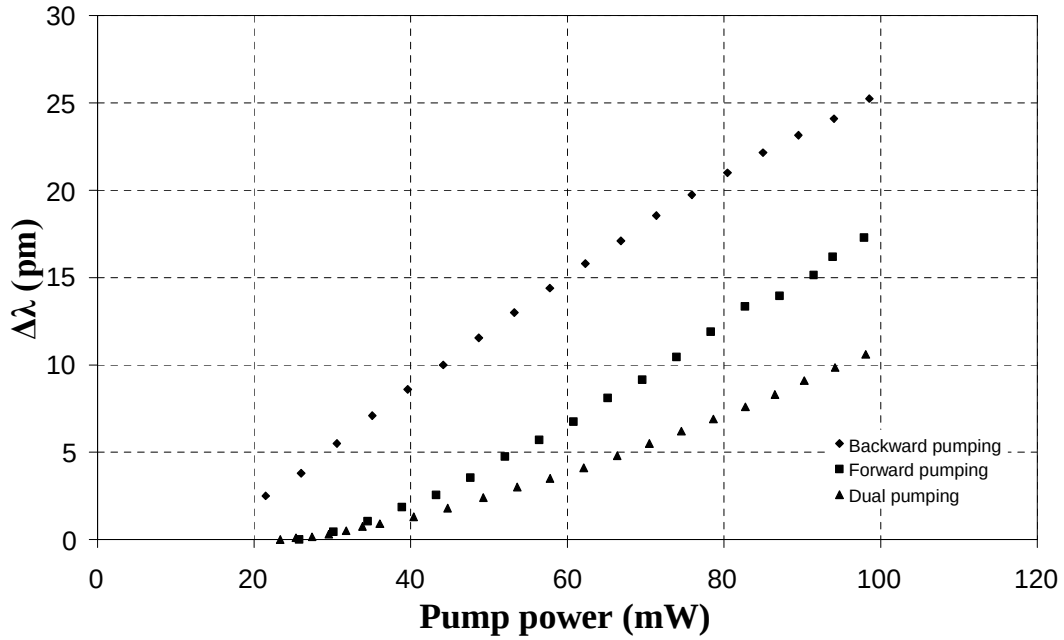

Figure 3.25: *Laser wavelength shift as a function of pump power.*

The DFB laser wavelength was measured and the laser wavelength shift, as a function of pump power, is plotted in Figure 3.25 for the three pump schemes. It is clearly shown that the backward pump has the largest laser wavelength shift, i.e. ~25 pm for ~100 mW pump power. The laser wavelength shifts, for the forward and dual pump schemes, were ~17 pm and ~11 pm, respectively. This laser wavelength shift was slightly higher than that when pumped with the 977 nm diode laser for the given pump power. Therefore, an increase in the laser linewidth would be expected.

Accordingly, the 3-dB laser linewidth of the laser, measured with the delayed self-heterodyne setup, is shown in Figure 3.26. The trendlines shown are simply a guide for viewing. The laser linewidth of the forward pumping configuration was the largest, i.e. 43 kHz – 68 kHz. The dual pumping configuration had the smallest linewidth at pump powers below 90 mW, from 26 kHz – 40 kHz, and these increased to 45 kHz at 100 mW pump power. The backward pumping scheme had a linewidth of ~ 40 kHz up to pump power of ~80 mW and then this decreased, at higher pump powers, to 35 kHz.

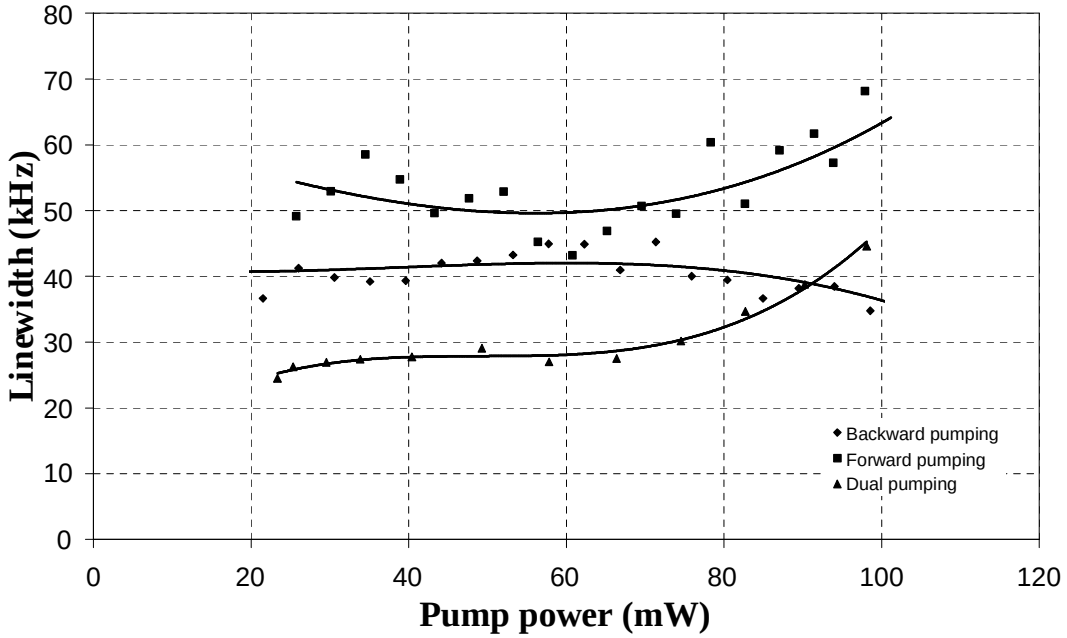

Figure 3.26: *Laser linewidth as a function of pump power.*

From the measured linewidth of the three different pump schemes, the results showed that the linewidths were constant at pump powers below 60 mW. These behaviours were different from those observed with the 977 nm pump diode. The reason for this was unclear. However, at high pump powers the linewidth behaviours were similar for both pump diodes. This may suggest that the RIN of the pump laser becomes dominant at high pump power. The linewidth of the backward pumping scheme was decreased at high pump power. For the forward- and dual- pumping configurations, its linewidths were increased as pump power increased. The increase in the $\partial\lambda/\partial P$, between 60 to 100 mW pump power, was ~26%, ~30% and ~24% as

compared with the 977 nm diode laser for the backward-, forward- and dual-pumping schemes, respectively. We observed a linewidth increase of 19%, 31% and 7% for the backward-, forward- and dual- pumping schemes, respectively.

Then, the RIN of the laser was also investigated. The results are shown in Figure 3.27. The ROF was higher for the backward and forward pump, and lower for the dual pump scheme as compared to the results for the 977 nm pump wavelength. This might be due to the spontaneous emission, during the laser operation being different. However, the RIN peak at the 975 nm pump wavelength was about the same as for the 977 nm pump.

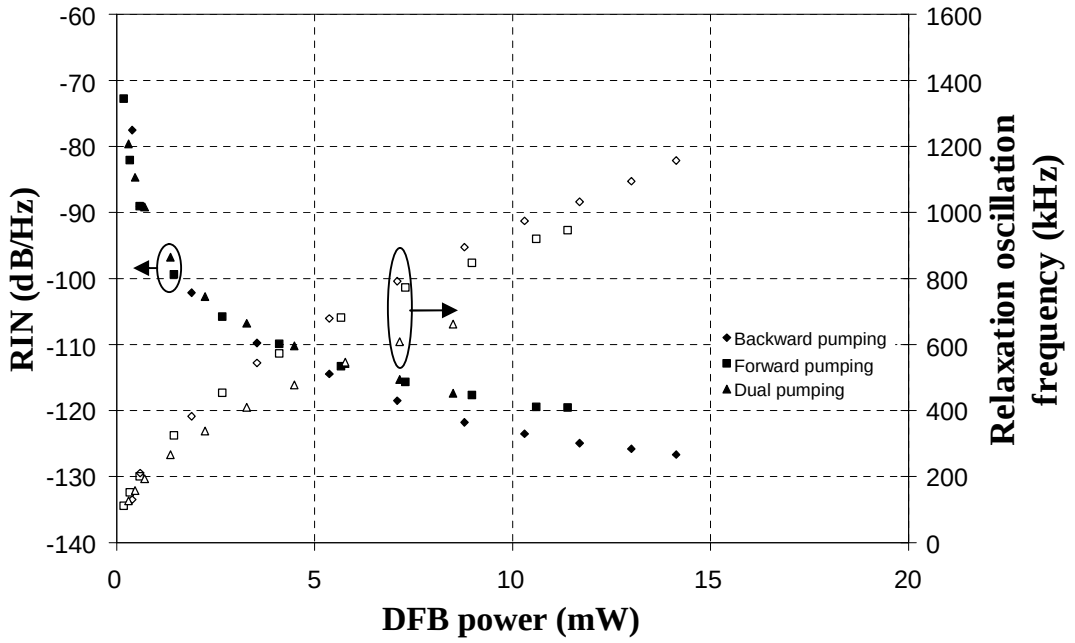

Figure 3.27: *RIN measured at the peak relaxation oscillation of the laser.*

3.6 Possibilities of reducing linewidth broadening

As observed, linewidth broadening of the DFB laser was due to the temperature fluctuation caused by the pump intensity noise. Therefore, one obvious solution is to use a very low noise pump. This may not be the most cost-effective solution. Another possibility is to use a material with a temperature-insensitive refractive

index ($dn/dT \approx 0$), e.g., through specially tailored phosphate glasses [43, 44]. This has the added advantage of reducing both pump-fluctuation-induced linewidth broadening and fundamental thermal noise.

Varying the length of the grating while keeping the grating strength constant modifies the fundamental thermal noise, which causes the associated linewidth floor to scale as $\Delta f \propto 1/\sqrt{L_{eff}}$, cf. Eq (3.11). On the other hand, assuming that the same fraction of the pump power is converted into heat within the entire grating, the pump-induced broadening is expected to scale as $\Delta f \propto 1/L_{eff}$. Similarly, the fibre core radius can be enlarged to increase the mode volume and thereby decrease the thermal effects.

Another approach to reduce the linewidth deterioration by pump noise is to use the DFB laser in the low power regime in a master oscillator power amplifier (MOPA) configuration.

3.7 Conclusion

This chapter described the experimental and theoretical linewidth characteristics of the 5 cm long Er^{3+}-Yb^{3+} doped fibre DFB laser operating in the region of 1.5 μm.

The experimental data were presented which highlight the anomalous linewidth behaviour of the single-frequency fibre lasers. It is shown that the linewidth deviates drastically from the Schawlow-Townes linewidth formula by increasing with pump and laser power, even when the laser was mounted on a temperature-controlled heat sink. For the same laser cavity, the choice of pumping configuration is also found to have a considerable bearing, not just on the threshold and laser efficiency, but also on the linewidths achievable. Although the cause was not yet fully understood at this point, the results on the anomalous linewidth behaviour strongly suggested that the design aimed at maximizing the laser efficiency and output power may well impact on its phase noise properties in unexpected and undesired ways.

A detailed analysis of the laser linewidth revealed that two noise sources are mainly responsible for limiting the linewidth. (i) At low pump power levels, a constant noise floor due to fundamental thermal noise limits the minimum achievable linewidth to ~15 kHz for our DFB design. This value is still many order of magnitude larger than the Schawlaw-Townes linewidth prediction and is due to the small mode volume. (ii) At higher pump powers, the main cause of the excess noise is due to the temperature fluctuations induced by pump intensity noise. This pump fluctuation effect is large due to high pump absorption over a small mode volume and is configuration dependent. A validation of the model was conducted with a 975 nm diode laser and good agreement was observed. Then, it followed by several discussions how to attempt to overcome these linewidth limitations of fibre lasers.

3.8 References

[1] G. A. Ball, W. W. Morey, and W. H. Glenn, "Standing-wave monomode erbium fiber laser," *IEEE Photonics Technology Letters*, vol. 3, pp. 613-615, 1991.

[2] J. T. Kringlebotn, J.-L. Archambault, L. Reekie, J. E. Townsend, G. G. Vienne, and D. N. Payne, "Highly-efficient, low-noise grating-feedback Er^{3+}:Yb^{3+} codoped fibre laser," *Electronics Letters*, vol. 30, pp. 972-973, 1994.

[3] V. C. Lauridsen, J. H. Povlsen, and P. Varming, "Optimising erbium-doped DFB fibre laser length with respect to maximum output power," *Electronics Letters*, vol. 35, pp. 300-302, 1999.

[4] W. H. Loh, B. N. Samson, L. Dong, G. J. Cowle, and K. Hsu, "High performance single frequency fiber grating-based erbium/ytterbium-codoped fiber lasers," *Journal of Lightwave Technology*, vol. 16, pp. 114-118, 1998.

[5] K. Yelen, L. M. B. Hickey, and M. N. Zervas, "A new design approach for fiber DFB lasers with improved efficiency," *IEEE Journal of Quantum Electronics*, vol. 40, pp. 711-720, 2004.

[6] G. A. Ball, C. G. Hull-Allen, and J. Livas, "Frequency noise of a Bragg grating fibre laser," *Electronics Letters*, vol. 30, pp. 1229-1230, 1994.

[7] N. Y. Voo, P. Horak, M. Ibsen, and W. H. Loh, "Linewidth and phase noise characteristics of DFB fibre lasers," in *SPIE European Symposium on Optics and Photonics in Security and Defence*, vol. 5620. London, 2004, pp. 179-186.

[8] N. Y. Voo, P. Horak, M. Ibsen, and W. H. Loh, "Anomalous linewidth behavior in short-cavity single-frequency fiber lasers," *IEEE Photonics Technology Letters*, vol. 17, pp. 546-548, 2005.

[9] P. Horak, N.Y. Voo, M. Ibsen, and W. H. Loh, "Dominant cause of linewidth in DFB Fiber lasers," in *CLEO/QELS 2005*. Baltimore, USA, 2005, pp. 1566-1568.

[10] P. Horak, N. Y. Voo, M. Ibsen, and W. H. Loh, "Pump-noise induced linewidth contributions in distributed feedback fiber lasers," *IEEE Photonics Technology Letters*, vol. 18, pp. 998-1000, 2006.

[11] J. L. Zyskind, V. Mizrahi, D. J. DiGiovanni, and J. W. Sulhoff, "Short single frequency erbium-doped fibre laser," *Electronics Letters*, vol. 28, pp. 1385-1387, 1992.

[12] W. H. Loh and R. I. Laming, "1.55 μm phase-shifted distributed feedback fibre laser," *Electronics Letters*, vol. 31, pp. 1440-1442, 1995.

[13] W. H. Loh, S. D. Butterworth, and W. A. Clarkson, "Efficient distributed feedback erbium-doped germanosilicate fibre laser pumped in 520 nm band," *Electronics Letters*, vol. 32, pp. 2088-2089, 1996.

[14] M. Sejka, P. Varming, J. Hubner, and M. Kristensen, "Distributed feedback Er^{3+}-doped fibre laser," *Electronics Letters*, vol. 31, pp. 1445-1446, 1995.

[15] J. J. Pan and Y. Shi, "166-mW single-frequency output power interactive fiber lasers with low noise," *IEEE Photonics Technology Letters*, vol. 11, pp. 36-38, 1999.

[16] W. H. Loh, L. Dong, and J. E. Caplen, "Single-sided output Sn/Er/Yb distributed feedback fiber laser," *Applied Physics Letters*, vol. 69, pp. 2151-2153, 1996.

[17] C. Spiegelberg, J. Geng, Y. Hu, Y. Kaneda, S. Jiang, and N. Peyghambarian, "Low-noise narrow-linewidth fiber laser at 1550 nm (June 2003)," *Journal of Lightwave Technology*, vol. 22, pp. 57-62, 2004.

[18] J. T. Kringlebotn, P. R. Morkel, L. Reekie, J.-L. Archambault, and D. N. Payne, "Efficient diode-pumped single-frequency erbium:ytterbium fiber laser," *IEEE Photonics Technology Letters*, vol. 5, pp. 1162-1164, 1993.

[19] L. Dong, W. H. Loh, J. E. Caplen, J. D. Minelly, K. Hsu, and L. Reekie, "Efficient single-frequency fiber lasers with novel photosensitive ErYb optical fibers," *Optics Letters*, vol. 22, pp. 694-696, 1997.

[20] E. Ronnekleiv, O. Hadeler, and G. Vienne, "Stability of an Er-Yb-doped fiber distributed-feedback laser with external reflections," *Optics Letters*, vol. 24, pp. 617-619, 1999.

[21] K.O. Hill, B. Malo, F. Bilodeau, D.C. Johnson, and J. Albert, "Bragg gratings fabricated in monomode photosensitive optical fiber by UV exposure through a phase mask," *Applied Physics Letters*, vol. 62, pp. 1035-1037, 1993.

[22] V. C. Lauridsen, J. H. Povlsen, and P. Varming, "Design of DFB fibre lasers," *Electronics Letters*, vol. 34, pp. 2028-2030, 1998.

[23] M. Ibsen, E. Ronnekleiv, G.J. Cowle, M.O. Berendt, O. Hadeler, M.N. Zervas, and R. I. Laming, "Robust high power (>20 mW) all-fibre DFB lasers with unidirectional and truly single polarisation outputs," in *CLEO*, 1999, pp. CWE4.

[24] T. Okoshi, K. Kikuchi, and A. Nakayama, "Novel method for high resolution measurement of laser output spectrum," *Electronics Letters*, vol. 16, pp. 630-631, 1980.

[25] P. Horak and W. H. Loh, "On the delayed self-heterodyne interferometeric technique for determining the linewidth of fibre lasers," *Optics Express*, vol. 14, pp. 3923-3928, 2006.

[26] "http://www.npphotonics.com/files/Laser_Module.pdf.," in *NP Photonics 'Scorpion' Laser Module, Product Data Sheet Rev 4*.

[27] A. Yariv, *Quantum electronics*: John Wiley & Sons, 1975.

[28] E. Yahel and A. Hardy, "Modeling high-power Er^{3+}-Yb^{3+} codoped fiber lasers," *Journal of Lightwave Technology*, vol. 21, pp. 2044-2052, 2003.

[29] G. Bjork and O. Nilsson, "A new exact and efficient numerical matrix theory of complicated laser structures: properties of asymmetric phase-shifted DFB lasers," *Journal of Lightwave Technology*, vol. 5, pp. 140-146, 1987.

[30] S. Foster, "Dynamical noise in single-mode distributed feedback fiber lasers," *IEEE Journal of Quantum Electronics*, vol. 40, pp. 1283-1293, 2004.

[31] M. Lax, "Classical noise. v. noise in self-sustained oscillators," *Physical review*, vol. 160, pp. 290-307, 1967.

[32] K. Kikuchi, "Effect of 1/f-type FM noise on semiconductor-laser linewidth residual in high-power limit," *IEEE Journal of Quantum Electronics*, vol. 25, pp. 684-688, 1989.

[33] W. H. Glenn, "Noise in interferometric optical systems: an optical Nyquist theorem," *IEEE Journal of Quantum Electronics*, vol. 25, pp. 1218-1224, 1989.

[34] K. H. Wanser, "Fundamental phase noise limit in optical fibres due to temperature fluctuations," *Electronics Letters*, vol. 28, pp. 53-54, 1992.

[35] M. K. Davis, M. J. F. Digonnet, and R. H. Pantell, "Thermal effects in doped fibers," *Journal of Lightwave Technology*, vol. 16, pp. 1013-1023, 1998.

[36] K.P. Koo, A.D. Kersey, A. Dandridge, and G. Ball, "Measurement of the thermal-noise-limited frequency stability of a fiber-optic Bragg-grating laser," in *Optical Fiber communication conference*. San Diego, 1995, pp. 297-298.

[37] E. Ronnekleiv, "Frequency and intensity noise of single frequency fiber Bragg grating lasers," *Optical Fiber Technology*, vol. 7, pp. 206-235, 2001.

[38] *Agilent 71400 Lightwave Signal Analyzer Application Note 371*.

[39] P.W. Milonni and J. H. Eberly, *Lasers*: Wiley-Interscience, 1998.

[40] G. De Geronimo, S. Taccheo, and P. Laporta, "Optoelectronic feedback control for intensity noise suppression in a codoped erbium-ytterbium glass laser," *Electronics Letters*, vol. 33, pp. 1336-1337, 1997.

[41] A. D. McCoy, L. B. Fu, M. Ibsen, B. C. Thomsen, and D. J. Richardson, "Intensity noise suppression in fibre DFB laser using gain saturated SOA," *Electronics Letters*, vol. 40, pp. 107-109, 2004.

[42] C. Lauer and M.-C. Amann, "Calculation of the linewidth broadening in vertical-cavity surface-emitting lasers due to temperature fluctuations," *Applied Physics Letters*, vol. 86, pp. 191108, 2005.

[43] E. T. Y. Lee and E. R. M. Taylor, "Compositional effects on the optical and thermal properties of potassium aluminophosphate glasses," *Optical Materials*, vol. 27, pp. 323-330, 2004.

[44] E. T. Y. Lee and E. R. M. Taylor, "Thermo-optic coefficients of potassium alumino-metaphosphate glasses," *Journal of Physics and Chemistry of Solids*, vol. 65, pp. 1187-1192, 2004.

Chapter 4

Non-Standard DFB Designs: A Comparative Study on Performance

This chapter presents the performance of the non-standard DFB designs: step-apodised and double discrete phase shifts designs. In this work, we compared the performance of the non-standard with the standard designs. This chapter also presents the experimental data for some of the suggested techniques, as described in Chapter 3, to reduce laser linewidth. The laser was operated in the MOPA configuration and lower coupling coefficient (κ) designs were used to test out the analytical model. Narrower laser linewidths were observed when the laser was pumped with a 1480 nm laser diode and the maximum output power of ~1 mW with an absorbed pump power of 20% was obtained. Subsequently, the laser was configured in the MOPA configuration for high power and its performance was analysed. For reducing the fundamental thermal noise, we modified the effective cavity length (L_{eff}) of the laser by using different coupling coefficients (κ). Then, a step-apodised phase shift design, in which the effective cavity length can be increased without deviating from the optimal cavity confinement, was fabricated and

its performance was compared with the standard laser design. In these designs, the signal intensity around the phase shift is very high as the fields propagating to the left and to the right are trapped by the two grating segments and they are circulating within a short effective cavity length. This intensity is dependent on the Q-factor of these gratings, and the laser will experience a much higher intensity at the phase shift with higher reflectivity gratings. Because the intensity profile of the single discrete phase shift is non-uniform, the peak intensity is built up in the vicinity of the phase shift and then decays exponential to both ends of the grating. Then, we designed a 2 x $\pi/2$ phase shifts DFB laser, with the phase shift separation of 5 mm and 10 mm, to investigate the effects of intra-cavity intensity. The significance of this double phase shift design is that the intensity distribution is much more uniform.

4.1 MOPA laser

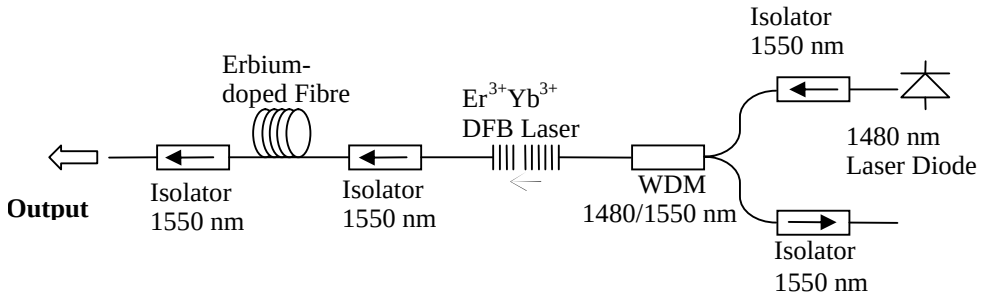

Figure 4.1: *DFB laser + MOPA configuration for high output.*

As observed in Section 3.4.6, the laser pumped at 1480 nm has a narrower linewidth, ~14 kHz, but its output power is ~ 1mW for ~30mW of absorbed pump power. A few MOPA configurations have been reported that were designed to boost the low output power of the laser [1, 2]. Consequently, our laser was configured in the MOPA configuration, as shown in Figure 4.1, for high output and its performance was experimentally analysed. In this MOPA configuration, the unabsorbed pump power was absorbed within the additional section of erbium-doped fibre, that acts as an amplifier, and is separated from the laser by a 1550-nm isolator. The additional length of the amplifier fibre used was 6-m long with an absorption loss of 7dB/m at 1480 nm. The DFB laser was operated in the forward direction. In this set-up, the

performance of the laser with the MOPA configuration was experimentally analysed not only for the threshold, output power, and linewidth but also the shift in lasing wavelength with pump power and the stability of the output power were measured.

4.1.1 Lasing threshold and output power characteristics

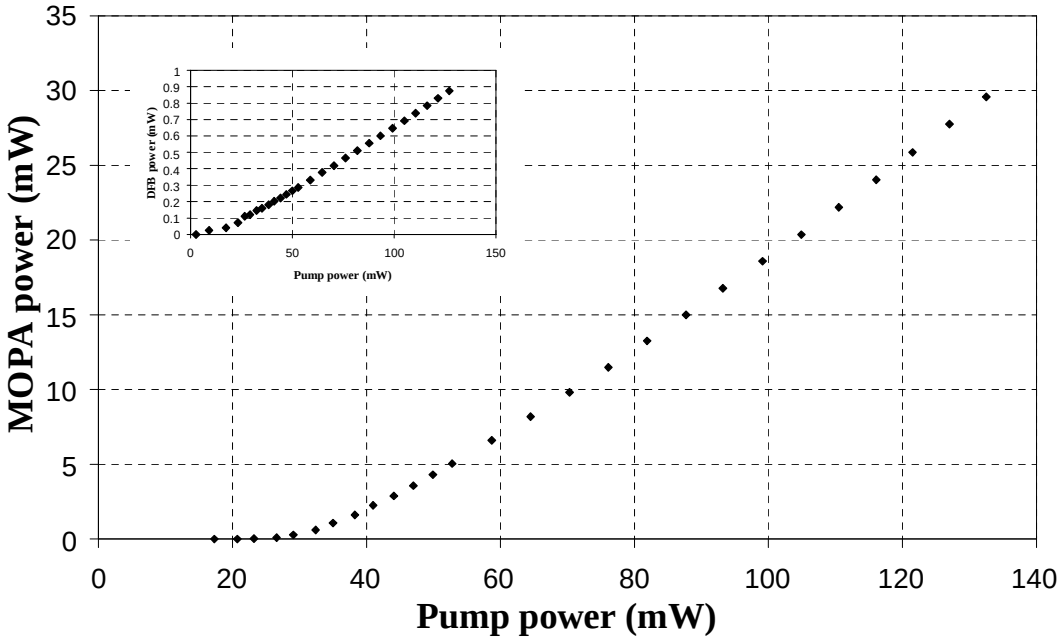

Figure 4.2: *MOPA output characteristics of the laser.*

A plot of the output of the MOPA laser, as a function of pump power is shown in Figure 4.2. The inset in the figure shows the laser output characteristics, in the forward pumping configuration, of the DFB laser itself. A maximum MOPA power of ~30 mW for ~130 mW of pump power was obtained. The slope efficiency of the MOPA laser was ~30 % with a lasing threshold of ~27 mW. The threshold power of the DFB laser was lower than in the MOPA configuration, as nearly full inversion can be easily achieved with a short length fibre. The output of the DFB laser was amplified to ~30 mW, i.e, a net gain of ~15 dB.

4.1.2 Laser linewidth

The 3-dB linewidth of the MOPA laser was measured to ensure that it was still maintaining the same linewidth as with the DFB laser itself. The results are shown in Figure 4.3. The measured linewidth was about the same as that without the amplifying fibre. A linewidth of ~ 14 kHz was observed over 130 mW pump power. In fact, 15 kHz linewidth has been observed in an Er^{3+} -doped DFB fibre laser with a MOPA configuration [2].

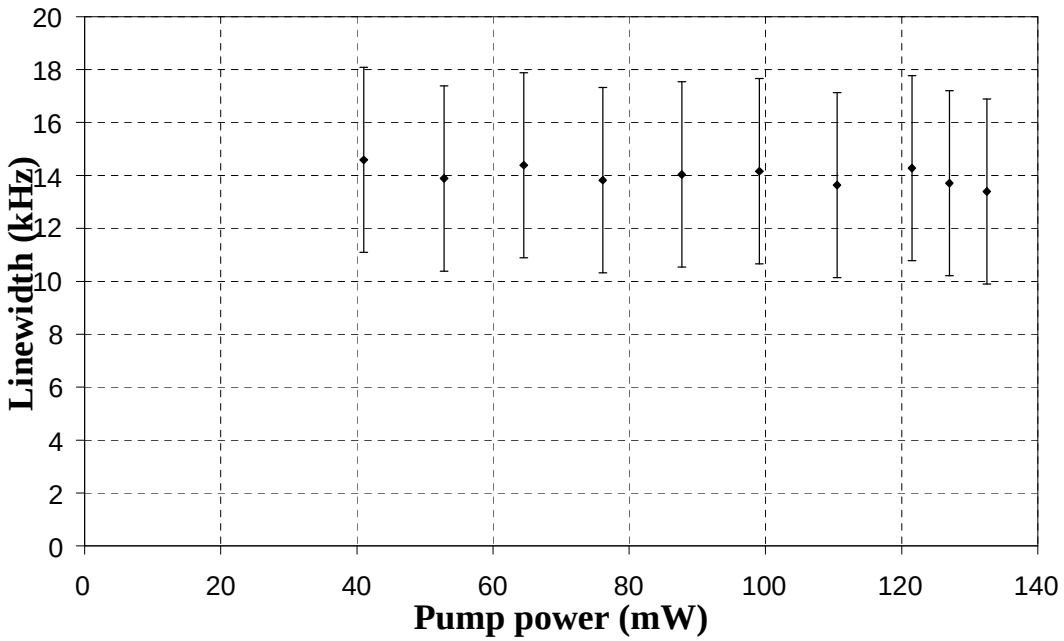

Figure 4.3: *Measured 3-dB linewidth of the MOPA laser.*

4.1.3 Lasing wavelength

The lasing wavelength shift was measured with the Burleigh wavemeter. Figure 4.4 shows the MOPA lasing wavelength as a function of pump power. The maximum shift in lasing wavelength observed in the MOPA configuration was ~1.4 pm for 130mW pump power. It was in Section 3.4.6 that the wavelength shift of the DFB laser itself in the forward pumping configuration was ~0.8 pm for the same pump power. This indicated that a small further increase in lasing wavelength of ~0.6 pm

was observed in the MOPA configuration. This implies a temperature rise in the fibre of not more than 0.2 ºC with 130 mW absorbed pump.

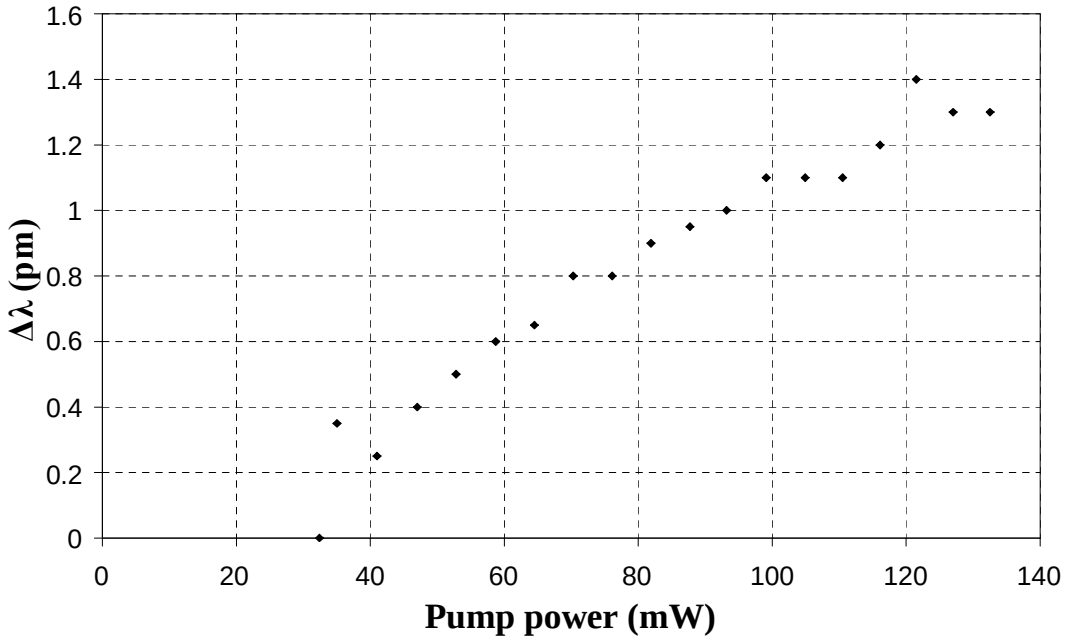

Figure 4.4: *The MOPA lasing wavelength shifted against pump power.*

4.1.4 RIN of the MOPA laser

As the cavity length of the laser had been increased, the stability of the laser output power needed to be investigated. The measured RIN and the ROF of the MOPA laser is shown in Figure 4.5. There was no penalty of instability of the laser output due to the additional length of amplifier fibre. The RIN of the MOPA laser was still maintained at ~-90 dB/Hz with the output power of 30 mW. In fact, it followed the RIN and ROF of the DFB laser itself and only the output power was amplified.

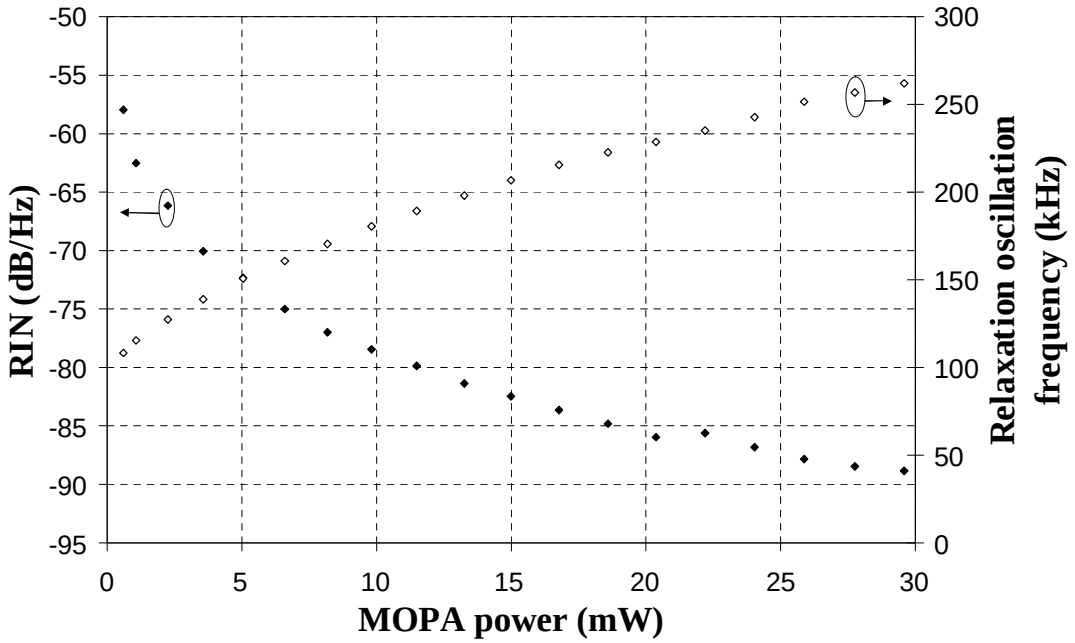

Figure 4.5: *Measured RIN at the ROF of the MOPA laser against output power.*

4.2 Laser performances with different effective cavity lengths

As mentioned in Section 3.6, the linewidth floor due to the fundamental thermal noise can be reduced by increasing the effective mode volume and this can be achieved by increasing the effective cavity length (L_{eff}) of the grating. The L_{eff} can be increased by decreasing the κ of the grating as $L_{eff} \simeq 1/\kappa$ [3]. In this work, the performance of three asymmetric π phase shift DFB lasers with κ values of 100 m^{-1}, 150 m^{-1} and 200 m^{-1} were experimentally analysed. The design of these lasers was the same as in Chapter 3, in which the phase shift of these lasers was located at 3 mm from the mid-point of the grating and the grating was 5 cm long. The L_{eff} of the grating with κ of 100 m^{-1}, 150 m^{-1} and 200 m^{-1} was 9.6, 6.6 and 4.9 mm. So far, the mentioned κ of the grating for the DFB lasers is uniform along the grating length and the L_{eff} is then divided equally at both sides of the phase shift. In this kind of design, the L_{eff} could not increase just by decreasing the κ of the grating, as this would reduce the reflectivity of the cavity and, therefore, decrease the optical feedback and, as a result, deviate from the optimal confinement condition. The step-apodised design is

capable of increasing the L_{eff} by a step change in the κ on either side of the phase shift and alters the length of the grating segments so as to restore the optimal reflectivity. This structure has been theoretically and experimentally analysed, and the pump to signal conversion ratio was increased by 40% [4]. This feature has led us to investigate its characteristics.

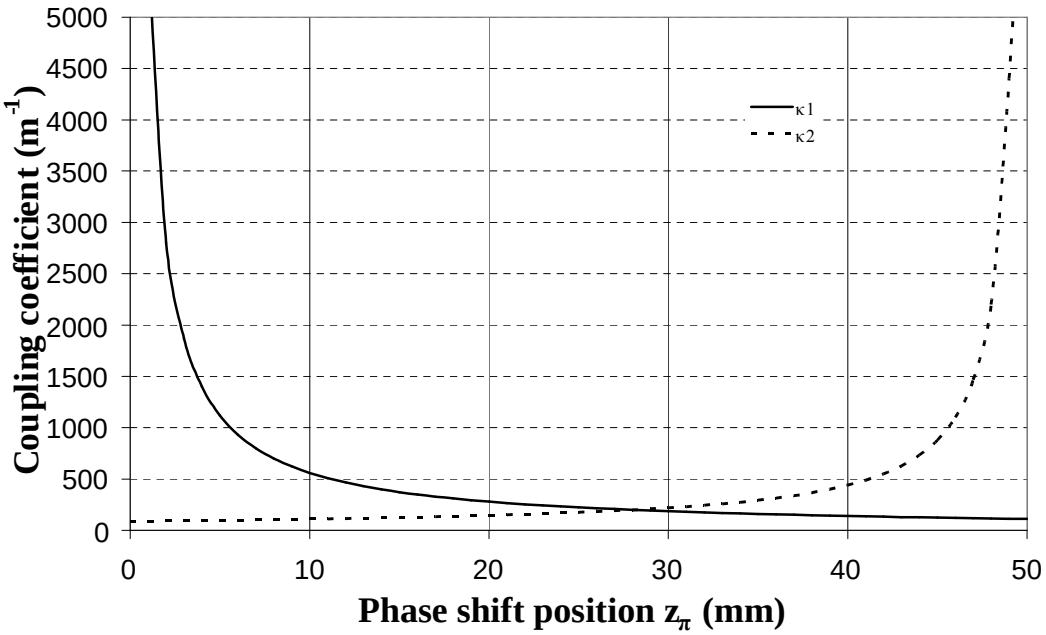

Figure 4.6 : *Coupling coefficients at different phase shift position.*

Our step-apodised DFB laser is fabricated with a grating strength (κL) of 10, the same κL as in the standard asymmetric π phase shift design with κ~200 m^{-1}. The phase shift location of the step-apodised design is restricted by the photosensitivity of the fibre which determines the maximum κ that can be attained, which in turn determines how short the highly reflective segment of the grating is. The coupling coefficients up to 310 m^{-1} are found to be feasible in the fibre we used. This value allowed us to place the phase shift at 18 mm from one end of the grating, and maintained the same reflectivity as in the laser with κ~200 m^{-1}, as seen in Figure 4.6. The grating strength (κL) of ~5.6 was achieved with this κ. This gives κ~140 m^{-1} on the other side of the phase shift, yielding a total grating strength of 10. The L_{eff} of this design was ~5.2 mm. Theoretically, the L_{eff} can be increased significantly when the phase shift is moved towards one of the ends of the grating, as was shown in [4]. For

our design, the L_{eff} can be made as high as ~5.7 mm in theory. The output of this laser was emitted predominately from the end with the lower κ.

These DFB lasers were constructed using the Er^{3+}-Yb^{3+} co-doped fibre with the B/Ge ring surrounding the core. The lasers were investigated under the three pumping configurations, as previously, i.e. backward-, forward- and dual- pumping configuration. The experimental set-up is shown in Figure 3.4. The characteristics of these lasers were investigated by measuring the threshold, output power, linewidth, laser wavelength shift with pump power, and the stability of the cavity due to different grating strengths or different L_{eff} was assessed.

4.2.1 Threshold and output power characteristics

The threshold and output power characteristics of the lasers, with κ~100 m^{-1}, κ~150 m^{-1}, κ~200 m^{-1} and the step-apodised design, for the three pumping schemes, are shown in Figure 4.7. In the backward configuration, it is clearly shown that the κ of 200 m^{-1} was the lowest in the lasing threshold and highest in efficiency as seen in (a). The slope efficiency of ~24% was obtained with a maximum output power of ~15 mW for a pump power of ~85 mW. The slope efficiency of the κ~150 m^{-1} and the step-apodised lasers was ~22%. The maximum output power of κ~100 m^{-1} was ~3.3 mW and the lasing threshold was ~27 mW. Its slope efficiency was ~5%.

The step-apodised design has the lowest lasing threshold in the forward pumping configuration, as shown in (b). As mentioned in the earlier section, the lasing threshold approximately corresponds to the pump power where the laser light experiences gain on one side of the phase shift and loss on the other. The phase shift position of the step-apodised design is the closest to the pump propagating end as compared with the other three lasers. The lasing thresholds of other lasers were increased for the same reason as explained. Once lasing, the slope efficiency of these lasers was almost similar, ~20%, except for the lowest κ. The lasing threshold of the κ~100 m^{-1} was ~35 mW and the maximum output power of ~2.7 mW was achieved for a pump power of ~90 mW.

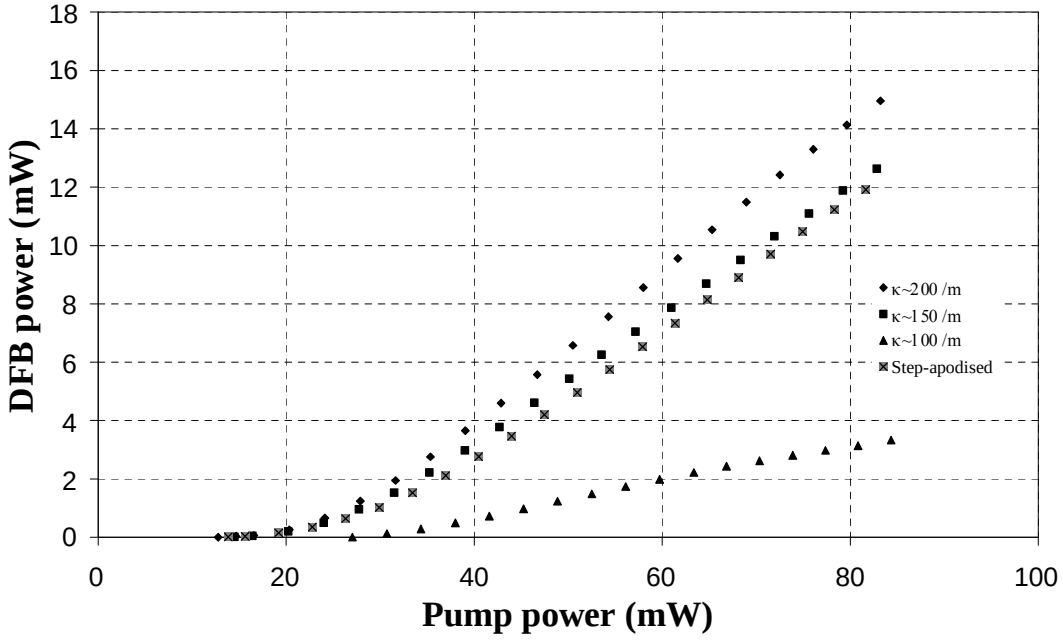
DFB power (mW)
Pump power (mW)
κ~200 /m
κ~150 /m
κ~100 /m
Step-apodised

(a)

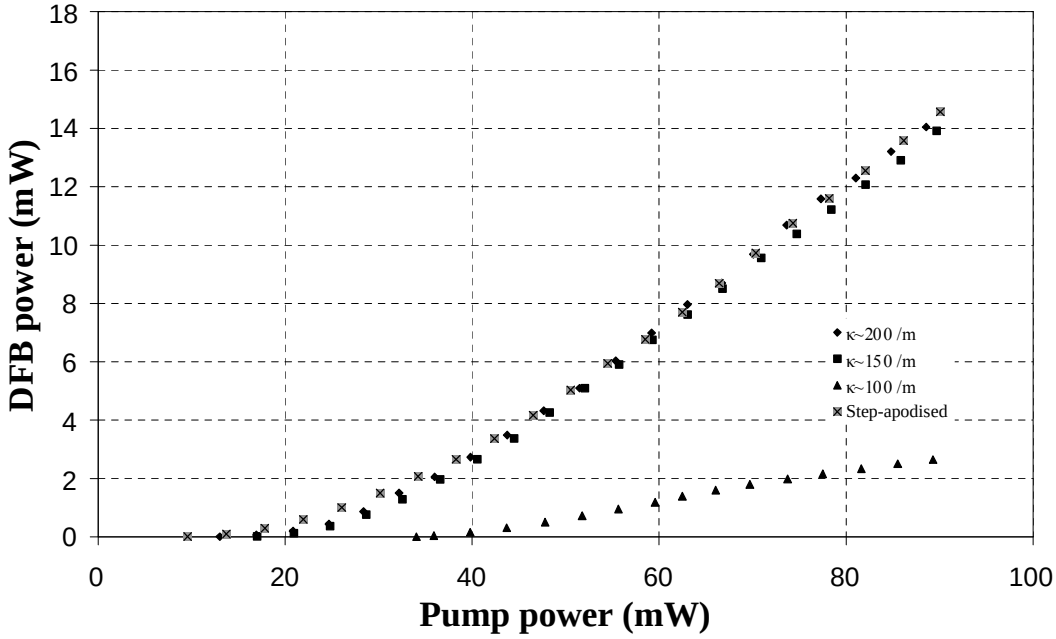
DFB power (mW)
Pump power (mW)
κ~200 /m
κ~150 /m
κ~100 /m
Step-apodised

(b)

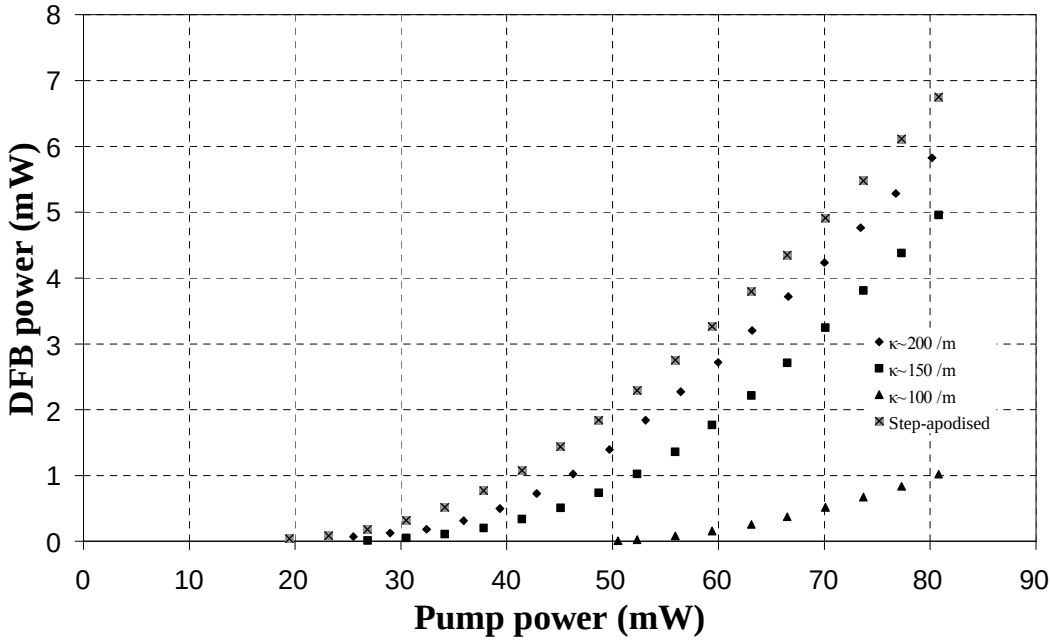

(c)

Figure 4.7: *Threshold and output power characteristics of the DFB lasers with different grating strengths in (a) backward-, (b) forward-, and (c) dual- pumping configurations.*

In the dual configuration, the threshold power of these lasers was higher than the two other pumping configurations, as observed in Chapter 3, and the reason for this was also explained, which is because the pump power was equally split and each input port received half of the pump power. Therefore, the threshold was slightly larger for the saturation of the Yb transition to begin. The lasing threshold of the step-apodised design was the lowest and had the highest output power, as seen in (c). The lasing threshold of ~20 mW and a maximum output power of ~6.7 mW, for a pump power of ~80 mW, were obtained. The slope efficiency of this laser was ~14%. The output power of the lowest κ was ~1 mW, with a slope efficiency of ~3.5%. The slope efficiencies of the κ~150 m^{-1} and the κ~200 m^{-1} laser were ~14% and ~15% respectively.

Generally, the highest laser efficiency and highest output power were observed with the backward pumping configuration for all the lasers. The κ~200 m^{-1} had the highest output power for the given pump power in the backward pump configuration. For the forward pumping configuration, the output powers of these lasers were

approximately similar except for the $\kappa \sim 100\ m^{-1}$. The cavity with a higher round-trip reflectivity will have a lower threshold and higher output. As observed in $\kappa \sim 200\ m^{-1}$, this has the lowest threshold and a higher laser efficiency because the round-trip reflectivity of the two grating segments was the highest. For a grating length of 5 cm, the round-trip reflectivity for $\kappa \sim 200\ m^{-1}$, $\kappa \sim 150\ m^{-1}$ and $\kappa \sim 100\ m^{-1}$ was 99.9% (-0.3×10^{-3} dB), 99.3% (-30×10^{-3} dB) and 94% (-300×10^{-3} dB), respectively. Although the effective cavity length of $\kappa \sim 100\ m^{-1}$ is the highest, the optical feedback is weak and, as a result, it gives the highest threshold and lowest output power for all the pumping configurations. For the step-apodised design, the round-trip reflectivity was 99.9%, which is the same as $\kappa \sim 200\ m^{-1}$. Their output powers were similar in the forward pumping configuration.

4.2.2 Laser linewidth and laser wavelength

Observing laser efficiencies of these different laser designs in different pumping configurations, it is interesting to compare the trade-off between the laser efficiencies and the linewidth as well as the laser wavelength shift. The 3-dB linewidths of these lasers were measured with the same delay self-heterodyne set-up as before. The lasers' wavelength shifted with pump power and was measured with the wavemeter.

Figure 4.8 shows the laser linewidth as a function of DFB power. The trendlines in the figure serve as a guide for the eye, not a rigorous fit. The largest linewidth was observed for $\kappa \sim 200\ m^{-1}$, in the forward pumping configuration, in which linewidths of 30 kHz – 60 kHz were obtained for a similar output power as in the backward pumping configuration. In the dual pumping scheme, the linewidths were 20 kHz – 50 kHz and its linewidth was lower than the backward pumping configuration at output powers below 2 mW. The narrowest linewidth of this laser was observed with the backward pumping configuration at output powers above 2 mW. The variations of linewidth were 25 kHz – 42 kHz in the backward pumping configuration. In the $\kappa \sim 150\ m^{-1}$, the narrowest linewidth was observed in the dual pumping configuration for the given output power. Its linewidth was 18 kHz – 41 kHz. The linewidth of the forward pumping configuration was lower at output powers below 5 mW and then

about the same as the backward pumping configuration at higher powers. Linewidths of 26 kHz – 42 kHz were observed for the forward pumping configuration and with 30 kHz – 40 kHz in the backward pumping configuration. The linewidths of the κ~100 m^{-1} design decreased as the output power increased. This followed the trend of Schawlow-Townes linewidth prediction, but its magnitude is still too large, so the spontaneous emission is believed not to be the effect. Also, the same argument applies as given in Chapter 3 that if the DFB power is increased by a certain fraction then the linewidth should be decreased by the same proportion if it is perturbed by spontaneous emission. This proportion was not observed in any of the pump configurations. In the backward pumping configuration, the linewidth was decreased from 37 kHz – 23 kHz when the output power increased from ~0.3 – 3.3 mW. The linewidth of the forward pumping configuration was the largest for the given output power. Its linewidth was decreased from 58 kHz – 25 kHz with output power increasing from ~0.05 – 2.7 mW. The narrowest linewidth was observed for the dual pumping configuration, in which linewidth of 34 kHz – 28 kHz was measured with power increasing from 0.2 – 1.2 mW. The narrowest linewidth of the step-apodised design was observed for the dual pumping scheme. Its linewidth was 30 kHz – 47 kHz with an output power of 0.5 – 7 mW. The linewidth of the forward pumping configuration was the largest for the similar output power. The variation of the linewidth for this configuration was 36 kHz – 55 kHz. The linewidth of the backward pumping configuration was 36 kHz – 52 kHz.

Now, we look at the laser design which offered the narrowest laser linewidth for the same pumping configuration. In the backward pumping configuration (a), it is clearly shown that the narrowest linewidth was observed in the lowest κ, at output powers above ~1.8 mW. The largest linewidth was observed with the step-apodised design with linewidth of 35 kHz – 52 kHz. At output powers below 6 mW, the linewidth of κ~200 m^{-1} was lower than κ~150 m^{-1}, then the linewidths were comparable above 6 mW. In the forward pumping configuration (b), the lowest linewidth was ~25 kHz which was observed with κ~100 m^{-1} at an output power of 2.6 mW and with κ~150 m^{-1} at an output power of ~0.1 mW. In this pumping configuration, the linewidth of κ~200 m^{-1} was larger than κ~150 m^{-1} for the given DFB power. The linewidth of the step-apodised design was the largest at output powers above 4 mW and then at

higher powers it was lower than κ~200 m^{-1}. In the dual pumping configuration (c), the κ~100 m^{-1} showed a decrease in the linewidth from 35 kHz – 28 kHz for output powers up to 1 mW. The trend shows that its linewidth will decrease with increasing output power. The narrowest linewidth was observed for κ~150 m^{-1}. The linewidth of the step-apodised laser was narrower than κ~150 m^{-1} at output powers above 4 mW.

In general, the effect of modifying the effective cavity length L_{eff} of the laser was observed particularly in the uniform refractive index profile with different κ values. We observed that the trend of linewidth of the lasers can be totally different depending on the κ. The L_{eff} of κ ~100 m^{-1} was two times longer for the κ ~200 m^{-1}, and a lower noise for a longer L_{eff} is expected as indicated in the analytical model. The decrease of the linewidth with increasing laser power is also attributed to the low reflectivity of the grating and the corresponding operation of the laser near the laser threshold, which is much higher than for κ ~200 m^{-1} and κ ~150 m^{-1}.

For κ ~200 m^{-1} and κ ~150 m^{-1}, the linewidth was increased as output power increased. As mentioned in the model, the linewidth floor of the laser is inversely proportional to L_{eff}, the scaling of the linewidth floor for κ ~200 m^{-1} and κ ~150 m^{-1} was analysed as the laser efficiencies were quite similar. The L_{eff} of κ ~200 m^{-1} was increased by 33%, so the linewidth floor of κ ~150 m^{-1} should be decreased by the same amount. The linewidth floor of the laser with κ ~200 m^{-1} was at ~20 kHz, as seen in the dual configuration, so the linewidth floor of κ ~150 m^{-1} should be at ~13 kHz. We observed the linewidth floor of 18 kHz which agreed with the prediction. For the step-apodised design, its L_{eff} was slightly longer than κ~200 m^{-1} and we expected a lower noise floor. However, it was higher and this could be associated with the laser cavity design as the L_{eff} was not the same at both sides of the phase shift.

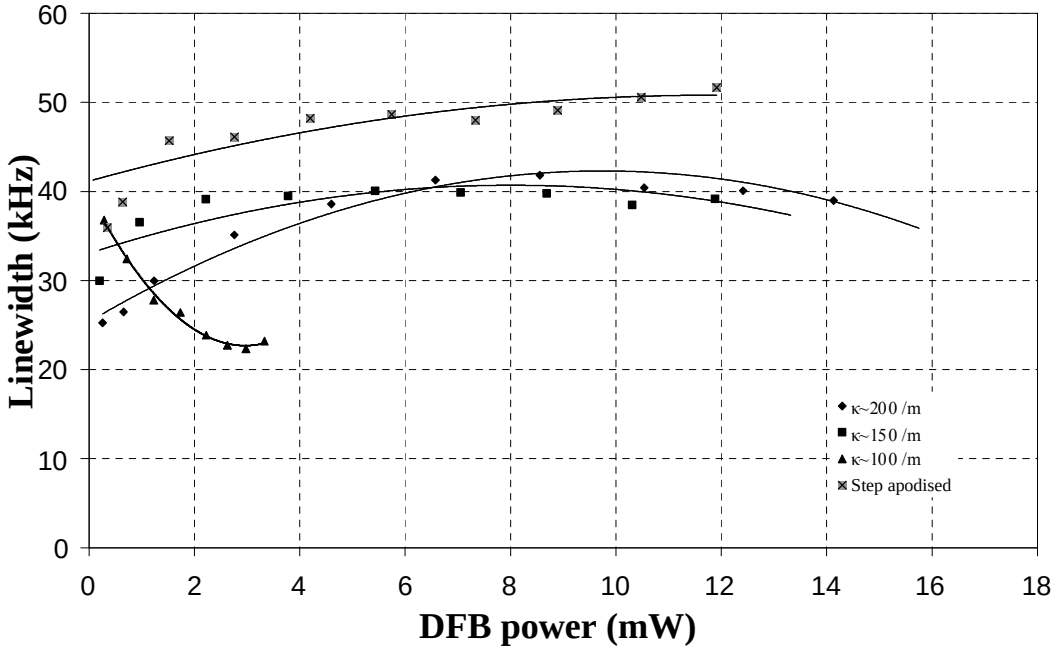
Linewidth (kHz)
DFB power (mW)
κ~200 /m
κ~150 /m
κ~100 /m
Step apodised

(a)

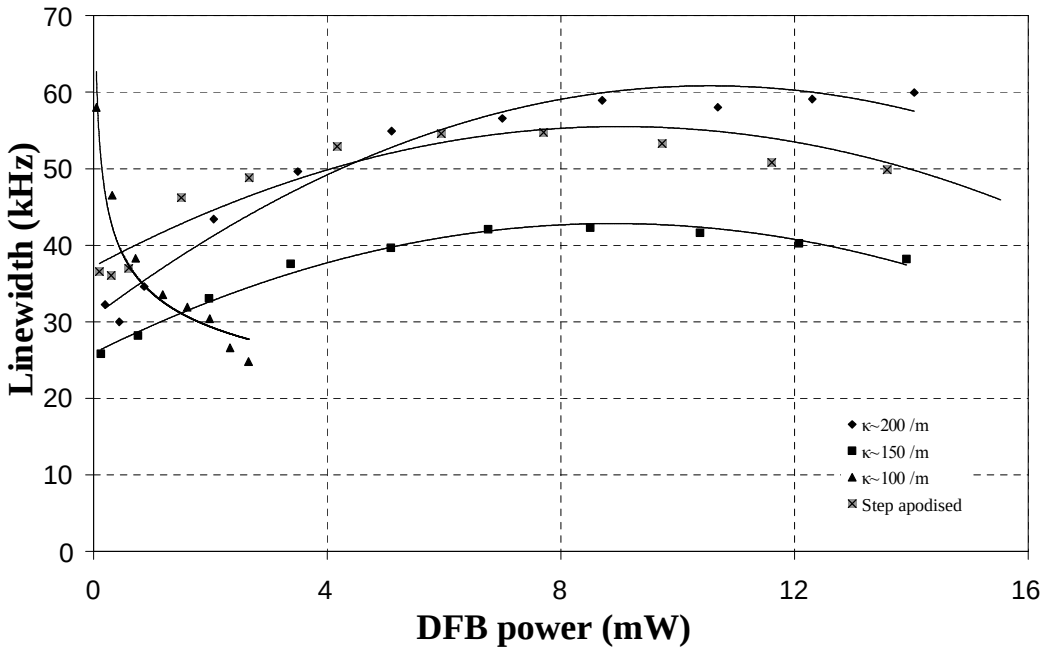
Linewidth (kHz)
DFB power (mW)
κ~200 /m
κ~150 /m
κ~100 /m
Step apodised

(b)

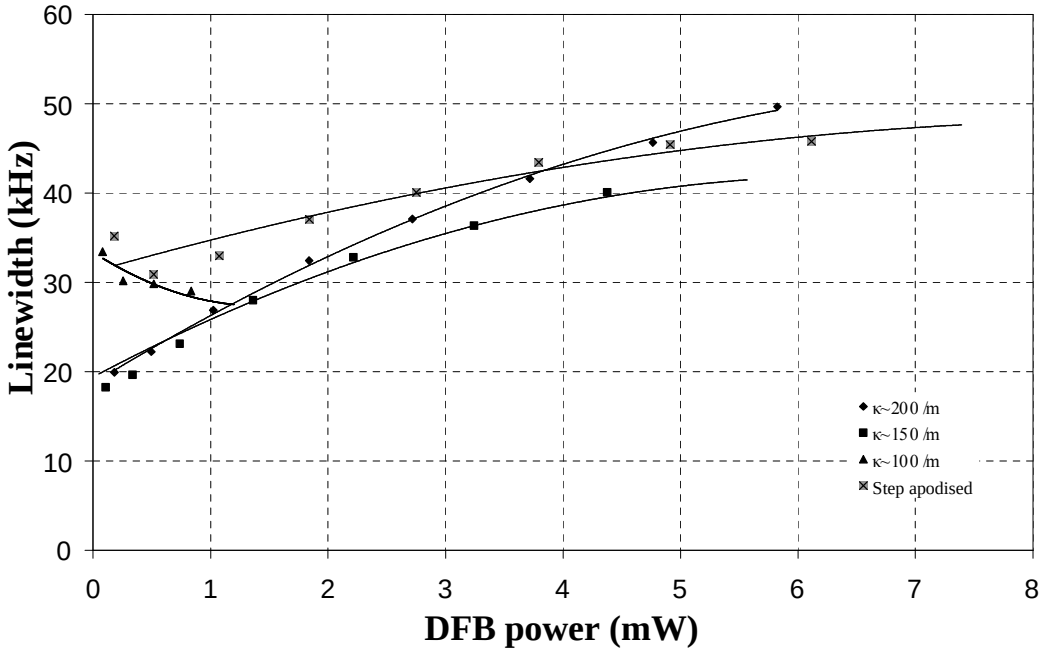

(c)

Figure 4.8: *Measured 3-dB laser linewidth of the DFB lasers with different grating strengths in (a) backward-, (b) forward-, and (c) dual- pumping configurations.*

After experimental investigation of the linewidths of the lasers, the lasing wavelength of the lasers was measured to analyse the temperature raise in the fibre due to the effect of modifying the L_{eff}. As mentioned in the earlier section the high intensity built up in the vicinity of the phase shift, due to the field propagating to the left and to the right being trapped by the two grating segments. This high intensity could create a heating effect and cause a variation in the refractive index and hence, in the lasing wavelength. The laser wavelength shifts of these lasers, as a function of pump power, were measured for the three pumping configurations. The results are summarised in Figure 4.9.

The laser wavelength shifting of $\kappa \sim 200$ m^{-1} in the backward pumping configuration was ~36 pm for ~85 mW pump power, indicating a temperature rise of ~4.5 ºC in the fibre. The wavelength shifts of the laser in the forward- and dual- pumping configurations were ~40 pm for ~90 mW of absorbed pump power and ~22 pm for ~80 mW of absorbed pump power, respectively. These wavelength shifts corresponded to an increase in the fibre temperature of ~5 ºC and ~2.8 ºC. The

temperature increases in the fibre of κ~150 m^{-1} in the backward- and forward-pumping configurations were both ~2.6 ºC. In the dual pumping configuration, a temperature rise of ~1 ºC was observed. The lowest κ showed the lowest shift in lasing wavelength for the three pumping schemes. The temperature increases in the fibre of this κ in the backward-, forward- and dual- pumping configurations were ~1.5 ºC, ~1.7 ºC and ~1 ºC, respectively. For the step-apodised design, the temperature increases in the fibre for the backward- and forward- pumping were ~4.3 ºC and ~1.8 ºC for the dual pumping scheme.

The plots in Figure 4.9 show the laser wavelength shift in different laser cavity designs. In the backward pumping configuration (a), it is clearly indicated that the larger laser wavelength shift was with the constant κ of higher value, i.e. higher reflectivity of laser cavity, because of the intensity increase with the Q-factor of the cavity and the resulting increase in temperature. The laser wavelength shifting for κ~200 m^{-1} was the largest and the lowest was in κ~100 m^{-1}. The laser wavelength shifts in the lowest κ and κ~150 m^{-1} were only ~32% and ~56% of that in κ~200 m^{-1}. The step-apodised design also showed a shift in lasing wavelength of ~23% less than in κ~200 m^{-1}. Plot (b), forward pumping configuration, shows that the largest laser wavelength shift was in κ~200 m^{-1} and that κ~100 m^{-1} was the lowest at the maximum pump power. The wavelength shift in κ~150 m^{-1} and κ~100 m^{-1} was ~52% and ~33% of the wavelength shift in κ~200 m^{-1}. In this configuration, the step-apodised design showed a lasing wavelength shift of ~10% lower than κ~200 m^{-1}. For the dual pumping configuration (c), the largest laser wavelength shift was again observed in κ~200 m^{-1} at the maximum pump power. The lowest shift in laser wavelength was observed in κ~150 m^{-1} and κ~100 m^{-1}. This was ~40% of the shift in the laser wavelength measured for κ~200 m^{-1}. For the step-apodised design, the laser wavelength shift was 75% of that for κ~200 m^{-1}.

In general, the laser wavelength shift for κ~200 m^{-1} was the largest, followed by the step-apodised design and then the κ~150 m^{-1} for the three different pumping schemes. The smallest wavelength shift was found to be for κ~100 m^{-1}. The laser wavelength increases with refractive index which increases with temperature. Assuming that the same amount of pump power is dissipated in the grating, the

temperature increase in the fibre is inversely proportional to the mode field volume which in turn depends on the L_{eff}. The longest L_{eff} is with κ~100 m^{-1} and hence less temperature variation is observed as compared with the others. Therefore, the laser wavelength shift is less for lower κ. For the step-apodised design, this showed a reduction in laser wavelength shift for a slightly longer L_{eff} as compared with κ~200 m^{-1}.

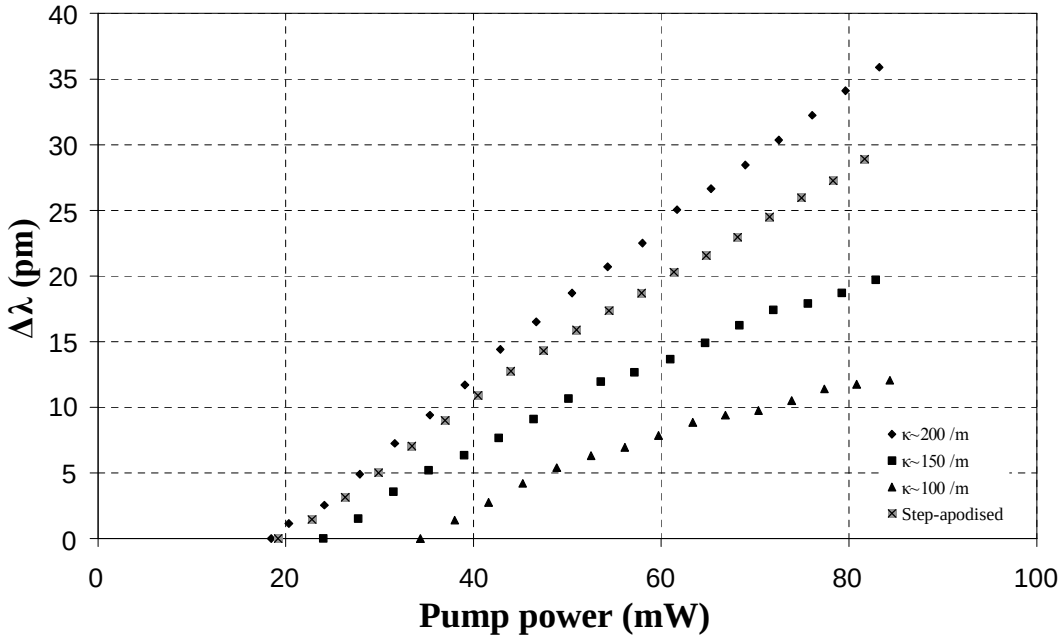

(a)

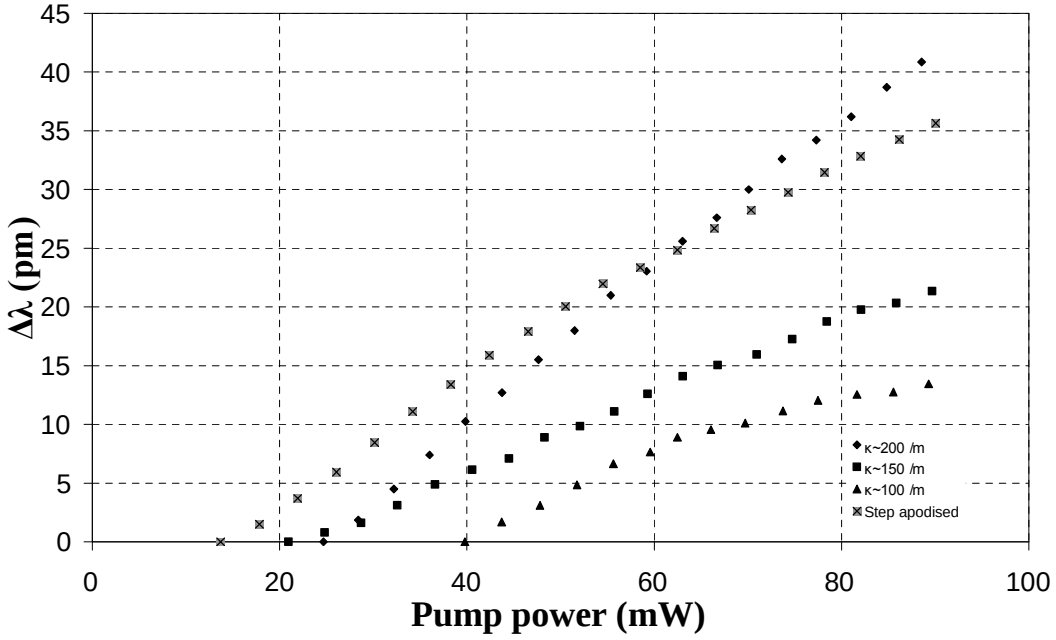

(b)

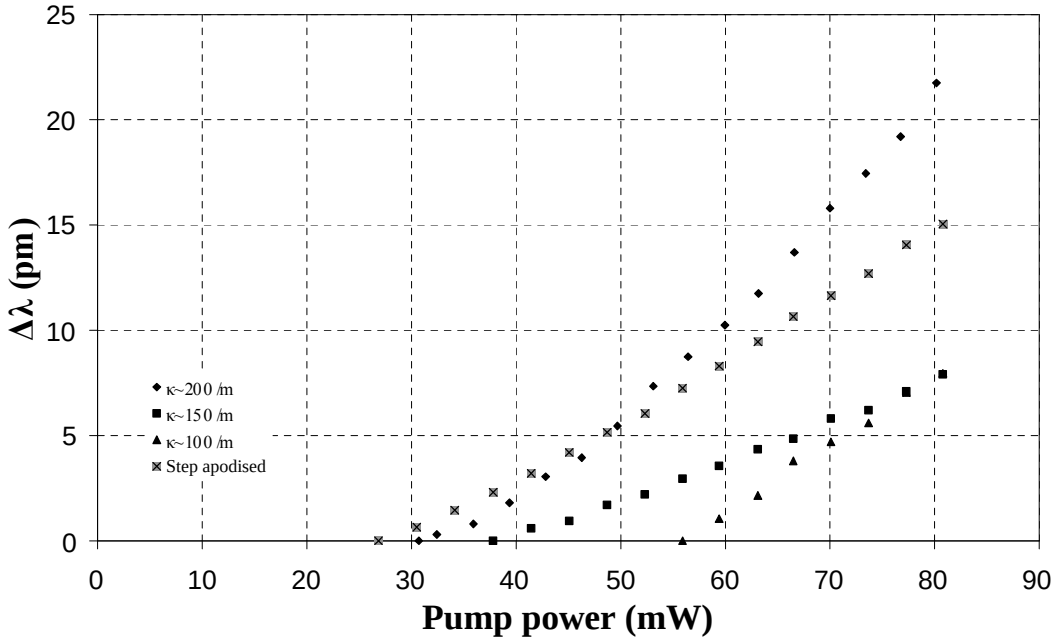

(c)

Figure 4.9: *The laser wavelength shift as a function of pump power for the DFB lasers with different grating strength in (a) backward-, (b) forward-, and (c) dual- pumping configurations.*

Now, verifying the analytical model developed in Chapter 3 for different laser cavity designs. The $\partial\lambda/\partial P$ for κ~100 m^{-1}, κ~150 m^{-1}, κ~200 m^{-1} and the step-apodised design were calculated. The change in the slope of the laser wavelength and the average of the observed linewidth with a pump power range of 60 – 80 mW, for the three pumping configurations, are shown in Table 4.1. From the table, it shows the shifting of laser wavelength for κ~100 m^{-1} was lower than κ~200 m^{-1} for the three pumping configurations. Its linewidth was narrower than κ~200 m^{-1}. This is expected as linewidth is directly proportional to laser wavelength shift due to temperature fluctuation caused by the pump intensity noise, as discussed in Section 3.5. The percentage change in the $\partial\lambda/\partial P$ and the linewidth for the forward- and dual-pumping configurations were compared with the backward pumping configuration. As seen in Table 4.1(b), the change in laser wavelength with the pump power was higher in the forward pumping configuration except for the step-apodised design. In the dual pumping configuration, Table 4.1(c), the laser wavelength shifts for κ~200 m^{-1} and 100 m^{-1} were higher than for the backward pumping configuration, except for κ~150 m^{-1} and the step-apodised design.

	$\kappa \sim 200\ m^{-1}$	$\kappa \sim 150\ m^{-1}$	$\kappa \sim 100\ m^{-1}$	Step-apodised
$\partial\lambda/\partial P$ (pm/mW)	0.503	0.277	0.185	0.424
Av. linewidth (kHz)	39.6	39.3	23.0	49.8

(a)

	$\kappa \sim 200\ m^{-1}$	$\kappa \sim 150\ m^{-1}$	$\kappa \sim 100\ m^{-1}$	Step-apodised
$\partial\lambda/\partial P$ (pm/mW)	0.602	0.314	0.222	0.404
Av. linewidth (kHz)	58.2	41.6	30.6	52.2
Change in $\partial\lambda/\partial P$ (%)	16.3	11.8	16.8	-4.9
Change in linewidth (%)	31.8	5.4	24.8	4.5

(b)

	$\kappa \sim 200\ m^{-1}$	$\kappa \sim 150\ m^{-1}$	$\kappa \sim 100\ m^{-1}$	Step-apodised
$\partial\lambda/\partial P$ (pm/mW)	0.569	0.194	0.256	0.318
Av. linewidth (kHz)	43.5	35.7	29.2	44.5
Change in $\partial\lambda/\partial P$ (%)	11.5	-42.6	27.9	-33.1
Change in linewidth (%)	8.9	-10.3	21.2	-12.1

(c)

Table 4.1: *The $\partial\lambda/\partial P$ and average linewidth of the (a) Backward- (b) Forward- and (c) Dual-pumping configurations.*

The change in the laser linewidth was of the same order of magnitude as the change in the $\partial\lambda/\partial P$ for the three different κ values of the three pumping configurations, except for the step-apodised design. For the step-apodised design, the change in the slope of the laser wavelength in the forward pumping configuration was smaller, but the linewidth was larger than for the backward pumping configuration. The reason for this is unclear. The linewidth of $\kappa \sim 200\ m^{-1}$ was largest in this configuration.

4.2.3 RIN of the lasers

We have seen that the behaviour of the linewidth and the laser wavelength shift varied with different κ in different pumping configurations. It is also important for us to investigate the intensity noise of these lasers to ensure that the RIN of these lasers are still maintained at a reasonable, or an even better, intensity noise level. The intensity noise of these lasers was experimentally investigated from their measured RIN peak. The measured RIN, at the ROF, versus DFB power for the three pumping configurations are shown in Figure 4.10.

For the backward pumping configuration (a), the ROF of κ~200 m^{-1} was lower than κ~150 m^{-1} and κ~100 m^{-1} and a higher RIN peak would be expected than the other two lower κ, however, it was not observed. Actually, this behaviour has been observed in [5] and was said to be caused by the spontaneous emission in the cavity which resulted in the perturbation of the optical field amplitude of the laser output. The RIN peak of ~-113 dB/Hz at 900 kHz was observed for κ~200 m^{-1} at an output power of ~15 mW. The difference in the RIN and ROF for κ~150 m^{-1} and κ~100 m^{-1} was not obvious in this configuration. For κ~150 m^{-1}, an RIN peak of ~-112 dB/Hz at ~950 kHz was observed at an output power of ~12 mW. The RIN peak of κ~100 m^{-1} was similar to κ~150 m^{-1} for the given DFB power. Its RIN peak of ~-96 dB/Hz was observed, at the ROF of 550 kHz, at the maximum output power of ~3.3 mW. The intensity noise of the step-apodised DFB laser reached ~-120 dB/Hz at a maximum output power of 12 mW. It had a similar ROF to κ~150 m^{-1}, but the RIN peak was ~7 dB lower at the maximum output power. This suggests that the cavity of this design responded to pump perturbation and that the cavity loss was actually lower.

In the forward pumping configuration (b), the ROF of the three different κ were expected to be different, as observed in (a), however, it was found to be similar for the given output power. The RIN peak would be expected to be similar, as ROF was similar, however it was observed to be quite different for all of these lasers. An RIN peak at 1 MHz was observed as low as -129 dB/Hz at the maximum output power of ~14 mW in κ~200 m^{-1}. This was 12 dB lower than the RIN of κ~150 m^{-1} for the same output power. The RIN peak of κ~100 m^{-1} was -95 dB/Hz at the maximum

output power of ~2.6 mW which was ~5dB higher than κ~150 m^{-1}. In fact, the ROF of κ~200 m^{-1} and the step-apodised design were higher in this pump configuration. This might be related to the spontaneous emission in the cavity depending on the direction of pumping. The RIN peak of the step-apodised configuration was -130 dB/Hz at 1.1 MHz and at output power of ~14 mW.

In the dual pumping configuration (c), the ROF of the lasers were observed to behave differently in this pumping configuration. As mentioned in (a), the lower ROF would be expected to have a higher RIN peak, however, the lowest RIN peak of -125 dB/Hz was observed at an output power of ~6 mW in κ~200 m^{-1} whose ROF was the lowest. This could be due to the spontaneous emission too. The RIN peak of κ~150 m^{-1} was similar to the backward pumping configuration for the given output power. The κ~100 m^{-1} showed a RIN peak reduction of ~5 dB as compared with the other pump configurations. For the step-apodised design, a RIN peak of -118 dB/Hz was observed at an output power of ~7 mW.

Overall, the intensity noise performance of κ~200 m^{-1} was better than the two other κ values for the given DFB output power. For the step-apodised design, the intensity noise in the forward pumping configuration was the lowest for the given DFB power.

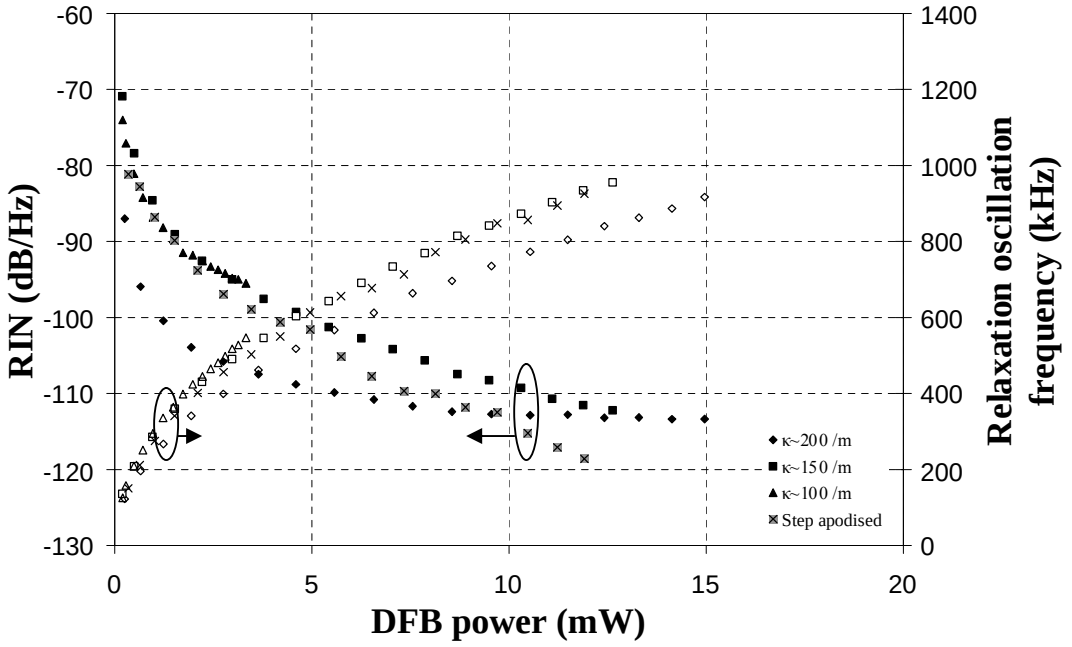

(a)

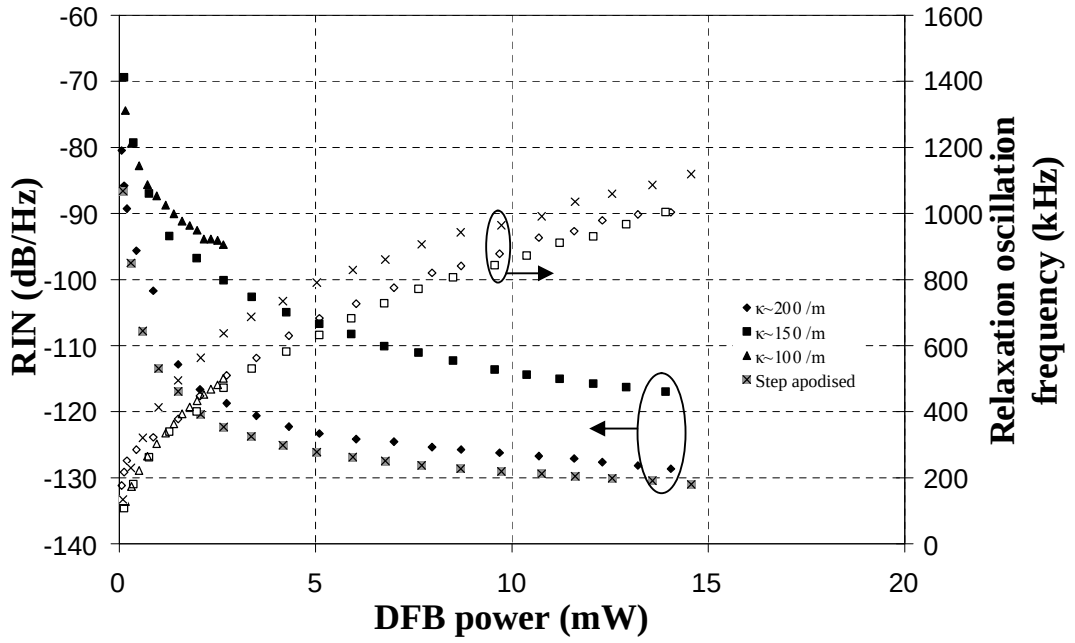

(b)

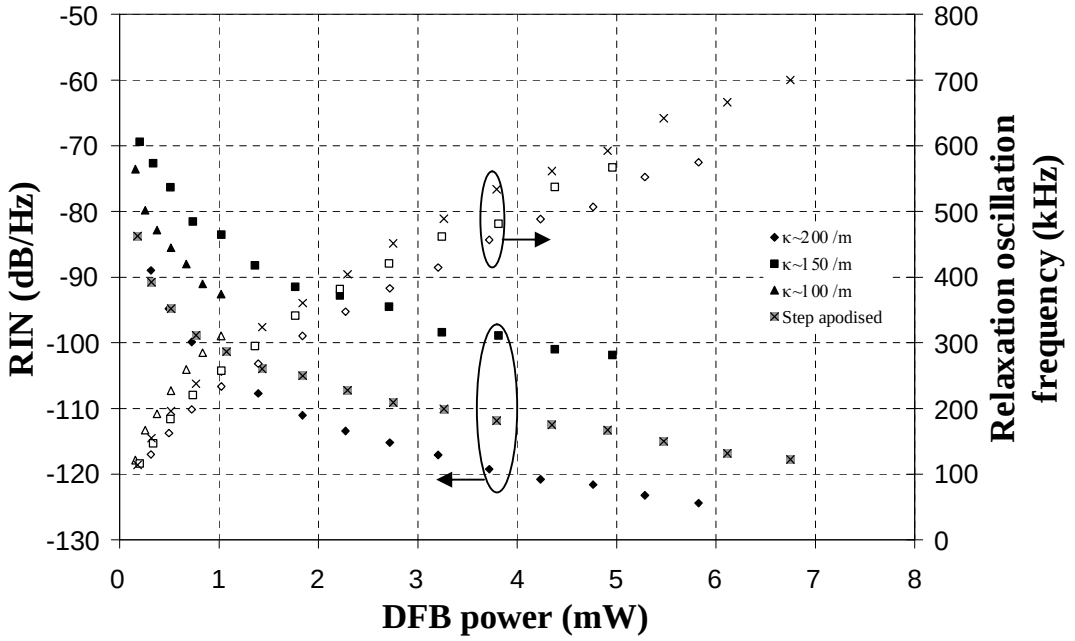

(c)

Figure 4.10: *RIN of the DFB lasers with different grating strengths in (a) backward-, (b) forward-, and (c) dual- pumping configurations.*

4.3 Two discrete π/2 phase shift DFB lasers

The lasing wavelength shifts with the pump power were observed previously. The remaining question is whether this measured wavelength shift is a result of the pump-induced temperature increase only, or is there also an intra-cavity effect arising from the high signal intensity around the phase shift itself? To investigate this point further, the 2 x π/2 phase shift DFB fibre laser was implemented and its performance was experimental analysed against the benchmark of a single asymmetric π phase shift DFB laser. The benchmark DFB laser was referred to the κ~200 m^{-1} DFB laser in the previous section. For single π phase shift DFB lasers, the peak intensity occurs around the phase shift location and decays 'exponentially' towards each end of the grating, giving a very non-uniform intensity profile, as mentioned in the previous section. This peak intensity can cause a variation of the refractive index and gain, giving rise to a change in the lasing wavelength and a decrease of the output power. Semiconductor multiple phase shift DFB lasers, with a 2 x π/2 phase shift structure, have been demonstrated which gave a near uniform intensity profile along their length, provided that the phase shifts were appropriately positioned [6]. Depending on the phase shift position, the intensity distribution in the cavity can then behave like a single π phase shift (phase shifts positioned at the centre of the cavity) and uniform (phase shifts positioned at the ends of the cavity), DFB structure. As indicated in Ref. [6], this flat intensity profile could give a more effective utilisation of the available gain, narrower linewidths because of the small variation in the refractive index along the structure and less variation in the output wavelength with power level.

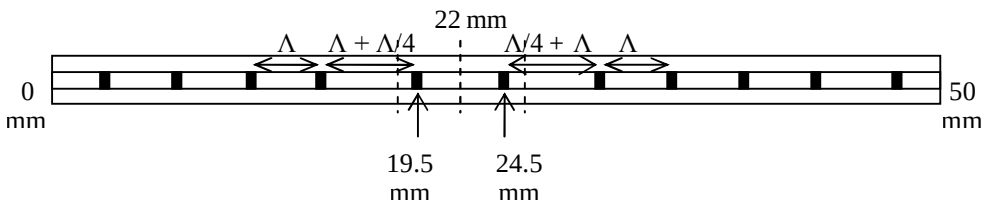

Figure 4.11: *Schematic diagram of a 2 x π/2 DFB fibre laser.*

The DFB fibre lasers were constructed with the Er^{3+}-Yb^{3+} phosphosilicate core having an annular photosensitive boron doped ring, the same fibre as was used

before. The feedback gratings of these lasers were 5 cm long with a $\kappa \sim 200\ m^{-1}$ and UV-written with the phase mask technique. For our asymmetric π phase shift design, the phase shift was located at 3 mm from the centre of the grating for the output power of the DFB laser to be predominantly at the end closer to the phase shift. In the 2 x $\pi/2$ DFB design, the two phase shifts were placed symmetrically about the position of the asymmetry phase shift design, unlike the semiconductor laser in which the phase shifts were positioned symmetrically about the centre of the cavity. These discrete phase shifts were placed 5 mm apart and positioned at 19.5 mm and 24.5 mm as shown in Figure 4.11 . As mentioned in [6], the intensity distribution in the cavity is a function of the position of the phase shifts and the strength of the grating. For this purpose, another double phase shifts laser, with the same grating strength, was fabricated with the phase shifts separated by 10 mm and positioned at 17 mm and 27 mm. The lasers were configured in the backward, forward and dual pumping schemes, as shown in Figure 3.5. The lasers were pumped at 977 nm with the laser diode. Their performance was investigated by measuring the laser threshold, output power, linewidth, lasing wavelength shift with the power and the RIN.

4.3.1 Threshold and output characteristics

Figure 4.12 shows the threshold power and the output power characteristics of the single π phase shift and the 2 x $\pi/2$ phase shifts DFB laser. It is clearly shown that the threshold of the single discrete phase shift was the lowest in the three pumping configurations. This can be explained by the high pump absorption and, because the phase shifts for the double phase shifts lasers were further apart, the round trip feedback was longer resulting in a slightly increased lasing threshold. This is evident by the performance of the 10 mm apart double phase shifts laser, the lasing threshold is even higher than the laser with the phase shifts of 5 mm apart. Overall, the backward pumping configuration gives the lowest lasing threshold and the dual pumping configuration is the worst, as observed earlier. This behaviour was, as explained in the earlier section, due to the asymmetry of the grating design and the pump absorption within the grating for the different pumping configurations.

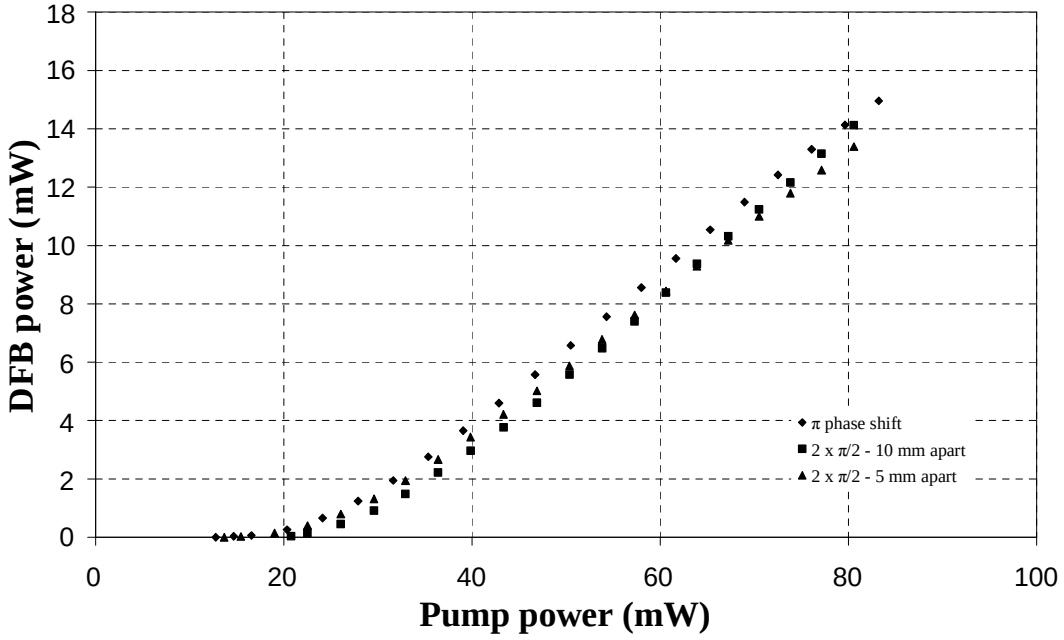
DFB power (mW)
Pump power (mW)
π phase shift
2 x π/2 - 10 mm apart
2 x π/2 - 5 mm apart

(a)

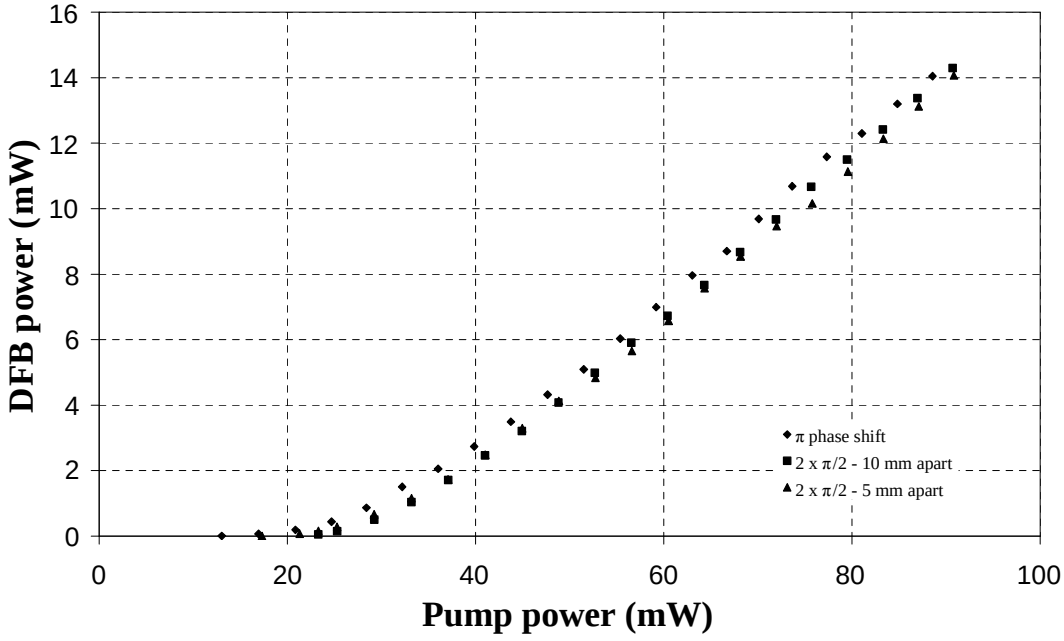
DFB power (mW)
Pump power (mW)
π phase shift
2 x π/2 - 10 mm apart
2 x π/2 - 5 mm apart

(b)

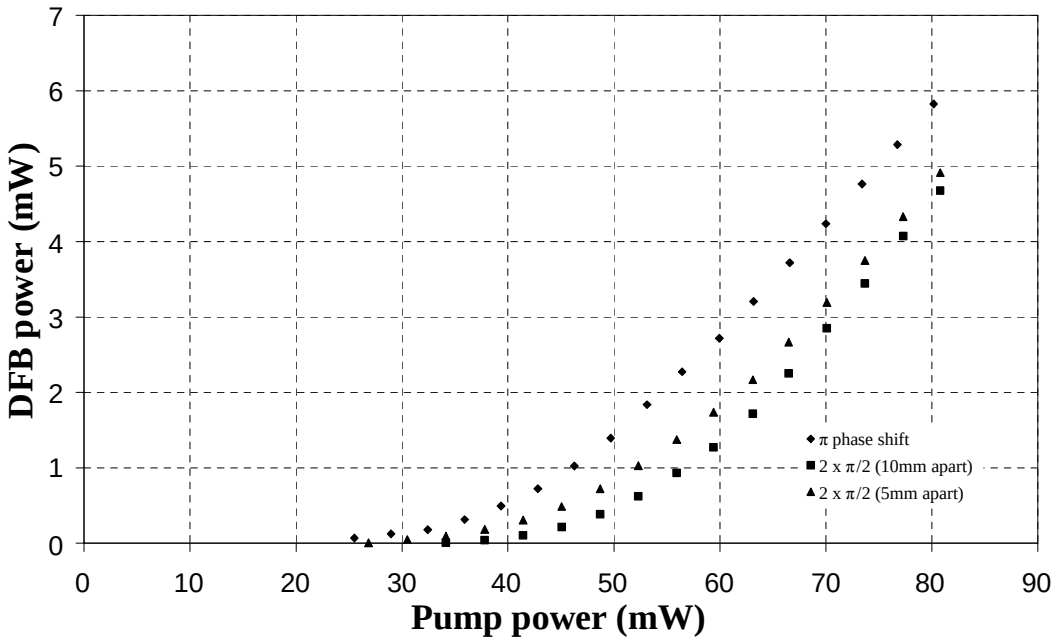

(c)

Figure 4.12: *Threshold and power characteristics of the single and two discrete phase shifts DFB structure in (a) backward-, (b) forward- and (c) dual-pumping configuration.*

For a better comparison, the laser efficiencies of these lasers were summarised in Table 4.2. Backward pumping is found to be marginally more power efficient than the other two configurations. Although the lasing thresholds of the double phase shifts lasers were higher than the single phase shift laser, once lasing, the slope efficiencies were similar or even higher in the case of the 10 mm apart double phase shifts laser for the backward and forward pumping configurations.

	Backward pump	Forward pump	Dual pump
π phase shift	24%	20%	15%
2 x π/2 – 5 mm apart	23%	21%	13%
2 x π/2 – 10 mm apart	27%	23%	14%

Table 4.2: *Slope efficiencies of the lasers in the three pumping configurations.*

4.3.2 Laser linewidth

The 3-dB laser linewidth behaviour, as a function of DFB power for the three configurations, is plotted in Figure 4.13. The trend-lines in the figures serve as a guide for viewing only, and this is not a rigorous fit. For the backward pump (a), the linewidth obtained for the double phase shifts, of 5 mm apart, design was ~10% lower than the single phase shift. Its linewidth exhibited an increase from 21 – 37 kHz over the given pump range. The 10 mm apart phase shifts laser was quite constant in linewidth at around 37 kHz.

For the forward pumping configuration (b), the laser linewidth of the 5 mm apart phase shifts laser was lower at powers below 10 mW and then it levels off with the single phase shift laser at linewidths of 60 kHz. The linewidth of the 10 mm apart phase shifts lasers shows a linear increase with the power. A linewidth of 42 – 58 kHz was observed and it was lower than the 5 mm phase shifts at powers above 5 mW.

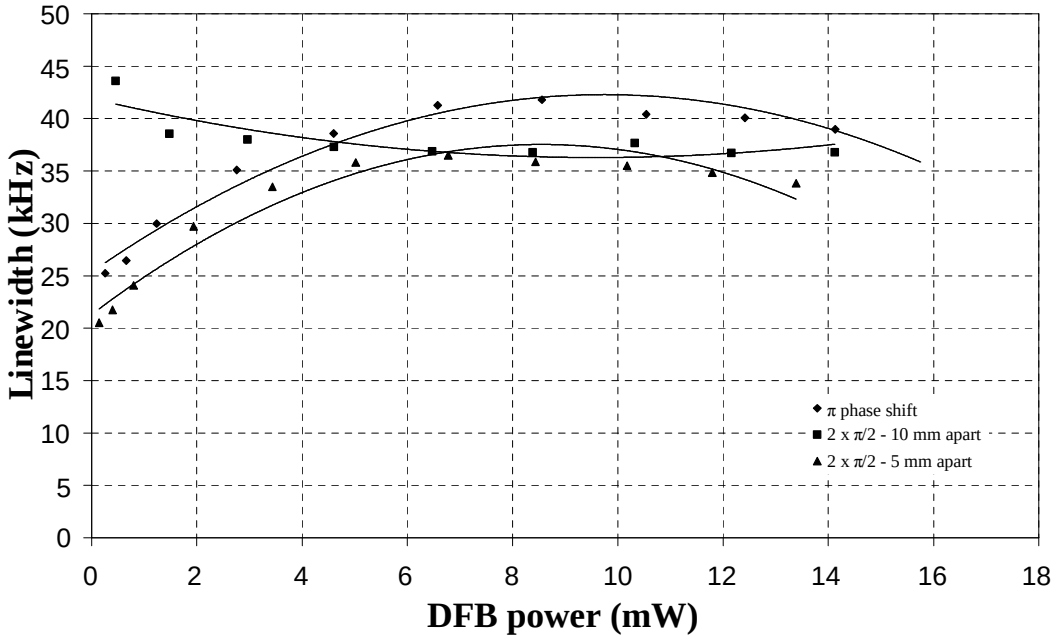

(a)

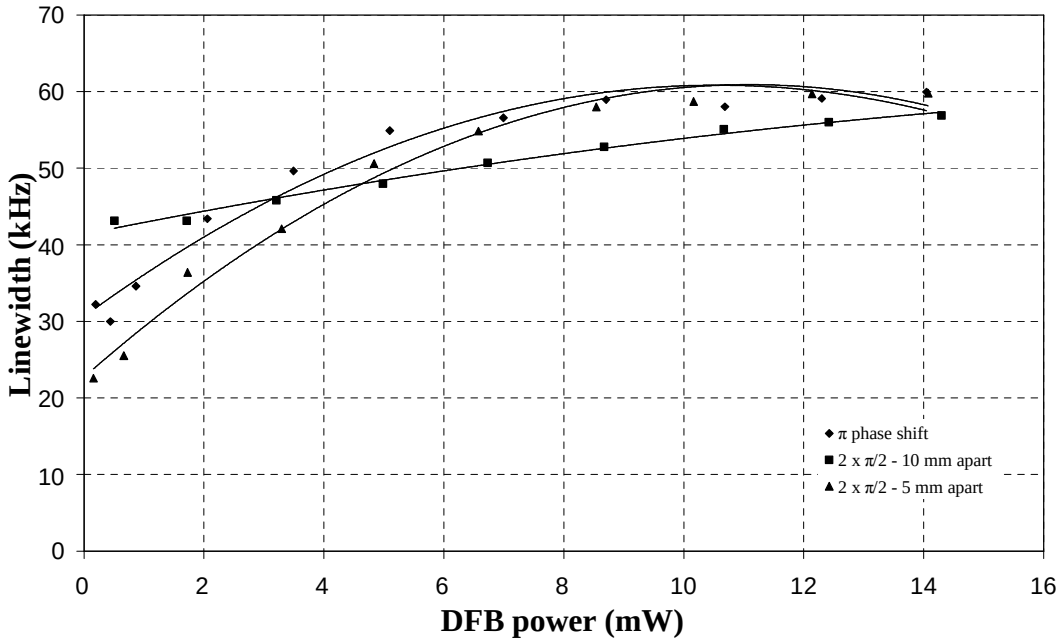

(b)

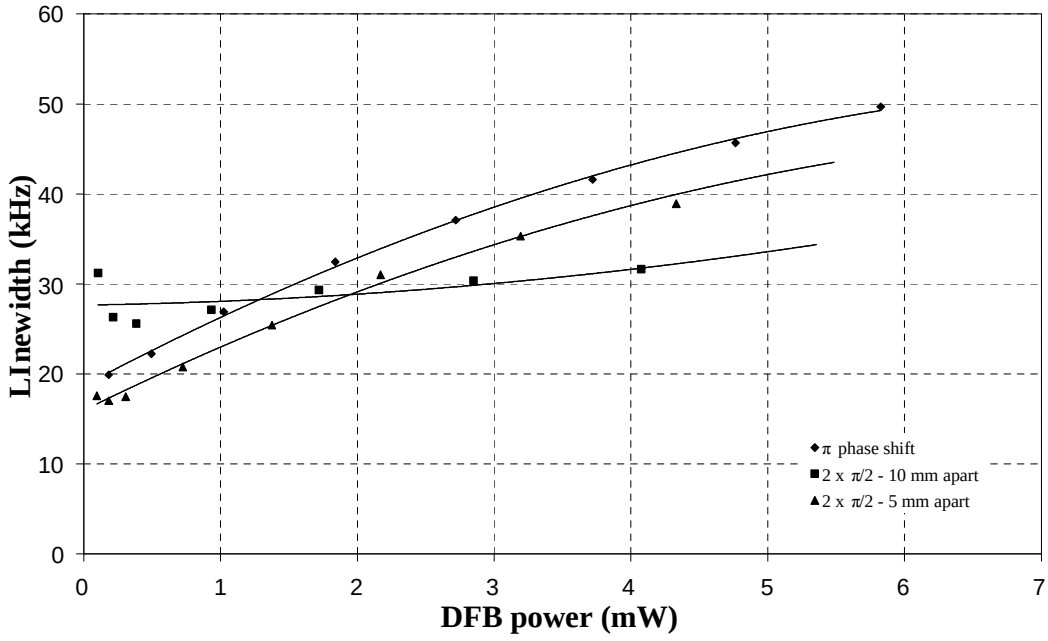

(c)

Figure 4.13: *The single and two discrete phase shifts lasers linewidth versus DFB power in (a) backward-, (b) forward- and (c) dual- pumping configurations.*

In the dual pumping configuration (c), the linewidth of the 5 mm phase shift laser was varied from ~17 – 42 kHz for the given DFB power range. It was still lower than the single phase shift laser. For the 10 mm phase shifts, the linewidth was varied

from ~28 – 33 kHz. It was lower than the 5 mm phase shifts at powers below 2 mW. The linewidth of the 10 mm apart phase shifts design behaved quite differently for the three pumping configurations. This may be because the separation of the phase shifts is too large, twice the $1/\kappa$, and the grating behaves basically as two (only weakly coupled) lasers around the two phase shifts and therefore it is no surprise that the linewidth behaviour differs. However, the linewidth of the 5 mm apart phase shifts design was always lower than the single phase shift design, as expected from the theory, but the difference is much smaller than expected from the change of the $d\lambda/dP$.

4.3.3 Laser wavelength

The lasing wavelength of the single and double phase shifts were measured as a function of the pump power to investigate whether the wavelength shifts are due to internal heating, because of dissipation of pump only, or the signal intensity around the phase shift. The results are shown in Figure 4.14. It is clearly seen that the lowest laser wavelength shift was in the double phase shifts of 5 mm apart design and the single phase shift design was the worst. For the single phase shift design, the wavelength was increased by ~35 pm for the backward and forward pumping configurations over the pump power range of 80 mW. The laser wavelength of the dual pump was increased by ~22 pm for the given pump power. For the double phase shifts of 10 mm apart design, increases in laser wavelength of ~25 pm, ~15 pm and ~13 pm were observed in the backward-, forward- and dual- pumping configurations, respectively. The wavelength increase in the double phase shifts of 5 mm apart design laser was ~17 pm, ~15 pm and ~7 pm for the backward, forward and dual pumping configuration, respectively.

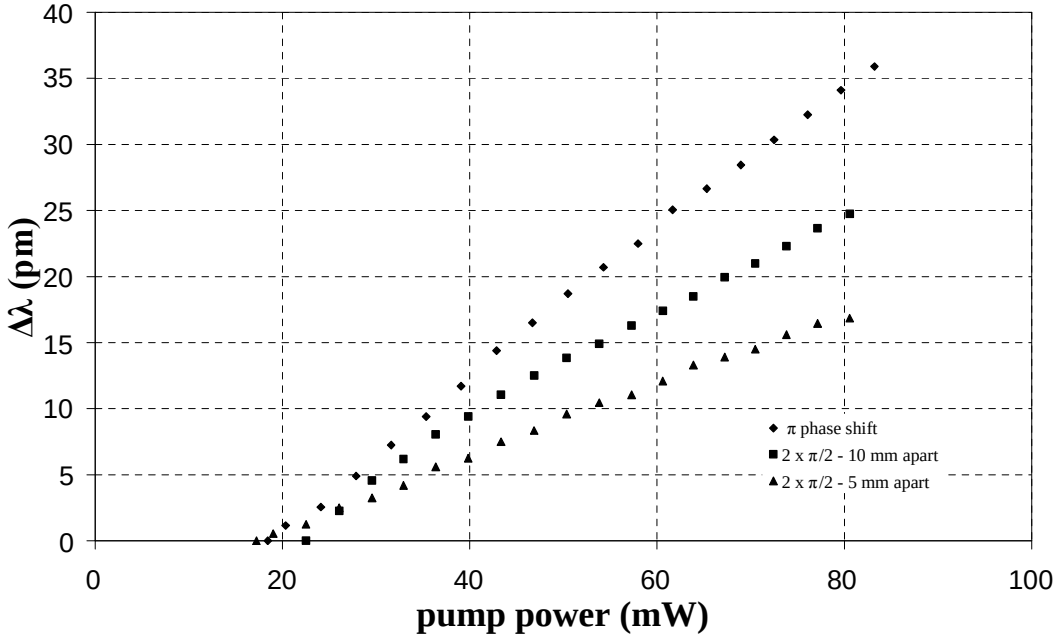
Δλ (pm)
pump power (mW)
π phase shift
2 x π/2 - 10 mm apart
2 x π/2 - 5 mm apart

(a)

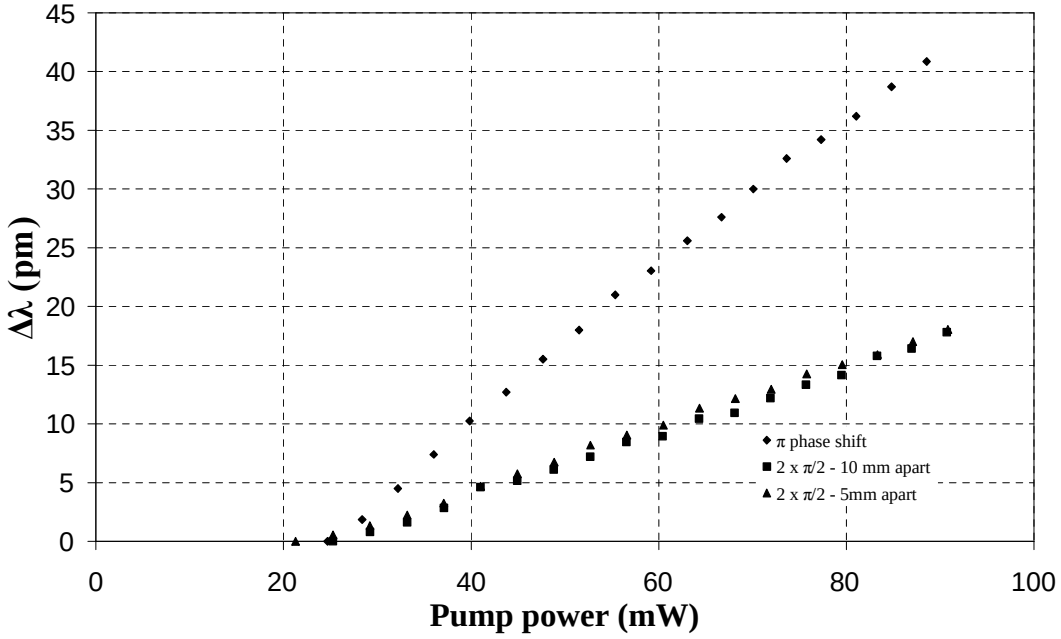
Δλ (pm)
Pump power (mW)
π phase shift
2 x π/2 - 10 mm apart
2 x π/2 - 5mm apart

(b)

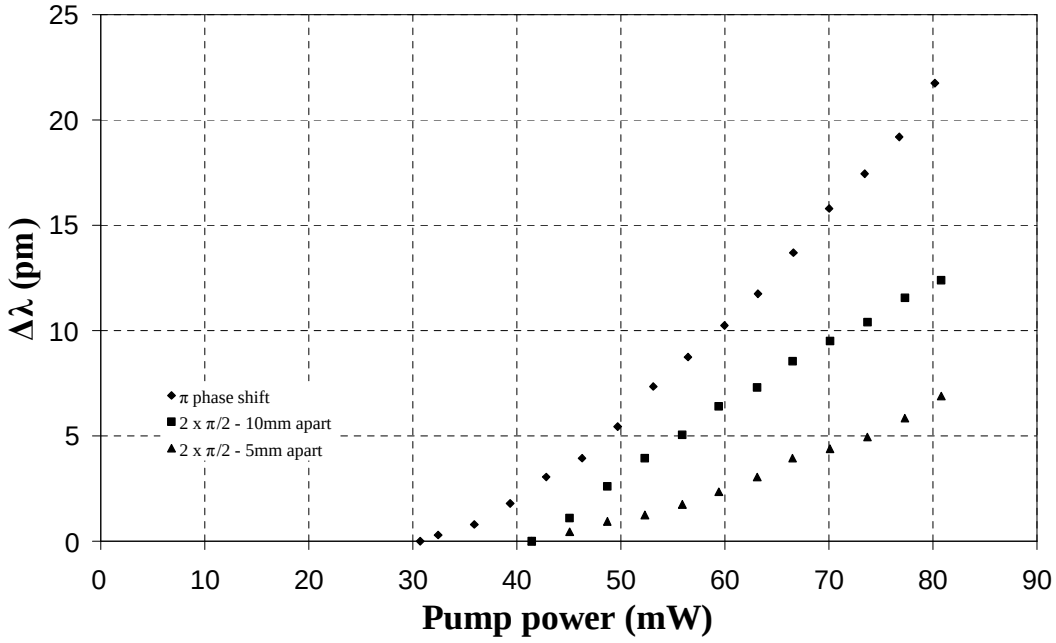

(c)

Figure 4.14: *Laser wavelength versus pump power of the single and two discrete phase shifts in (a) backward-, (b) forward- and (c) dual- pumping configurations.*

A lasing wavelength reduction of 30% and 50% was observed in the double phase shifts lasers of the 10 mm and 5 mm apart designs for the backward pump. Both double phase shifts lasers showed a reduction of ~60% for the forward pumping configuration. For the dual pumping configuration, a nearly 70% reduction in the wavelength shift was observed in the 5 mm apart phase shifts design and 40% in the 10 mm apart phase shifts design. This suggests that there was some intra-cavity intensity contributing to the wavelength shift of the lasers.

4.3.4 RIN of the lasers

It is important to observe the linewidth characteristics as well as the lasing wavelength shifts of the lasers, but it is also simultaneously important to examine the stability of the lasers due to the intra-cavity intensity. The RIN was measured with the signal analyser. Figure 4.15 shows the RIN of the lasers, measured at the relaxation oscillation frequency, as a function of output power.

In the backward pumping configuration (a), the ROF of these lasers was about the same for the given DFB power, but the RIN peak of the 10 mm apart phase shifts design was the highest and then levelled off with the single phase shift design. The 5 mm apart phase shifts design exhibits a lower RIN for output powers above 5 mW in the backward pumping configuration.

In the forward pumping configuration (b), the ROF of these lasers deviated from each other, with the largest oscillation in the single phase shift design. As a result the RIN of the single phase shift design was the lowest. The lowest ROF was observed in the 10 mm apart phase shifts design and hence, its RIN was the highest. The intensity noise of the single phase shift design was the lowest for all output power levels. Its RIN level 'approached below' -127 dB/Hz for powers above 14 mW. For the 5 mm apart phase shifts design, its RIN was at 125 dB/Hz at ~14 mW DFB power.

In the dual pumping configuration (c), the ROF for these lasers was about the same for the given output power. The single phase shift design was the lowest, -122 dB/Hz, and the 10 mm phase shifts design was the worst, -100 dB/Hz.

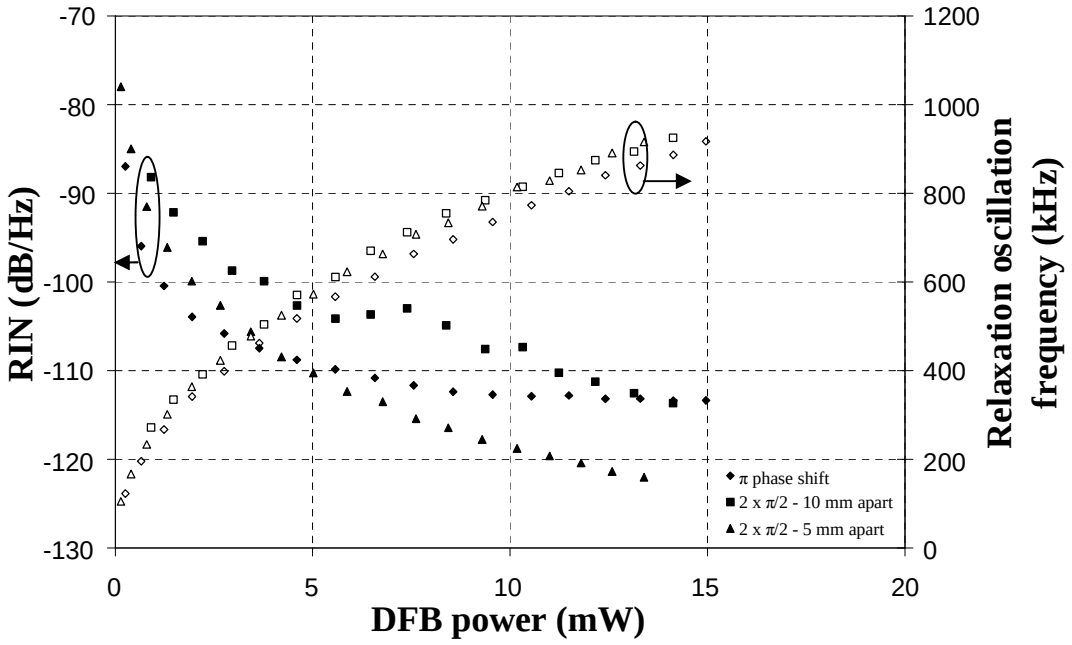

(a)

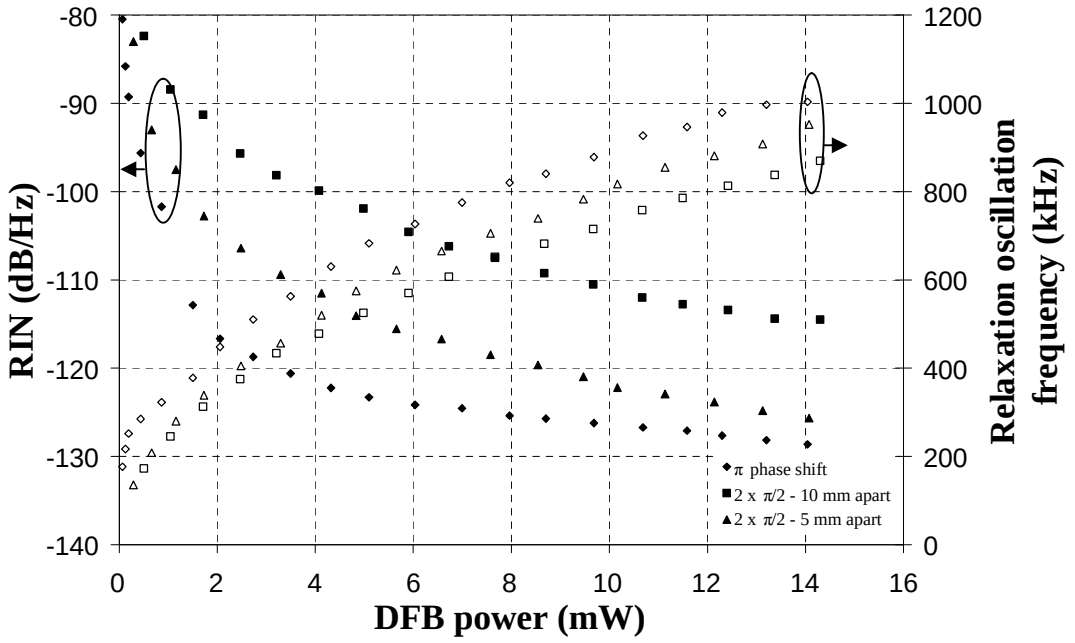

(b)

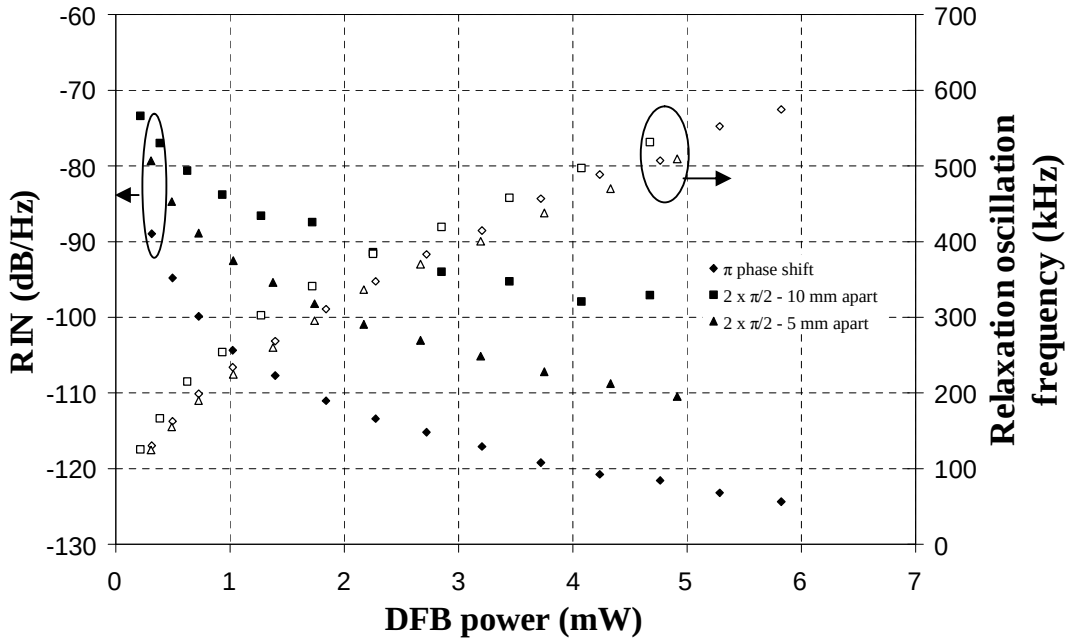

(c)

Figure 4.15: *The RIN characteristics of the single and two discrete phase shifts laser in (a) backward-, (b) forward- and (c) dual- pumping configurations.*

Overall, the RIN of the 5 mm apart phase shifts design was the lowest with a value of -122 dB/Hz at output powers of 13 mW in the backward pumping configuration. The

RIN of the single phase shift design was the lowest in the forward pumping configuration with a value of -127 dB/Hz at a DFB power ~14 mW. The reason for this amplitude noise behaviour is not yet fully understood.

4.4 Conclusion

In this work, we investigated the MOPA configuration and lower coupling coefficient designs as suggested by the analytical model for reducing the laser linewidth. The step-apodised design was fabricated to compare with the performance of the standard DFB fibre laser. The intensity profile of the single phase shift design is non uniform, as high intensity builds up around the phase shift and causes a variation in the refractive index and hence, lasing wavelength. The 2 x $\pi/2$ phase shift was designed to investigate the intra-cavity effect of the laser as well as the laser linewidth.

The laser linewidth of ~14 kHz was observed when the DFB laser was in-band pumped with a pump wavelength of 1480 nm. With the MOPA configuration, the output of the laser was amplified to ~30 mW with a net gain of ~15 dB. Its characteristics followed exactly the DFB laser itself, apart from a slight increase in laser wavelength of ~1.4 pm with a 130 mW pump power.

The laser linewidths of κ~200 m^{-1}, κ~150 m^{-1} and κ~100 m^{-1} and a step-apodised design were experimental investigated. Its linewidth was configuration dependent. For κ~200 $m^{-1}$and κ~150 m^{-1}, the linewidth was increased as DFB power increased. The laser linewidths of κ~100 m^{-1} followed the inverse power rule that was predicted by the Schawlow-Townes formula, but its magnitude was a few orders higher than predicted. This is due to the low reflectivity of the cavity and the corresponding operation of the laser near the laser threshold, which is much higher than the others. It had the narrowest linewidth at output powers above 1.8 mW, in the backward pumping configuration. In the forward pumping configuration, the narrowest linewidths were observed in κ~100 m^{-1} at an output power of 2.6 mW and κ~150 m^{-1} at an output power of 0.1 mW. The narrowest linewidth was observed for κ~150 m^{-1}

in the dual pumping configuration. The laser efficiencies of κ~100 m^{-1} were the lowest due to the weak optical feedback. The efficiencies of κ~150 m^{-1} and κ~200 m^{-1} were similar. The fundamental thermal noise contributed to the laser linewidth at low pump levels and was reduced by increasing the L_{eff}, as observed in the dual pumping configuration with κ~150 m^{-1} and κ~200 m^{-1}. We also observed that the laser wavelength shift is less with longer L_{eff}, i.e lower κ value. This is because the mode field volume increases with L_{eff} and hence reduces temperature raise in the fibre. Consequently, the refractive index change is lower and caused a decrement in lasing wavelength shift.

The 2 x π/2 phase shift DFB laser with phase shifts located at 5 mm and 10 mm apart has shown a reduction in lasing wavelength shift as compared with the single phase shift design for similar laser efficiencies. This suggests that the laser wavelength shift was not only due to the absorbed pump power but was also affected by the signal intensity distribution in the cavity. We also observed a decrease in the laser linewidth with the 5 mm apart phase shifts laser.

4.5 References

[1] C. Alegria, Y. Jeong, C. Codemard, J. K. Sahu, J. A. Alvarez-Chavez, L. Fu, M. Ibsen, and J. Nilsson, "83-W single-frequency narrow-linewidth MOPA using large-core erbium-ytterbium Co-doped fiber," *IEEE Photonics Technology Letters*, vol. 16, pp. 1825-1827, 2004.

[2] M. Sejka, P. Varming, J. Hubner, and M. Kristensen, "Distributed feedback Er^{3+}-doped fibre laser," *Electronics Letters*, vol. 31, pp. 1445-1446, 1995.

[3] E. Ronnekleiv, M. Ibsen, M.N. Zervas, and R. I. Laming, "Characterization of fiber distributed-feedback lasers with an index perturbation method," *Applied Optics*, vol. 38, pp. 4558-4565, 1999.

[4] K. Yelen, L. M. B. Hickey, and M. N. Zervas, "A new design approach for fiber DFB lasers with improved efficiency," *IEEE Journal of Quantum Electronics*, vol. 40, pp. 711-720, 2004.

[5] G. A. Cranch, M. A. Englund, and C. K. Kirkendall, "Intensity noise characteristics of erbium-doped distributed-feedback fiber lasers," *IEEE Journal of Quantum Electronics*, vol. 39, pp. 1579-1587, 2003.

[6] J. E. A. Whiteaway, B. Garrett, G. H. B. Thompson, A. J. Collar, C. J. Armistead, and M. J. Fice, "The static and dynamic characteristics of single and multiple phase-shifted DFB laser structures," *IEEE Journal of Quantum Electronics*, vol. 28, pp. 1277-1293, 1992.

Chapter 5

Development of an Improved Efficiency Thulium-doped DFB Fibre Laser for 2 μm Applications

---

Development of laser sources operating around the 2 μm 'eye-safe' region has started to gather pace, mainly driven by a number of applications in areas such as medicine [1], Light Detection And Ranging (LIDAR) [2], remote gas sensing [3] and spectroscopy [4-7]. Thulium (Tm^{3+}) is a particular attractive ion for such applications since it has an emission spectrum ranging from ~1.7 to 2.1 μm. This spectral range covers the absorption bands of water, methane, carbon dioxide and nitrous oxide. In fact, recently, a single-frequency Tm^{3+}-doped fibre laser operating at 1735 nm, with maximum output power of 1 mW for 590 mW of launched pump power at 800 nm, was demonstrated [8]. However, this laser suffered from very moderate efficiency and low output power. It was probably limited by the quantum efficiency as well as

the three-level operating system which requires at least half of the ions to be excited to obtain population inversion.

In this work, a continuous-wave (CW), DFB, single-frequency, thulium (Tm^{3+}) co-doped with antimony (Sb^{3+}), fibre laser operating at 1836 nm was realised and characterised. This is the longest reported operating wavelength of a DFB fibre laser [9, 10]. The laser itself shows an output power of 5 mW and, with the aid of a MOPA, the power of the DFB fibre laser was amplified to 345 mW. In this chapter, the photosensitivity of the fibre, that is required for the UV Bragg gratings written into the core, and the design and characterisation of the laser is discussed. The pump-bands for Tm are also reviewed. Here, the DFB fibre laser was in-band pumped at 1565 nm in the forward pumping configuration and then it was configured in the MOPA to amplify the signal power. Then, the DFB laser was configured in the intracavity pumping scheme by using a cladding-pumped Raman fibre laser at 1660 nm. The possible applications of this DFB laser operating in this wavelength region are also discussed.

5.1 Review of pump absorption bands of Tm^{3+} -doped fibre being used

This section reviews the pump absorption bands that have been used to pump Tm^{3+}-doped fibre lasers and single-frequency DFB fibre lasers. Three main pump bands in a Tm^{3+}-doped silica fibre are available to achieve lasing at 1.7 to 2.1 μm: $^3F_4$, $^3H_5$ and $^3H_4$. Tm has laser transition bands at 0.47, 1.47, and 1.9 μm, as seen in Figure 5.1. Pumping wavelengths of 0.79, 1.09 and 1.57 μm have been demonstrated for 1.9 μm Tm^{3+}-doped silica fibre lasers [11-13]. Pumping at 0.8 μm, transition $^3H_6 \rightarrow {}^3F_4$, has been used to pump a length of 27 cm Tm^{3+}-doped fibre to produce a CW laser at 1.96 μm with an output power of 2.7 mW [11]. The slope efficiency of this laser was 13%. For the transition $^3H_6 \rightarrow {}^3H_5$, a Yb^{3+}-doped silica double-cladded fibre laser, operating at 1.1 μm, can be used as pump source, this has been demonstrated by [13]. The maximum output power achieved was 1.1 W, with a fibre length of 0.42 m, and

the slope efficiency was 27% (quantum efficiency 58%). However, pumping into the $^3H_5$ level of the Tm^{3+} produces excited state absorption, in which energy is lost through $^3F_{2,3}$ and $^1G_4$ excited levels [13, 14]. Direct pumping into the upper level ($^3H_4$) of the 1.9 μm with the Er^{3+}-doped fibre laser at 1.57 μm has also been demonstrated [12]. A slope efficiency of 71% (quantum efficiency 79%), with an output power of 21 mW, was obtained from a 4 m long fibre. An even longer pump wavelength of 1.63 μm has been used to pump Tm^{3+}-doped fluoride fibre [15]. The output power of the 6 m long fibre laser was 5.5 mW, with a pump power of 8 mW. Slope efficiency of 81.9% (quantum efficiency 84%) was obtained. In this pumping scheme, Tm ions are directly excited to the $^3H_4$ level of the 1.9 μm transition, in which the photon conversion efficiency is much higher than with 0.8 or 1.06 μm pumping. Whereas with pumping wavelengths of 0.79 and 1.06 μm, Tm ions pumped to $^3F_4$ or $^3H_5$ levels then rapidly phonon-decay to the upper level of 1.9 μm. For the Tm^{3+}-doped DFB fibre laser, demonstrated with a pump wavelength of 790 nm, lasing at 1735 nm has been demonstrated with a slope efficiency of 0.2% [8]. This efficiency was probably limited by the quantum efficiency and reduced because the three-level system lases from the $^3H_4$ level to the ground $^3H_6$ level, which requires at least half of the thulium ions to be excited to obtain population inversion. In this work, we demonstrate in-band pumping of the DFB fibre laser at 1565 nm, in which the theoretical quantum efficiency limit is ~85%. With this pump wavelength the Tm ions are excited to the upper laser level $^3H_4$ directly, so the photon conversion efficiency for 1.8 μm emission will be higher than with the other pumping schemes.

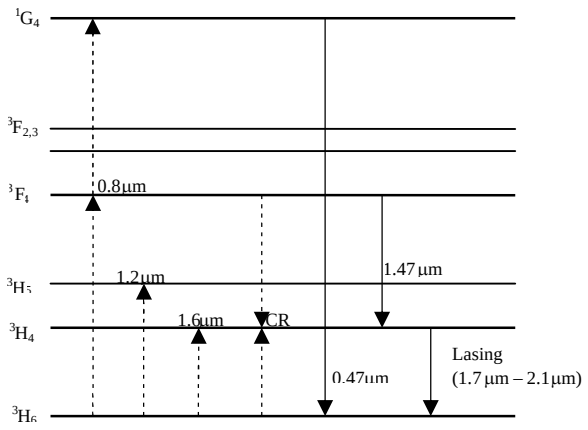

Figure 5.1: *Schematic diagram of the Energy-level diagram of Tm^{3+} in silica [16], showing the pump, absorption, and emission bands*

5.2 Tm^{3+}-Sb co-doped alumino-silicate fibre

The details of the Tm^{3+} co-doped Sb fibre used for constructing the DFB laser, such as the fabrication of the fibre, fibre photosensitivity and photostabilisation of gratings inscribed, is described in this section. The fibre used for fabricating the DFB laser, the same as that reported in [17], was made in the ORC by the modified chemical vapour deposition (MCVD) method. Both thulium (Tm) and antimony (Sb) were incorporated into the fibre-preform through the solution doping technique during the preform preparation. Al^{3+} was also added to the solution to homogenize the spatial distribution of the dopants. The synthesized silica preform was drawn into a fibre, with an outer diameter of 120 μm, and the numerical aperture (NA) was around 0.16. The cut-off wavelength of the fibre was designed at 1.55 μm, the pump and signal wavelengths used were both single-mode at this cut-off wavelength. The concentration of Tm and Sb is 1000 ppm and 800 ppm respectively. This fibre is germanium-free, the only photosensitive material for UV written Bragg gratings is Sb. The gain medium of the DFB laser was provided by Tm. The small signal absorption (background loss) of the gain fibre was obtained using a cut-back technique, with a broadband semiconductor optical amplifier source operating from ~1480 to 1620 nm, and it was found to be ~0.46 dB/cm at 1565 nm.

5.2.1 Photosensitivity of the fibre

This section briefly reviews photosensitization of different types of glass hosts and the experimental set-up used to study the photosensitivity that can be achieved by our Tm^{3+}-Sb co-doping fibre, as it is essential for realising UV written Bragg gratings in the core for cavity feedback of our DFB lasers. Most of the photosensitivity studies of the fibre for photoinduced refractive index changes have so far concentrated on germano-silicate (Ge/Si) core optical fibres. Enhancement of photosensitivity in Ge/Si fibre has been reported by co-doping with boron [18] or tin [19], as well as by loading the fibre with hydrogen prior to grating writing with UV [20]. The loading process involved the diffusion of H_2 molecules into the fibres at low temperatures

and high pressures. When exposed to UV, the dissolved H_2 reacted at the Si-O-Ge sites resulting in the formation of Si-OH and oxygen deficient Ge defects which contribute to the index changes. However, the Ge/Si glass hosts limit the incorporation of large concentrations of rare-earths which can impose problems such as clustering [21]. In order to avoid energy being transferred to the neighbouring ions, i.e. ion pair-induced quenching, the concentration of the rare-earth has to be low and hence the pump absorption is low which leads to poor laser efficiency. Recently, antimony (Sb) -doped optical fibre, made by sol-gel techniques, was found to be highly photosensitive achieving refractive-index modulation growth rates six times higher than that of the equivalent Ge-doped fibres [22].

The photosensitivity of our fibre was tested by writing uniform Bragg gratings and then by analysis of the transmission spectrum. The gratings were written using a frequency doubled Ar^+-ion laser operating at 244 nm, with a beam-intensity of 300W/cm^2, to operate strictly in a type I regime, where the refractive index change is linearly proportional to the fluence. The fibre was hydrogen loaded at 200 atm for 2 weeks at 70 ˚C prior to writing UV Bragg gratings, so as to enhance the photoinduced refractive index changes, using the same technique as in [20]. The index-modulation of this hydrogen-loaded fibre was 15 times higher than the unloaded fibre as reported in [17]. After the inscription of the gratings, they were annealed at 100 ˚C for 24 hours to outgas any residual hydrogen in the fibre and to stabilise the index-modulations. The experimental set-up for testing consists of a broadband semiconductor source and an OSA (Advantest Q8384 optical spectrum analyser) to measure the transmission spectrum of the grating. One end of the grating was spliced to the output of the broadband semiconductor source, having a 3-dB bandwidth of 60 nm ranging from 1500-1560 nm, and the transmission spectrum was analysed with the OSA from the other end of the grating. The coupling coefficient was extracted from the reflectivity of the grating using the coupled-mode theory. The reflection coefficient is given by [23]

$$R = \tanh^2(\kappa L)$$

Where L is the length of the fibre grating and κ is the coupling coefficient. The reflectivity of the grating was determined from the transmission spectrum as reflection = 1 – transmission. It was much simpler to use the transmission spectrum

to determine the reflectivity of the gratings, as the maximum transmission loss through this can be directly observed from the transmission spectrum. From the coupling coefficient, the index modulation change, Δn, was obtained by the following equation [23]

$$\kappa = \frac{\pi \Delta n \, \eta}{\lambda_B}$$

where η is a transverse overlap integral of the modal distribution with gratings ~0.85. The Bragg wavelength (λ_B) was at 1597 nm. The DFB fibre laser operating wavelength was designed to be at 1836 nm. However, due to the limitation of the OSA, the maximum wavelength of the OSA is 1750 nm, the grating was written at 1597 nm for the photosensitivity studies. The measured index modulation change is then used to calculate κ at 1836 nm.

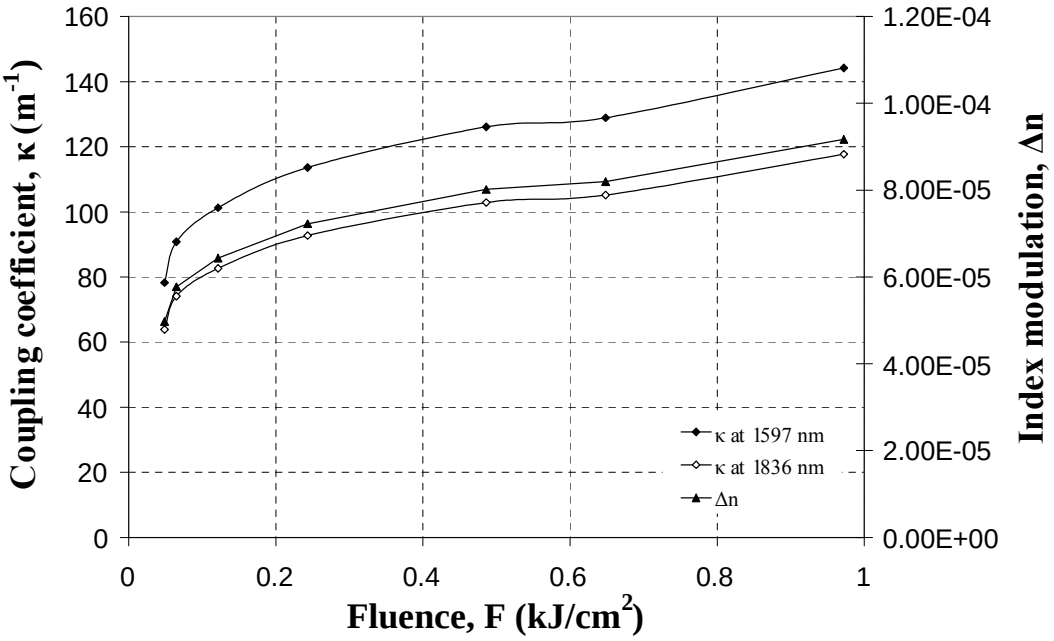

Figure 5.2: *Measured index growth and coupling coefficient at 1597 nm against 244 nm CW-fluence and the calculated coupling coefficient at 1836 nm.*

The index growth of the fibre was studied at different fluences. Figure 5.2 shows the measured index growth and the coupling coefficient plotted against fluence, together with the calculated κ at 1836 nm. The index modulation change of ~$1x10^{-4}$ was obtained at a fluence of ~1 kJ/cm^2. The UV induced refractive index changes in this

hydrogen-loaded fibre can be explained in the same way as [20], i.e. the formation of Si-OH and oxygen deficient Ge defects have been involved with index change for the hydrogenated Ge/Si fibre. For our fibre's refractive index changes, these could also be due to the formation of Si-OH and oxygen deficient Sb defects.

As for our 5-cm long Er^{3+}-Yb^{3+} co-doped DFB lasers, a total grating strength of 10 was used in which the optical feedback in the cavity was high and resulted a better laser efficiency as compared with a grating strength of 5 and 7.5, observed in Section 4.2. In this case, due to the low concentration of Tm^{3+} ions, i.e. low gain, the length of the DFB laser is increased to 8 cm. The maximum index growth of this fibre is ~9 x 10^{-5} and the maximum κ can be obtained at 1836 nm is ~120 m^{-1}. With this maximum κ and a fibre length of 8 cm, the grating strength of 9.6 can be achieved.

5.2.2 Thermal stability of the Sb Bragg grating

Temperature stability of the Bragg grating was assessed, it was annealed at temperature increments of 100 °C starting at 200 °C until the reflectivity of the grating was completely erased. At each temperature the grating was annealed for 24 hours to be able to analyse the stabilised level of the induced index-modulations. The grating was spliced to the output of the broadband semiconductor source and placed in an oven, and the transmission spectrum of the grating was analysed with the OSA. The temperature stability of the gratings with coupling coefficients (κ) of 140 m^{-1} and 90 m^{-1} were tested. Figure 5.3 summarises these results through a plot of the coupling-coefficient, normalised against the coupling coefficient observed after the initial annealing at 100 °C. It is clearly indicated that the stronger the initial grating, the greater the value of coupling coefficient that remains after annealing. The reflectivity decays as gratings are annealed at elevated temperatures, this is due to the dynamics of trapping thermally activated carriers in a distribution of defect sites, which occurred during gratings' writing, returning to their initial sites under high-temperature excitement [24].

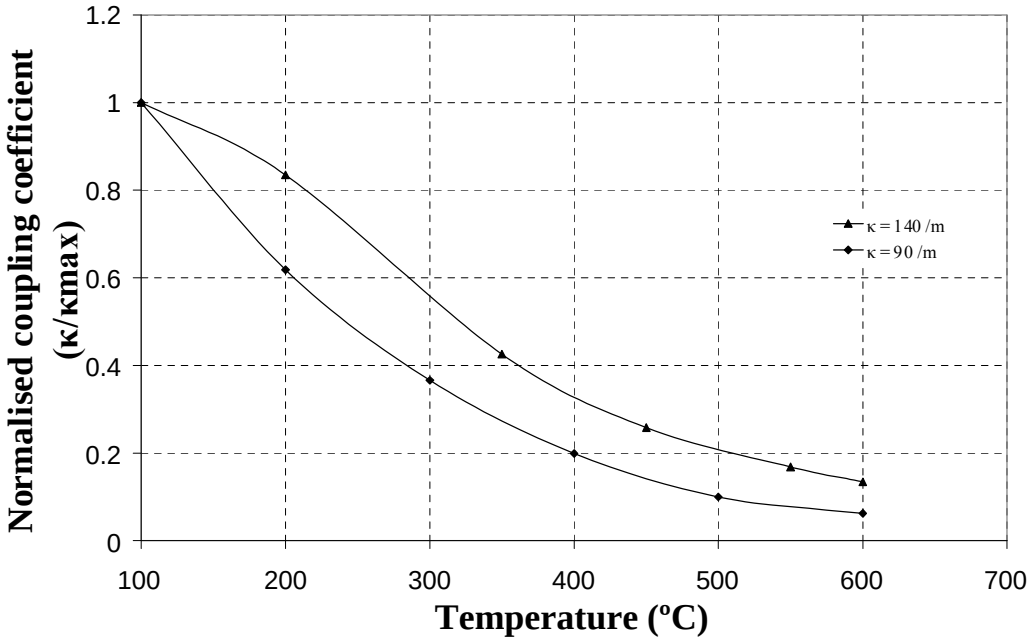

Figure 5.3: *Thermal decay of the refractive index modulation of the FBG in the Sb co-doped fibre.*

At 200 °C the coupling coefficient of the grating, with κ~140 m^{-1}, was maintained at ~ 80% of its initial strength, whereas the strength dropped to ~ 60% in κ~90 m^{-1}. At 600 °C, the grating with κ~90 m^{-1} remained at ~5%, and for κ~140 m^{-1} remained at ~10%, of its initial strength. Hence, gratings with a higher coupling coefficient are more resistant to high temperature. The gratings in the Sb co-doped fibre show a slow decay in grating strength above 500 °C, and would be able to endure at least up to 700 °C. This is comparable with the grating thermal stability of the germanosilicate and tin-silicate fibres, being completely erased at 680 °C and enduring at 780 °C respectively [19]. The high temperature sustainability of the grating written in this fibre is another important feature for high temperature sensing applications e.g. gaseous emissions in volcanic sites (above 150 °C), in oil field etc.

5.3 The Structure of the DFB fibre laser

The Tm^{3+}-Sb co-doped fibre, as mentioned in Section 5.2, was used for constructing the DFB fibre laser. The designed operating wavelength of the DFB was at 1836 nm which is at the peak emission of the Tm. The laser cavity was based on Bragg

gratings, that are UV written by the phase-mask technique [25], with a period of Λ = 636 nm. The DFB grating is written directly into the core of the fibre and is 8 cm in length, with a $\lambda/4$ phase-shift located 4.8 mm from the mid-point of the grating. This asymmetry enables the output power to be emitted predominantly from the end of the laser closest to the phase shift. Single polarisation operation of the laser was obtained by writing the phase-shifted gratings with CW UV light at 244 nm, polarized perpendicular to the propagation axis of the fibre, as reported in [26]. After writing, the grating was annealed for 24 hours at 100 ºC to stabilise the index modulation. The writing time of the grating was 3 minutes with a fluence of ~1 kJ/cm^2. The resulting coupling coefficient of the grating was 120 m^{-1}, yielding a total grating strength of 9.6. The DFB laser is operated in the forward direction and the output characteristic is determined in the following section.

5.4 Experimental set-up and result of the DFB laser

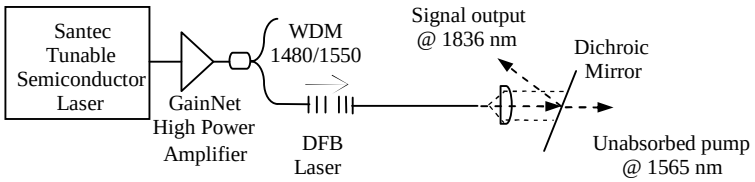

Figure 5.4: *Experimental configuration of the single-frequency DFB fibre laser, in a forward pumping scheme.*

Figure 5.4 shows the experimental set-up of the DFB fibre laser MOPA configuration. The source used to pump the laser was a 9 mW Santec, tunable semiconductor source, operating at 1565 nm, which was subsequently amplified to 1.4 W, by a high-power amplifier from SPI Lasers. The output of the amplifier was then coupled into the DFB laser, via a WDM, in order to reduce the back reflection of the source. The fibre laser is operated in a forward pumping configuration in which the pump copropagates with the laser output. A dichroic mirror, with a high reflectivity at around 1.8 μm and having a high transmission at the pump wavelength, was then used to extract the forward propagating signal. The lasing wavelength was designed to be at 1836 nm, which was confirmed and measured with a Bentham

M300 monochromator, having a resolution of 0.5 nm. Figure 5.5 shows the output power of the 1836 nm DFB fibre laser operated on it own. The laser has a threshold power of 95 mW with respect to the absorbed pump power and has a maximum output power of ~5 mW, with a slope efficiency of 1%, at a pump power of ~550 mW. One explanation for such a relatively low slope efficiency could be related to the background loss of the silica-based fibre at wavelengths longer than 1.8 μm [27]. The background loss in our fibre was ~0.7 dB/m. However, without Sb codoping, we usually get a background loss ~0.4 dB/m [personal discussion with J.K. Sahu]. It suggests that the Sb co-doping increased the background loss by ~0.3 dB/m.

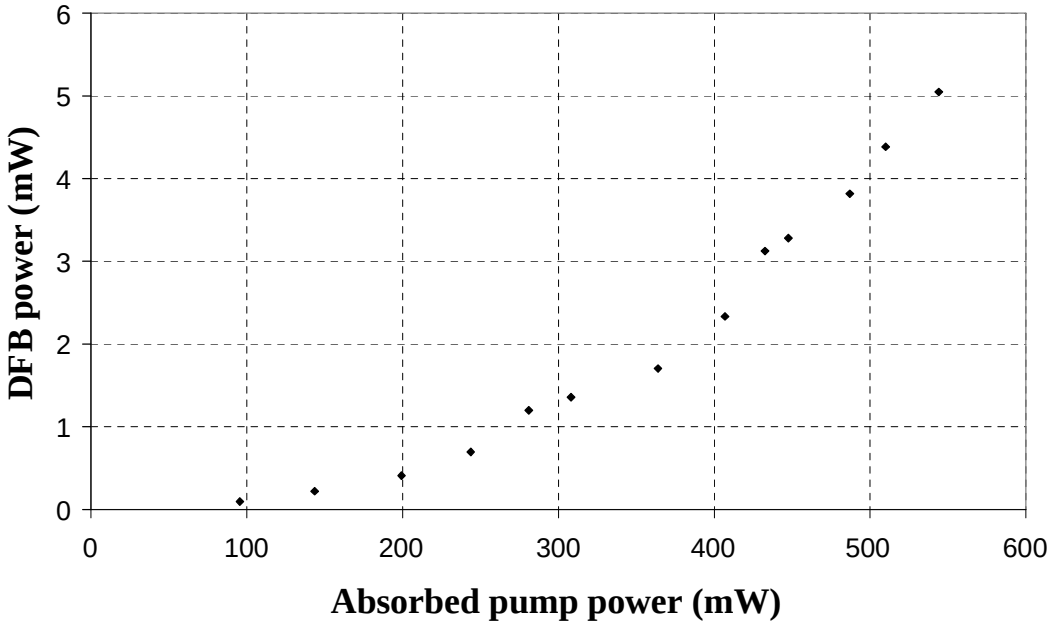

Figure 5.5: *Output of the single-frequency DFB fibre laser, at a wavelength of 1836 nm, as a function of absorbed pump power.*

Many applications require moderate power, low noise, narrow-linewidth sources for increased sensitivity and signal to noise ratio. However, due to the, in some cases, low gain, low material concentration, and associated low pump absorption in a short cavity, it might be necessary to boost the low output with an amplifier to reach a satisfactory power level. To do this, the master-oscillator power amplifier (MOPA) design was constructed to overcome the power limitation sometimes associated with short single-frequency fibre lasers. A typical combined laser and MOPA design

includes the short fibre laser and is followed by a length of amplifier fibre identical to that of the laser. It is a very simple configuration yet it still ensures that key characteristics of the laser, such as, for example, low noise and narrow-linewidth performance, are maintained [28-30].

5.5 DFB fibre laser with MOPA configuration and result

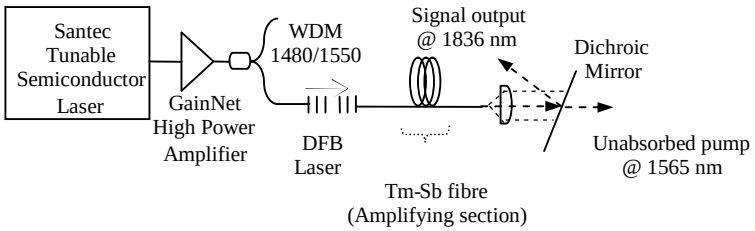

Figure 5.6: *Experimental set-up of DFB laser with MOPA configuration.*

The experimental configuration of the DFB MOPA laser is shown in Figure 5.6. The DFB fibre laser is spliced to an additional section of Tm^{3+}-Sb fibre used to amplify the signal output by utilizing the residual pump power not absorbed in the laser. The single-frequency operation of the DFB laser + MOPA was verified by using an in-house scanning Fabry-Pérot interferometer (FPI), with the plane mirrors used in the FPI cavity having a reflectivity of 3% at the lasing wavelength. The separation of the mirrors was 17.3 mm, giving a free-spectral range (FSR) of 8.67 GHz. The possible polarisation effect that could be present in this laser is the orthogonal linear polarisation mode splitting of this fibre which is calculated to be ~1.13 GHz. Figure 5.7 shows a scan over one FSR and confirms that only one longitudinal mode, with no other polarization or longitudinal modes, is present in the MOPA DFB fibre laser. From our experience in fabricating asymmetrical DFB fibre lasers in the region of 1550 nm, the typical linewidth of the lasers is a few tens of kilohertz, although it is difficult to measure this value accurately here due to the equipment limitations. We believe that the linewidth of this laser will be close to this value, not least due to the 8-cm length of the laser.

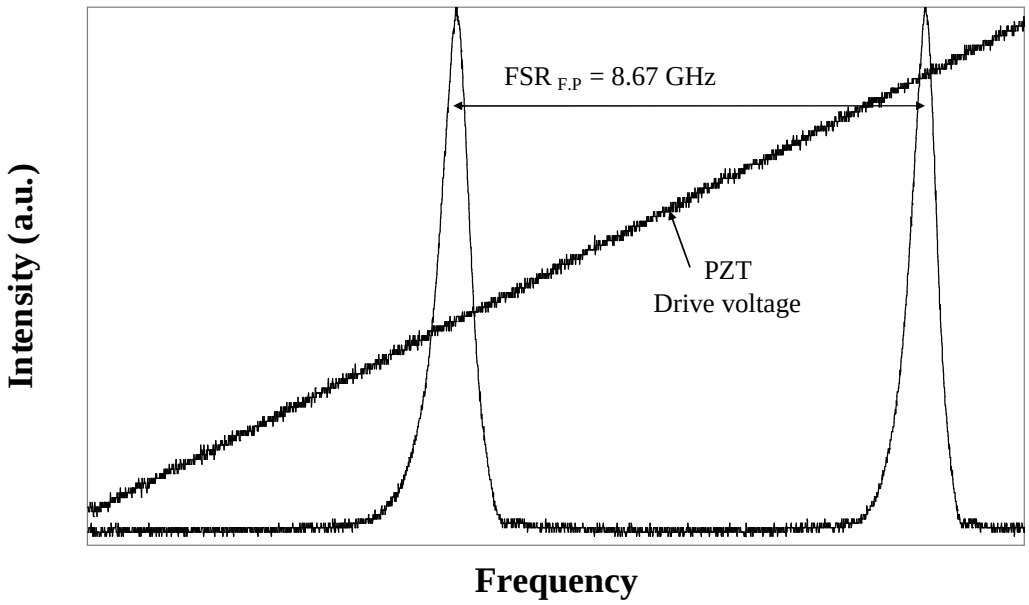

Figure 5.7: *Single-frequency operation of the DFB fibre laser verified by scanning Fabry-Perot interferometer with FSR of 8.67 GHz.*

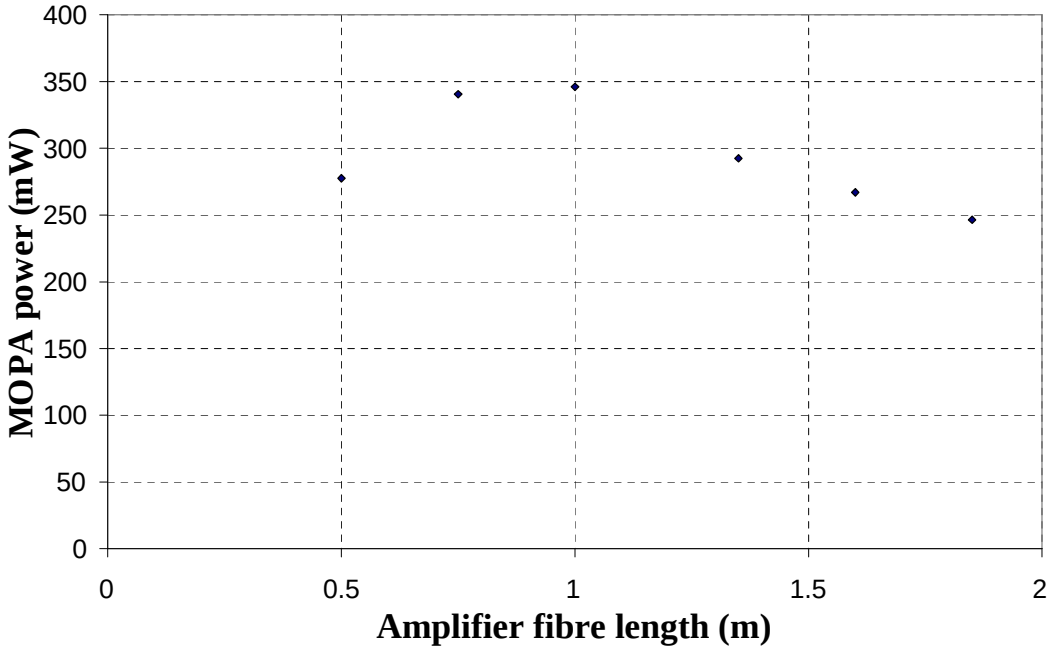

Figure 5.8: *Dependence of the output laser power for a constant pump power of 1.4 W on active fibre length.*

In order to investigate the optimal amplifier fibre length that gives a maximum MOPA power for a constant pump power of 1.4 W, a length of 1.85 m of amplifier

fibre was started with. The fibre was then cut short and the power was measured. The results are shown in Figure 5.8. It showed that the dependence of the MOPA output power on the active fibre length. It can be seen that a maximum power of 345 mW was obtained with a fibre length of 1-m. As the fibre length increases, the power tends to decrease. The decrease in output power with increasing fibre length is due to reabsorption of the laser signal. With the aid of a length of 1-m amplifier fibre, the output of the DFB at 5 mW was amplified to 345 mW, i.e., a net gain of ~18 dB.

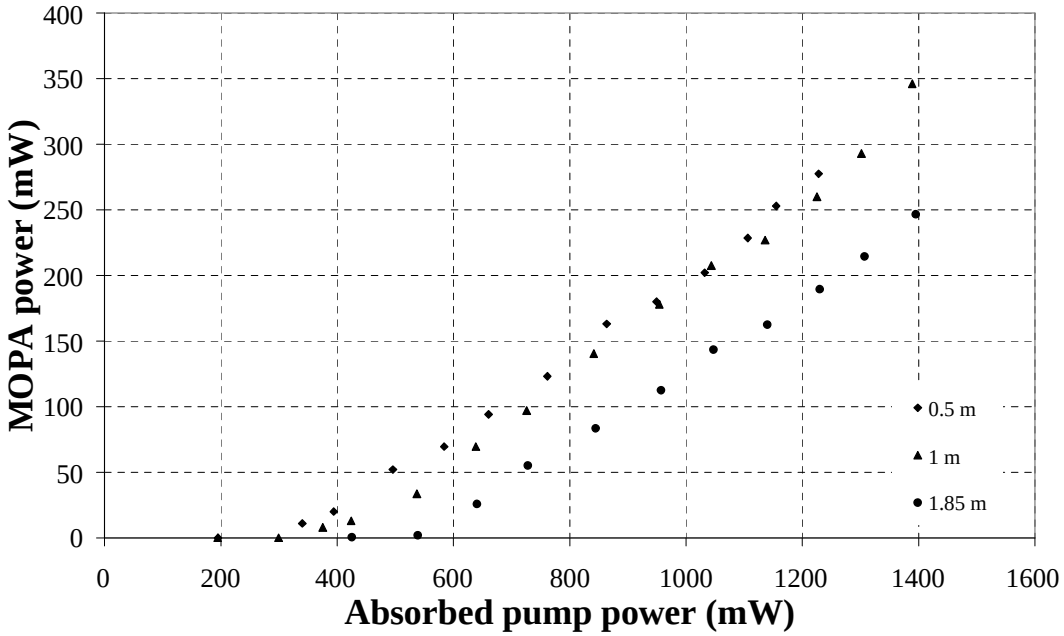

Figure 5.9: *MOPA output of the DFB fibre laser against absorbed pump power at 1565nm, for an active fibre length of 0.5, 1 and 1.85 m.*

The threshold and output powers of the DFB laser with MOPA characteristics for active fibre length of 0.5, 1 and 1.85 m are plotted, in Figure 5.9, as a function of absorbed pump power. Slope efficiencies of the MOPA at 0.5, 1 and 1.85 m of active fibre length, relative to the absorbed pump power, were ~28%, 34%, and 26%, respectively. All the pump power has been absorbed in the 1 and 1.85-m active fibre length as seen in the figure above. At 0.5-m active fibre, the unabsorbed pump power was ~170 mW.

5.6 Intracavity pumping set-up and result

Because of the low concentration of the Tm^{3+}-Sb co-doped DFB fibre laser, there is a low pump absorption and, as a consequence, low output power results. In this section an intracavity pumping scheme is described that is designed to improve the output power of the DFB laser, as compared with direct pumping configuration. This is by placing the DFB laser inside a high reflective cavity of the pump laser, so that the power that circulates inside the cavity is much greater than the output power. In Ref [31], the 10 cm long Er^{3+} fibre DFB laser was placed inside the cavity of the Yb^{3+}-doped fibre laser operated at 975 nm, the output power from the DFB laser has shown an improvement of threefold as compared with the direct pumping configuration. In this set-up, the Tm^{3+}-doped DFB laser was placed inside the cladding-pumped Raman fibre laser's cavity operating at 1660nm so as to recycle the unabsorbed pump power inside the cavity. The estimated absorption loss of the Tm^{3+}-Sb co-doped fibre at this wavelength, from Figure 5.10, is ~0.4 dB/cm which is about the same as at 1565 nm (~0.46 dB/cm).

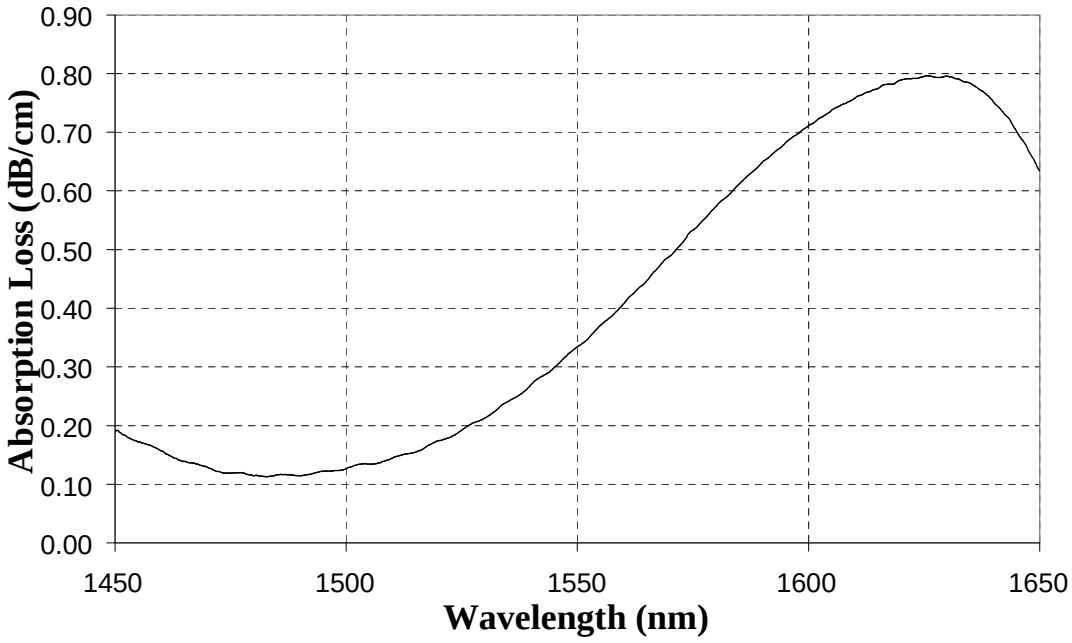

Figure 5.10: *Absorption loss of Tm^{3+}-Sb co-doped fibre.*

The experimental configuration for the intracavity pumping scheme is shown in Figure 5.11. The cladding-pumped Raman fibre laser used was the same as reported in [32]. Basically, it consisted of a high-power continuous-wave pump source at 1552 nm and a 1.2 km length of double-cladding Raman fibre (DCRF). The pump source for the Raman fibre laser was a two-stage fibre master-oscillator power-amplifier (MOPA) based on Er^{3+}-Yb^{3+} co-doped fibre amplifiers (EYDFAs). The seed source of the MOPA was a high-power tunable fibre ring laser which used a commercial 2W EYDFA from SPI Lasers and a tunable fibre Bragg grating. The power of the ring laser was set at 1.4 W, at a wavelength of 1552 nm, and it was then free-space coupled through a pair of lenses and a dichroic mirror into a 4-m long EYDFA. The 972 nm pump of the EYDFA, together with the 1552 nm signal, is launched into the EYDF so that the fibre output end can be free-space launched into the DCRF laser. The Raman laser cavity consisted of a FBG, with 80 % reflectivity at 1660 nm, written in the core of the DCRF at the 1552 nm launch end and the laser output coupler was formed by, a flat cleave in the SMF-28 fibre at the output end of the DFB, the 4% Fresnel reflection. The other end of the DFB laser was spliced to a piece of double-cladding fibre (DCF) to absorb the backward propagating radiation of the DFB laser.

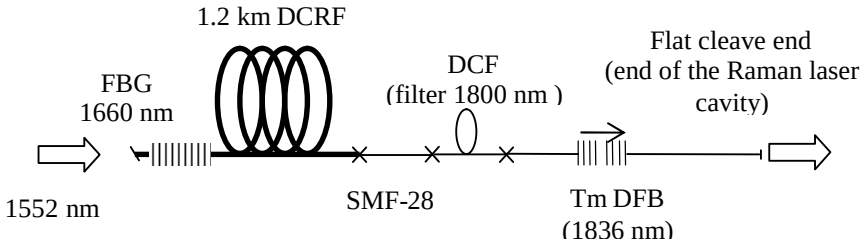

Figure 5.11: *Experimental configuration for intracavity pumping.*

The output of the laser was observed with an automatic monochromator, having a resolution of 3 nm, which is computerised. From the scans of the monochromator, it was difficult to obtain an accurate picture of the DFB as the cavity was unstable in time. In addition, it was not possible to know the 1660 nm power being absorbed by the DFB as it was not possible to measure the power in the cavity. Figure 5.12 shows

the spectrum obtained with the monochromator. The total power, measured with a thermal power meter at the end of the Raman laser cavity, was 18 W. This was a combination of the Raman pump, Raman laser and DFB laser powers. With the aid of "Origin", a mathematics software program to perform the integration, the DFB power was estimated to be ~144 mW. Basically, the software calculated the areas of the spectrum and then the total power was divided accordingly.

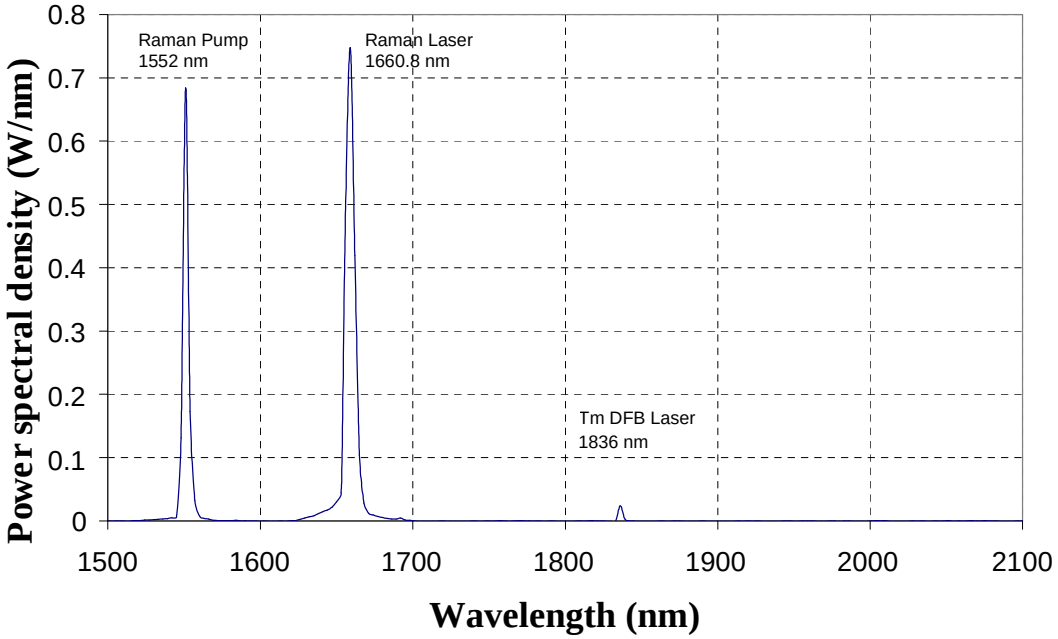

Figure 5.12: *Experimental spectrum obtained for 100 W of 972 nm pump power/ 25 W of 1552 nm.*

5.7 Possible applications of the single-frequency DFB fibre laser at 1.7 – 2.0 μm

Lasers operating at a wavelength around the 2 μm eye-safe region have been extensively used for the development of instrumentation for environmental or industrial monitoring applications [3-7]. Methane (CH_4), carbon dioxide (CO_2) and nitrous oxide (N_2O) are important trace gases in the atmosphere as active greenhouse gases. These gases absorb the infrared radiation from the sun and trap the heat in the atmosphere and as a result are increasing the average temperature of the Earth. Rising temperatures may produce changes in weather, sea levels, and land use patterns, commonly referred to as "climate change." There are other applications in

the region such as in LIDAR [2] and also in medical fields due to the strong absorption of the 2 μm radiation in water and biological tissues. Incisions in porcine tissue and chicken breast have been demonstrated with a 1.98 μm CW Tm-doped silica fibre laser[1].

A number of research studies are being conducted to determine the isotope ratio of N_2O [4, 5] and CH_4 [5]. The isotope abundance ratio in the molecule reflects different production processes of the molecule and different transportation histories in the atmosphere. A laser-spectroscope was developed for N_2O isotope ratio measurements using 2 μm wavelength-modulated distributed-feedback diode lasers combined with a multipass cell. In this set-up, the centre wavelength of the lasers, stabilised to the centre of the selected absorption line, were made to travel different distances in the cell to compensate the large abundance differences. The isotope ratio is determined by comparing the ratio of the absorbencies for the selected absorption lines in the sample gas with that in the reference gas of known isotopic composition. In Ref [5], the DFB semiconductor lasers' wavelengths were fixed at the centre of the absorption lines of CH_4 and NO_2, around 1.7μm and 2μm respectively.

In Ref [3], a diode-laser spectrometer employed a single mode DFB diode laser at a wavelength of 1.999 μm, with a linewidth of about 10 MHz, for measuring the concentration of CO_2 and H_2O in gaseous mixtures. The spectrometer was built on two separate breadboards. For the first breadboard, a portion of the laser beam was directed into a Fabry-Pérot interferometer, which provided a precise frequency calibration of the laser frequency scans, and the remaining part of the beam was focused into a 10-m-long single mode fibre, by means of a lens, and transmitted to the second breadboard which contained a multiple reflection cell and an InGaAs photodiode. Then, the laser beam was collimated in air and into the cell. The transmitted beam was detected by the photodiode during continuous and periodic scans of the laser frequency over the absorption lines. However, this spectrometer involved some optics which is sensitive to the environmental vibration.

Another possible application of our DFB fibre laser operating wavelength is to use it as the source for the measurement of the second overtone of NO. A DFB diode laser

sensor at 1.8 μm has been developed for measuring the combustion-generated NO, such as in the emission from an aircraft [6]. The researchers were trying to determine the emission of NO, with emission levels below 40 parts in 10^6 by volume (ppmv), as this is the minimum requirement for a ground certificate of a new engine, for an aircraft during flight. The DFB laser had an output of 15 mW and the tuning range was from 1.8068 to 1.8106 μm. Due to the limited temperature tuning range of the DFB lasers, typically only several nanometers, it is necessary to specify the desired operation wavelength range to tolerance before fabrication. Figure 5.13 shows the calculated absorption spectrum obtained by Ref [6] for the second overtone band of NO. It is clearly seen that the NO at 800 K has an absorption range from ~1.79 to 1.86 μm.

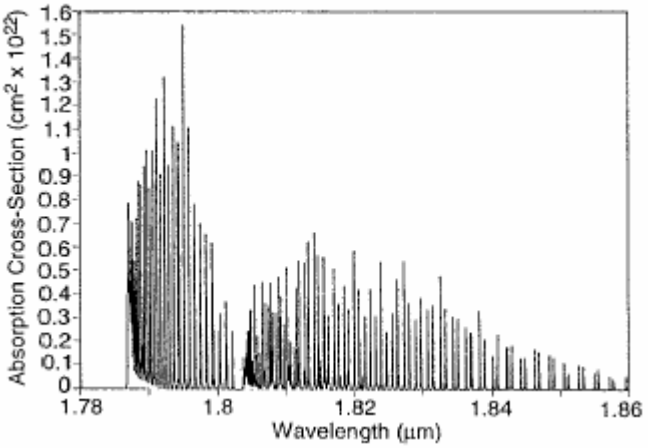

Figure 5.13: *Calculated absorption spectra for the (3,0) band of NO at 800 K[6].*

Water exhibits an absorption band at wavelengths around 1.8 μm and has been detected by the fluorescence of a Tm^{3+}-doped fluoride fibre pumped with a laser diode at 785nm [7], and also by [6] in which water vapour absorption features were detected in their NO monitoring system.

For a high performance coherent radar system, the laser source has to be frequency as well as amplitude stabilised, where the laser wavelength has to be held typically to within a few pm from the absorption line centre and the relative intensity noise has to be less than -110 dB/Hz. The effective technique used to control emission wavelength is by injection seeding, where a low power output laser with a narrow spectral linewidth is used to control the emission wavelength of the Q-switched

oscillator, as discussed in [2]. Laporta et al. developed a cw single-frequency Tm-Ho:YAG laser tunable from 2087 to 2099 nm for injection seeding of a coherent LIDAR system for wind velocity measurement. The laser has both amplitude and frequency stabilisation by means of an electronics circuit and by locking the oscillator to an absorption line of a molecule, respectively.

5.8 Conclusion

In this chapter, an in-band-pumped, continuous-wave, single-frequency Tm^{3+}-Sb co-doped DFB fibre laser operated at 1836 nm was realised and characterised. This is the first report of a Tm^{3+} co-doped, single-frequency, DFB fibre laser that is in-band pumped at 1565 nm and the longest reported operating wavelength of a DFB fibre laser. The laser itself shows an output power of 5 mW with a slope efficiency of 1%, at an absorbed pump power of ~550 mW. The laser is then subsequently amplified to 345 mW using a MOPA configuration with an amplifier fibre length of 1 m, corresponding to a gain of ~18 dB. The single-frequency and single polarisation of the laser was confirmed with the Fabry-Pérot interferometer. In this work, the DFB laser was configured in an intracavity pumping scheme by placing it inside the Raman laser cavity and the DFB output power of 144 mW was obtained. However, the laser cavity was unstable as a consequence this affected the stability of the DFB power.

The λ/4 phase shift is located 4.8 mm from the mid-point of the grating. The DFB laser is 8 cm long with a cavity feedback grating strength of 10. The gratings were UV written into the core of the Tm^{3+} co-doped Sb fibre. The photosensitisation of the fibre is provided by the Sb and by using hydrogen loading technique to enhance the photoinduced refractive index by 15 times. The κ of the grating remaining at 600 ºC, for κ~140 and 90 m^{-1}, were ~ 10% and ~5% of its initial κ. The thermal stability of the grating written in this fibre is suitable for high temperature sensing applications.

The possible applications of this DFB laser were discussed. We believe that it could be a practical source for spectroscopy, LIDAR, and medical applications because the

lasing wavelength is in the 'eye-safe' spectral region and furthermore, the characteristics of the DFB lasers such as compact size, wavelength stability and narrow linewidth.

5.9 References

[1] M. Pierce, S. Jackson, P. Golding, B. Dickinson, M. Dickinson, T. King, and P. Sloan, "Development and application of fibre lasers for medical applications," *Proceedings of SPIE*, vol. 4253, pp. 144-154, 2001.

[2] P. Laporta, M. Marano, L. Pallaro, and S. Taccheo, "Amplitude and frequency stabilisation of a Tm-Ho:YAG laser for coherent lidar applications at 2.1 μm," *Optics and Lasers in Engineering*, vol. 37, pp. 447-457, 2002.

[3] G. Gagliardi, R. Restieri, G. Casa, and L. Gianfrani, "Chemical and isotopic analysis using diode laser spectroscopy: applications to volcanic gas monitoring," *Optics and Lasers in Engineering*, vol. 37, pp. 131-142, 2002.

[4] K. Uehara, K. Yamamoto, T. Kikugawa, S. Toyoda, K. Tsuji, and N. Yoshida, "Precise isotope abundance ratio measurement of nitrous oxide using diode lasers," *Sensors and Actuators B: Chemical*, vol. 90, pp. 250-255, 2003.

[5] K. Uehara, K. Yamamoto, T. Kikugawa, and N. Yoshida, "Isotope analysis of environmental substances by a new laser-spectroscopic method utilizing different pathlengths," *Sensors and Actuators B: Chemical*, vol. 74, pp. 173-178, 2001.

[6] D. M. Sonnenfroh and M. G. Allen, "Absorption measurements of the second overtone band of NO in ambient and combustion gases with a 1.8- μm room-temperature diode laser," *Applied Optics*, vol. 36, pp. 7970-7977, 1997.

[7] F. J. McAleavey and B. D. MacCraith, "Diode-pumped thulium-doped zirconium fluoride fibre as a fluorescent source for water sensing," *Electronics Letters*, vol. 31, pp. 1379-1380, 1995.

[8] S. Agger, J. H. Povlsen, and P. Varming, "Single-frequency thulium-doped distributed-feedback fiber laser," *Optics Letters*, vol. 29, pp. 1503-1505, 2004.

[9] N. Y. Voo, J. K. Sahu, and M. Ibsen, "345 mW single-frequency Tm^{3+}-Sb co-doped DFB fibre laser MOPA at 1836 nm," in *OAA*. Budapest, Hungary, 2005, pp. TuD2.

[10] N. Y. Voo, J. K. Sahu, and M. Ibsen, "345-mW 1836-nm single-frequency DFB fiber laser MOPA," *IEEE Photonics Technology Letters*, vol. 17, pp. 2550-2552, 2005.

[11] D. C. Hanna, I. M. Jauncey, R. M. Percival, I. R. Perry, R. G. Smart, P. J. Suni, J. E. Townsend, and A. C. Tropper, "Continuous-wave oscillation of a monomode thulium-doped fibre laser," *Electronics Letters*, vol. 24, pp. 1222-1223, 1988.

[12] T. Yamamoto, Y. Miyajima, and T. Komukai, "1.9 μm Tm-doped silica fibre laser pumped at 1.57 μm," *Electronics Letters*, vol. 30, pp. 220-221, 1994.

[13] Y. H. Tsang, D. J. Coleman, and T. A. King, "High power 1.9 μm Tm^{3+}-silica fibre laser pumped at 1.09 μm by a Yb^{3+}-silica fibre laser," *Optics Communications*, vol. 231, pp. 357-364, 2004.

[14] D.C. Hanna, I.R. Perry, and J. R. Lincoln, "A 1-watt thulium-doped cw fibre laser opearting at 2 μm," *Optics Communications*, vol. 80, pp. 52-56, 1990.

[15] R. M. Percival, D. Szebesta, C. P. Seltzer, S. D. Perrin, S. T. Davey, and M. Louka, "A 1.6-μm pumped 1.9-μm thulium-doped flouride fibre laser and amplifier of very high efficieny," *IEEE Journal of Quantum Electronics*, vol. 31, pp. 489-493, 1995.

[16] S. D. Jackson and T. A. King, "Theoretical modeling of Tm-doped silica fiber lasers," *Journal of Lightwave Technology*, vol. 17, pp. 948-956, 1999.

[17] J. K. Sahu, M. R. Mokhtar, N. Y. Voo, D. N. Payne, and M. Ibsen, "Photosensitivity in germanium-free antimony doped alumino-silicate optical fibre prepared by MCVD," presented at ECOC, 2004, pp. Th3.35.

[18] D. L. Williams, B. J. Ainslie, J. R. Armitage, R. Kashyap, and R. Campbell, "Enhanced UV photosensitivity in boron codoped germanosilicate fibres," *Electronics Letters*, vol. 29, pp. 45, 1993.

[19] G. Brambilla and V. Pruneri, "Enhanced photorefractivity in tin-doped silica optical fibers (review)," *IEEE Journal of Selected Topics in Quantum Electronics*, vol. 7, pp. 403-408, 2001.

[20] P. J. Lemaire, R. M. Atkins, V. Mizrahi, and W. A. Reed, "High pressure H_2 loading as a technique for achieving ultrahigh UV photosensitivity and thermal sensitivity in GeO_2 doped optical fibres," *Electronics Letters*, vol. 29, pp. 1191-1193, 1993.

[21] W. H. Loh, L. Dong, and J. E. Caplen, "Single-sided output Sn/Er/Yb distributed feedback fiber laser," *Applied Physics Letters*, vol. 69, pp. 2151-2153, 1996.

[22] K. Oh, P. S. Westbrook, R. M. Atkins, P. Reyes, R. S. Windeler, W. A. Reed, T. E. Stockert, D. Brownlow, D. DiGiovanni, P. S. Westbrook, R. M. Atkins, P. Reyes, R. S. Windeler, W. A. Reed, T. E. Stockert, D. Brownlow, and D. DiGiovanni, "Ultraviolet photosensitive response in an antimony-doped optical fiber," *Optics Letters*, vol. 27, pp. 488-490, 2002.

[23] A. Ghatak and K. Thyagarajan, *Introduction of fibre optics*: The press syndicate of the University of Cambridge, 1998.

[24] Yonghang Shen, Jinglei He, Tong Sun, and K. T. V. Grattan, "High-temperature sustainability of strong fiber Bragg gratings written into Sb-Ge-codoped photosensitive fiber: decay mechanisms involved during annealing," *Optics Letters*, vol. 29, pp. 554-556, 2004.

[25] K.O. Hill, B. Malo, F. Bilodeau, D.C. Johnson, and J. Albert, "Bragg gratings fabricated in monomode photosensitive optical fiber by UV exposure through a phase mask," *Applied Physics Letters*, vol. 62, pp. 1035-1037, 1993.

[26] M. Ibsen, E. Ronnekleiv, G.J. Cowle, M.O. Berendt, O. Hadeler, M.N. Zervas, and R. I. Laming, "Robust high power (>20 mW) all-fibre DFB lasers with unidirectional and truly single polarisation outputs," in *CLEO*, 1999, pp. CWE4.

[27] S. D. Jackson and M. S, "Efficiency Dependence on the Tm^{3+} and Al^{3+} Concentrations for Tm^{3+}-Doped Silica Double-Clad Fiber Lasers," *Applied Optics*, vol. 42, pp. 2702-2707, 2003.

[28] C. Alegria, Y. Jeong, C. Codemard, J. K. Sahu, J. A. Alvarez-Chavez, L. Fu, M. Ibsen, and J. Nilsson, "83-W single-frequency narrow-linewidth MOPA using large-core erbium-ytterbium Co-doped fiber," *IEEE Photonics Technology Letters*, vol. 16, pp. 1825-1827, 2004.

[29] G. A. Ball, C. E. Holton, G. Hull-Allen, and W. W. Morey, "60 mW 1.5 μm single-frequency low-noise fiber laser MOPA," *IEEE Photonics Technology Letters*, vol. 6, pp. 192-194, 1994.

[30] J. J. Pan and Y. Shi, "166-mW single-frequency output power interactive fiber lasers with low noise," *IEEE Photonics Technology Letters*, vol. 11, pp. 36-38, 1999.

[31] W. H. Loh, B. N. Samson, Z. E. Harutjunian, and R. I. Laming, "Intracavity pumping for increased output power from a distributed feedback erbium fibre laser," *Electronics Letters*, vol. 32, pp. 1204-1205, 1996.

[32] C.A. Codemard, P. Dupriez, Y. Jeong, J.K. Sahu, M. Ibsen, and J. Nilsson, "High power cladding-pumping Raman fiber laser with true single-mode output at 1660 nm," in *OFC*. Anaheim, California, 2006, pp. OThJ2.

Chapter 6

Holmium-doped DFB/DBR Fibre Laser at 2.1μm

Lasers operating in the eye-safe 2 μm wavelength region can find a number of important applications as discussed in Chapter 5. Holmium (Ho^{3+}) is an rare-earth ion which has been studied as an active ion in silicate [1-7] and fluoride [8, 9] glass hosts for lasers operating at ~2.1 μm. Although a highly efficient laser oscillation is achieved when using fluoride glass hosts [2], due to a lower non-radiative phonon energy than the silica glass, there are some problems such as fibre strength, durability, and splicing techniques to be solved to enable fluoride fibre to be practically applied. The cavity of the fibre lasers is based on the Fabry-Pérot type cavities which are formed by a high-reflectivity input mirror and an output coupler. The shortest cavity length of Ho^{3+}-doped silica fibre lasers was 13 cm, having a slope efficiency of 2.5%, and the maximum laser output power was 6.4 mW [2].

The motivation of this research was to develop a continuous-wave (CW), DFB, single-frequency, holmium (Ho^{3+}) doped silica fibre laser operating at 2140 nm. The design of the DFB was aimed to be as compact as possible, with a stable operating wavelength and a target output power of <10 mW. This chapter describes the fibre

design, the loss and emission measurements of Ho^{3+}, and an assessment of the efficiency of the designed DFB fibre laser operating in the forward pumping scheme. Section 6.1 reviews the pump absorption bands of Ho^{3+} in silica being used here. Pump sources used to investigate the efficiency of the designed DFB laser were an Yb^{3+}-doped fibre laser at 1119 nm and a Tm^{3+} co-doped DFB laser at 1836 nm. The details of the fibre used for constructing the DFB laser such as the fibre's photosensitivity, concentration of Ho^{3+}, core diameter, numerical aperture (NA) and cut-off wavelength as well as measurements of loss and emission of Ho^{3+} are found in Section 6.2. Based on this information, the DFB laser was designed and the details of the designed DFB laser are given in Section 6.3. The assessments of the laser efficiency are given in Section 6.4. The pump absorption for this DFB laser was too low, a DBR fibre laser was then constructed and assessed. The final section is the summary and outcome of this research.

6.1 Review of pump absorption bands of Ho^{3+}-doped silica fibre lasers being used

The $^5I_7 \rightarrow {}^5I_8$ laser transition of Ho^{3+} is used to achieve laser emission at 2.1 μm. A wide range of pumping sources has been used to pump the relevant laser transitions of Ho^{3+}, as it has large, broad, absorption bands which cover the wavelengths from the visible blue band to the near-infrared band. Ho^{3+}-doped silica fibre lasers operated at ~2 μm wavelength have been pumped by the use of Tm^{3+} [2, 6] or Yb^{3+} [4] sensitization, direct Yb^{3+}-doped silica fibre laser pumping [3, 5, 10], and direct pumping with lasers operating at non-standard wavelengths [1]. The commercially available semiconductor lasers have emission wavelengths longer than 750 nm which cannot be used to pump the strongest absorption bands of Ho^{3+} located in the visible range. Therefore, for the first demonstration of Ho^{3+}-doped fibre lasers it was pumped by an argon laser at 457.9 nm and had a slope efficiency of 1.7% with a threshold power of 46 mW [1]. Unfortunately, because of the lack of a suitable absorption band in the near infrared region which could be pumped by commercially available laser diodes, the Ho^{3+} has to be co-doped with sensitizer ions, either Tm^{3+}

or Yb^{3+}, in which there is energy transfer from the sensitizer ions to Ho ions. In [2, 6] laser oscillations of Ho in the 2 μm region have been demonstrated by pumping the absorption bands of Tm at $^3F_4$ and $^3H_5$ levels with a 786 nm Ti:sapphire laser and a Raman fibre laser operated at 1212 nm respectively; the excited ions drop by phonon relaxation to the $^3H_4$ level of Tm^{3+} and by utilising energy transfer from the $^3H_4$ level of Tm^{3+} to the $^5I_7$ upper laser level of Ho^{3+}. Yb^{3+} as a sensitizer ion was demonstrated in [4], the Ho^{3+} was co-doped with Yb^{3+} and the fibre laser was pumped with a 50 W 975 nm diode laser system, whereby Yb^{3+} absorbed the pump radiation and then energy transfer occurred from the $^2F_{5/2}$ level of Yb^{3+} to the $^5I_6$ level of Ho^{3+}, and multiphonon relaxation from the $^5I_6$ level to the $^5I_7$ upper laser level. The weak point of the configuration of these lasers is the strong competition between the sensitizer ions to Ho energy transfer and the processes of excited state absorption and the fluorescence of the sensitizer ions [3]. The use of direct pumping, with Yb^{3+}-doped silica fibre lasers, has also been demonstrated. In Ref [3] it was shown that the 4.5 m-long Ho fibre laser, pumped at 1150 nm with a double-clad Yb-doped fibre laser, has a slope efficiency of 20% and a maximum output power of 280 mW for 2W absorbed pump power. Ref [5] pumped a length of 2m Ho^{3+}-doped fibre laser at 1100 nm with a Yb^{3+}-doped silica fibre laser, a maximum slope efficiency of 35% and a maximum output power of 2.7 W was demonstrated for ~10 W launched pump power. Then, tuning of the 2 μm Ho^{3+}-doped silica fibre laser over 144 nm, from 2019 to 2163 nm, achieving a maximum output power of 1.58 W, has been demonstrated by [10].

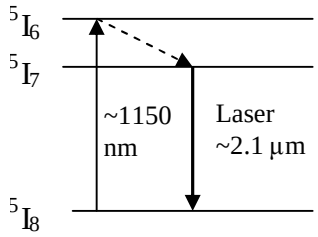

Figure 6.1: *Simplified three-level energy diagram of Ho^{3+} in silica.*

Figure 6.1 shows the simplified three-level energy diagram of Ho^{3+}. In this work, the Ho^{3+}-doped DFB laser was pumped in the $^5I_6$ level, the excited Ho ions decay rapidly, by phonon decay, to the upper lasing level $^5I_7$. The pump source used was an

Yb^{3+}-doped fibre laser whose operating wavelength was determined by the Bragg gratings at 1119 nm. The quantum efficiency limit, at the lasing wavelength of 2140 nm, is ~52%. Pumping at 1836 nm with the Tm^{3+} DFB MOPA laser was also performed in which the theoretical quantum efficiency limit is ~86%.

6.2 Ho^{3+}-doped alumino-silicate fibre

This section is about our Ho^{3+}-doped fibre used for implementing the DFB laser. This was the first trial of fabricating the Ho^{3+}-doped fibre by the ORC fibre fabricators. The fibre preform was made by conventional modified chemical vapour deposition (MCVD). Holmium and aluminium were incorporated into the core of fibre-preform through the solution doping technique during the preform preparation. Germanium and boron were added through MCVD deposition into the core for photosensitive mechanism. The function of aluminium is mentioned in Section 5.2, i.e. to even out the distribution of the dopants as well as increase the solubility of the Ho^{3+} while reducing the possibility of concentration quenching. The preform was then drawn into fibre having a diameter of 95 μm. The estimated concentration of Ho^{3+} in the fibre is ~12000 ppm, it has a core diameter of 7.9 μm, NA ~ 0.162, and a cut-off wavelength of 1670 nm. The gain medium was achieved by Ho^{3+}. The small signal absorptions of Ho^{3+} at 1119 and 1836 nm were found to be ~0.2 dB/cm. The experimental details for measuring the absorption loss are in Section 6.2.2.

6.2.1 Photosensitivity of the fibre

The photosensitivity of the Ho^{3+} fibre is studied in this section. The technique used to measure the photosensitivity of the fibre is the same as in Section 5.2.1. The fibre was hydrogen loaded at 200 atm for 2 weeks at 70℃ prior to UV writing the Bragg gratings and then 1 cm long test gratings, with a Bragg wavelength at 1597 nm, were written into the core of the fibre with the same Ar^{+}-ion laser operating at 244 nm. After gratings inscription, they were annealed at 100 ℃ for 24 hours to outgas any residual hydrogen in the fibre and to stabilise the index-modulations. The gratings

were spliced to the output of the semiconductor source and the transmission spectra of the gratings were measured with the OSA, having a resolution of 0.01 nm. The coupling coefficient (κ) was extracted in the same way as in Section 5.2.1. The index growth of the fibre was studied at different fluence. The coupling coefficient at 2140 nm, the operating wavelength of the DFB laser, was then calculated from the measured modulation index of the fibre. Figure 6.2 shows the measured index growth and coupling coefficient at 1597 nm, as a function of fluence, as well as the calculated κ at 2140 nm. The index modulation change of ~3 x 10^{-5} was achieved by this fibre with a fluence of ~2.2 kJ/cm^2. The photosensitivity of the fibre is low as indicated by the index modulation change. With a fluence of ~2.2 kJ/cm^2, the κ at 2140 nm that can be obtained is ~30 m^{-1}, this means that a cavity length of ~30 cm is needed in order to achieve a grating strength of 10. For a robust single-frequency output, the cavity length of the laser needed to be only a few centimetres so as to increase the axial mode spacing. In order to keep the DFB short and to have enough gain, the length of the DFB gratings chosen is 12 cm and hence a κL of ~4 was attained. After assessing the photosensitivity, the next section is regarding the pump absorption loss at the pump wavelengths used, by measuring the absorption bands of our Ho^{3+}-doped fibre.

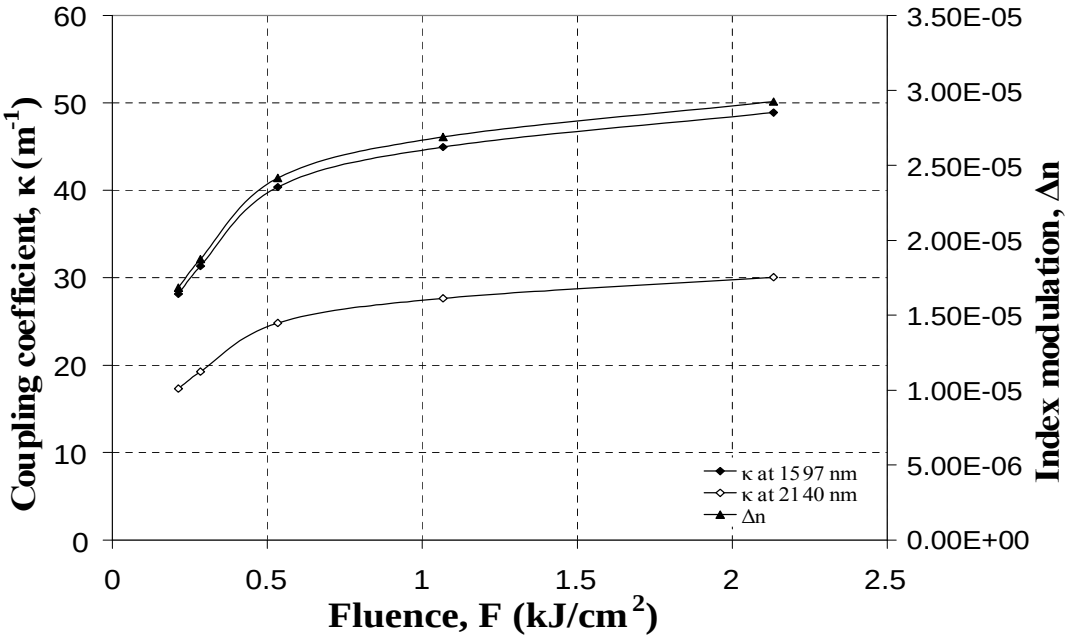

Figure 6.2: *Measured index growth and coupling coefficient at 1597 nm against 244 nm CW-fluence, together with the calculated coupling coefficient at 2140 nm.*

6.2.2 Absorption of the Ho^{3+}-doped fibre

The white light was coupled into the Ho^{3+}-doped fibre and the absorption spectrum was obtained with the OSA by a cut-back technique. The measured absorption spectrum of the fibre in the range 700-1750 nm is shown in Figure 6.3. A very similar absorption spectrum was observed as in [5], in which the spectrum showed the absorption bands of Ho^{3+} at $^5I_4$, $^5I_5$ and $^5I_6$. The absorption peak of $^5I_6$ is at 1150 nm with a loss of ~0.7 dB/cm. The pump sources used to pump the DFB laser were an Yb^{3+}-doped fibre laser operating at 1119 nm and a Tm^{3+} DFB MOPA laser at 1836 nm. As observed from the figure below, the absorption loss at 1119 nm was ~0.2 dB/cm. The absorption at 1836 nm, using the Tm^{3+} DFB MOPA laser as a light source, was found to be ~0.2 dB/cm by the cut-back method.

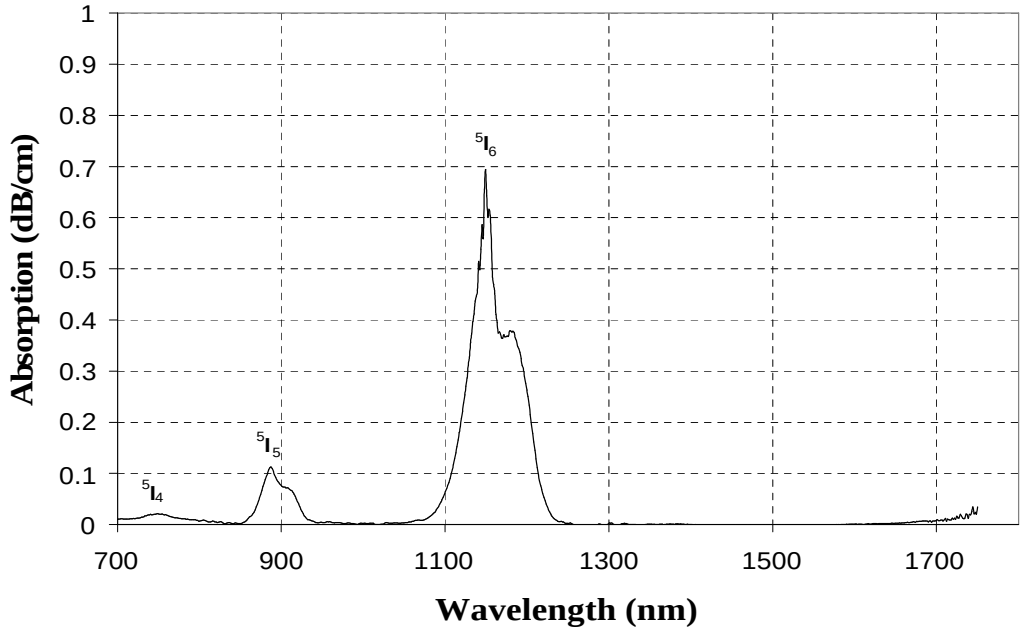

Figure 6.3: *The measured absorption spectrum of our Ho^{3+}-doped silica fibre.*

6.2.3 Emission of Ho^{3+}-doped fibre

This section describes the experimental set-up for measuring the emission of Ho^{3+}. From the laser efficiency point of view, the operating wavelength of the DFB laser

needed to be at the gain peak. The experimental set-up for investigating the emission of Ho^{3+} is shown in Figure 6.4, in which the Tm^{3+} DFB MOPA laser, operated at 1836 nm, is used to excite a 45 cm length of Ho^{3+}-doped fibre. The DFB laser was pumped with a 1 mW Tunics, tunable laser diode source, operating at 1565 nm, and then amplified to 1W by a high power amplifier from SPI Lasers. The length of the amplifier fibre was 1.75 m and the power after the MOPA laser, measured with a Melles-Griot 13PEM001 thermal power meter, with all the pump power being absorbed, was 22 mW at a pump power of 680 mW. The Ho^{3+}-doped fibre was spliced to the output of the MOPA and the other end was spliced to an angle connector, to prevent back reflections. The emission spectrum at the end of the doped fibre was measured with the automatic monochromator.

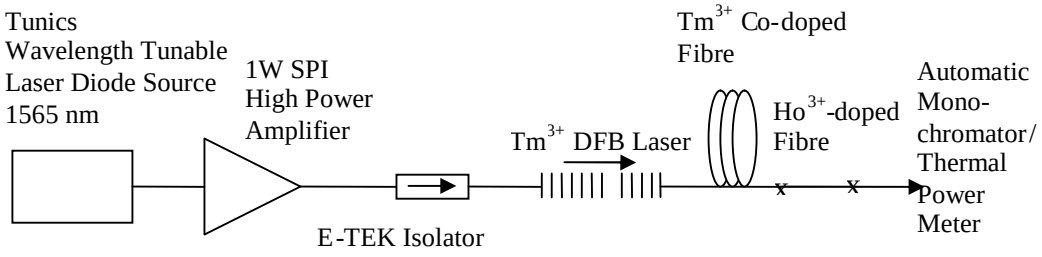

Figure 6.4: *Experimental set-up for measuring the emission of our Ho^{3+}-doped silica fibre.*

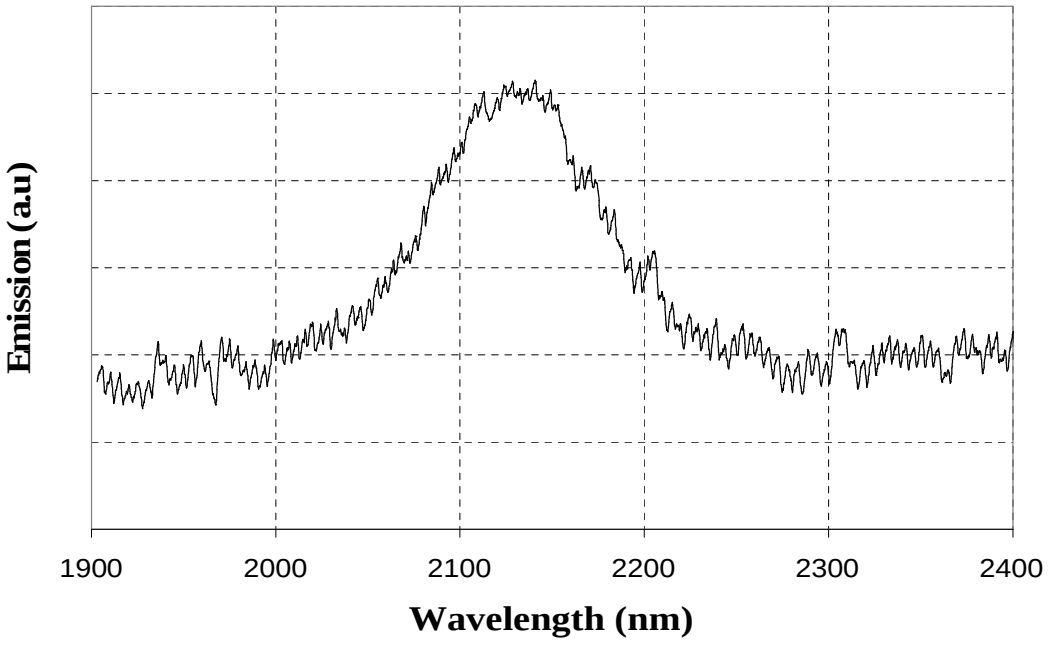

Figure 6.5: *The measured emission of Ho^{3+}- doped silica fibre as a function of wavelength.*

Figure 6.5 shows the emission spectrum of the Ho^{3+}-doped fibre, scanned with the monochromator having a resolution of 0.16 nm. The measured full-width half maximum (FWHM) emission bandwidth of the Ho^{3+}-doped fibre is found to be in the range of 2080 – 2180 nm and the peak wavelength is at ~2140 nm. The operating wavelength of the DFB laser is designed at this peak wavelength.

6.3 Structure of the DFB fibre laser

This section outlines the design of the Ho^{3+}-doped DFB laser, which is basically having a similar structure to the Er^{3+}-Yb^{3+} and Tm^{3+} DFB fibre lasers, in which the π phase shift is placed slightly off-centre with respect to the centre of the grating, i.e. at a ratio of 0.44: 0.56. The length of the DFB gratings is 12 cm and the phase shift was placed at 7.2 mm from the mid point of the grating. The gratings were written directly into the core of the fibre with the phase mask technique that was used in the Er^{3+}-Yb^{3+} or Tm^{3+} DFB fibre laser. The period of the phase mask (Λ) is 1476 nm and the operating wavelength of the DFB is 2140 nm. Single polarisation operation was obtained as mentioned in Chapter 3. As mentioned in the earlier section on the photosensitivity of the fibre, prior to the fabrication of the UV written Bragg gratings, the Ho^{3+}-doped fibre was hydrogen loaded to make it more photosensitive. After writing, the grating was annealed for 24 hours at 100 ^{o}C to outgas the residual hydrogen and to stabilise the index modulation. The final grating strength of ~4 was obtained with a $\kappa \sim 30\ m^{-1}$.

6.4 Experimental set-up and result

Two pump wavelengths were used to investigate the DFB laser performance. As mentioned in Section 6.1, the quantum efficiency limit for 1119 nm and 1836 nm, at the lasing wavelength, is ~52% and ~86%, respectively.

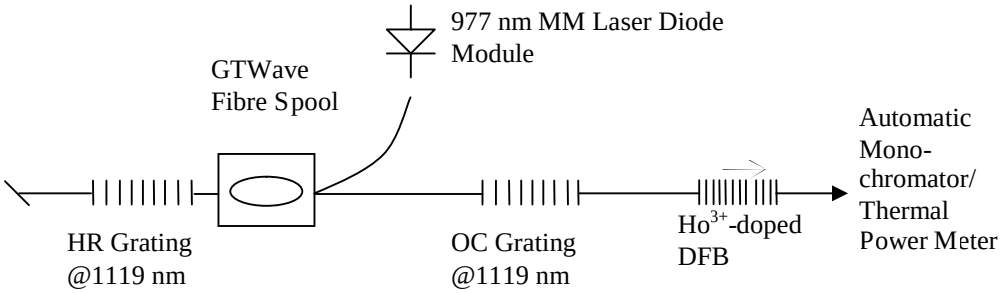

Figure 6.6: *Experimental set-up of the $^5I_6$ pump band of the Ho^{3+} -doped DFB fibre laser.*

Figure 6.6 shows the experimental set-up for the $^5I_6$ pump band of the Ho^{3+}-doped DFB fibre laser. The pump source was an Yb^{3+}-doped fibre laser operated at 1119 nm. The Yb^{3+}-doped fibre laser basically consisted of a spool of GTWave fibre, a high reflectivity grating and an output coupler (OC) grating at 1119 nm. The GTWave fibre assembly consists of an Yb^{3+}-doped fibre and two un-doped silica pump fibres wrapped around the doped fibre. The GTWave fibre is 1 km long and is pumped by a pigtailed 977 nm multimode laser diode which was spliced to the pump fibre. As the pump light propagates along the pump fibre, its evanescent field is coupled to the Yb^{3+}-doped fibre where it is absorbed. The operating wavelength of the Yb^{3+}-doped fibre laser was determined by the Bragg gratings at 1119 nm which coincides with the optimal performance of the Yb^{3+}-doped laser. The output power of the laser, measured at the end of the OC grating, was ~230 mW with an input power from the pump diode of 3W. The DFB fibre laser was configured in the forward pumping scheme in which a WDM coupler is eliminated. One end of the DFB laser, the end further away from the phase shift, was spliced to the output end of the Yb^{3+}-doped fibre laser. The output end of the DFB laser, the end closer to the phase shift, was measured with the automatic monochromator.

The DFB laser was pumped with 230 mW and the power at the output end of the laser, measured with the thermal power meter, was ~120 mW. The measured power might consist of the signal and unabsorbed power, for this reason, the monochromator was used to investigate the spectrum at the output end of the DFB laser. Figure 6.7 shows the spectrum at the output end of the DFB laser as a function

of wavelength that was scanned by the monochromator. From the spectrum, a peak was observed at 2123 nm. This peak wavelength was far from the designed operating wavelength of the laser, which is at 2140 nm. So, in order to further investigate the possibility of this being due to the pump source itself, the DFB laser was broken at the splice point and a 50 cm piece of Ho^{3+}-doped fibre was spliced at the OC grating end. A peak at 2123 nm was still observed with a decreasing in amplitude. Obviously, this cannot be due to the pump source as the amplitude should be the same for both cases. The other possibility was lasing actually occurred at the maximum emission peak of Ho^{3+} as the threshold power of the cavity could be lower than the DFB cavity. As observed in Section 4.2, the DFB laser with $\kappa L \sim 5$ required a much higher threshold power than $\kappa L \sim 10$. This could be the reason as the κL of the Ho^{3+} DFB was low, i.e. ~4, and the threshold power is even higher in order for lasing to occur.

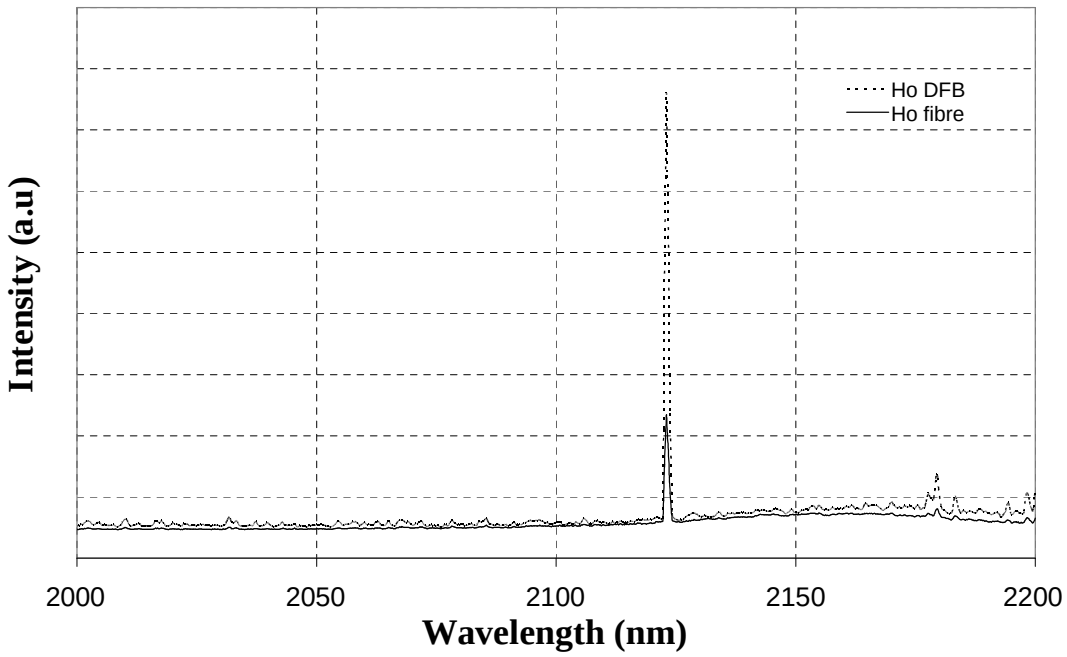

Figure 6.7: *Spectrum with and without DFB fibre laser at 230 mW pump power.*

From the measured unabsorbed power ~120 mW, the absorption of the fibre at 1119 nm was ~0.27 dB/cm, which is about the same as the absorption loss measured earlier. The absorption of this fibre is low and the pump power available to reach the threshold of the DFB laser is limited. In addition, the pump wavelength was below

the 1670 nm cut-off wavelength of the fibre, higher order modes could therefore be presented and hence power competition between the modes would occur. The following experimental set-up was used to pump the DFB laser above the cut-off wavelength of the fibre. Using the 1836 nm Tm^{3+} DFB MOPA laser as pump source, the V-number at this pump wavelength was 2.19 so there was only one mode present. In addition, it is an in-band pumping scheme at 1836 nm, in which the theoretical quantum efficiency limit is ~86%. With this pump wavelength, the Ho^{3+} ions are excited to the upper laser level $^5I_7$ directly, so the photon conversion efficiency for 2.1 μm emission will be higher than with the other pumping schemes. Figure 6.8 shows the experimental set-up of the $^5I_7$ pump band of the Ho^{3+}-doped DFB laser.

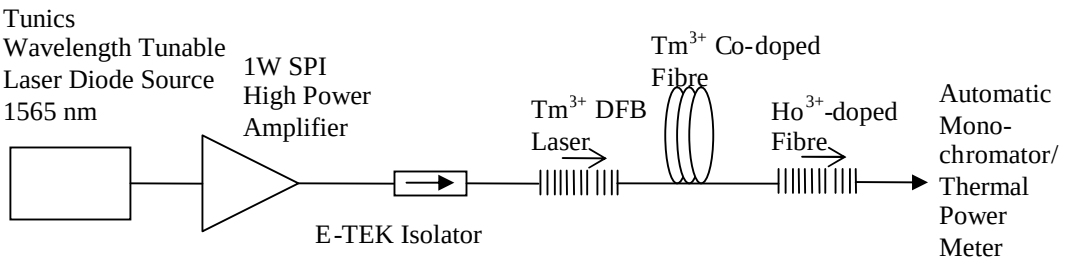

Figure 6.8: *Experimental set-up for the $^5I_7$ pump band of Ho^{3+}-doped DFB laser.*

The same experimental set-up for the Tm^{3+} DFB MOPA laser as in Section 6.2.3, used for obtaining the emission of Ho^{3+}, was used to pump the Ho^{3+}-doped DFB laser. The amplifier fibre length of 1.295 m was used, instead of 1.75 m. The maximum MOPA output power of ~110 mW was obtained with 960 mW pump power. The end further away from the phase shift was spliced to the MOPA laser output and the power after the Ho^{3+}-doped DFB laser was ~ 45 mW, measured with the power meter. Again, the monochromator was used to investigate the output characteristics of the laser. Figure 6.9 shows the output characteristics of the DFB laser at a pump power of 110 mW and also 65 mW. For 65 mW pump power, the power at the output of the DFB laser was 27 mW. Results show that the ASE of the Ho^{3+}-doped fibre was increased as the pump power increased and the DFB laser did not lase with these pump power levels. The pump absorption at this wavelength was ~0.2 dB/cm.

Pump wavelengths at 1119 nm and 1836 nm were used to pump the DFB laser, neither wavelength showed that lasing occurred. This could be due to the quality, Q, of the cavity that is reduced as compared with the Q-value of a grating strength of ~10. Consequently, the loss in the cavity has increased as a result of decreasing the Q of the cavity. Furthermore, the gain in the fibre could be low and hence, it is insufficient to overcome the losses. The estimated loss introduced by the reflective gratings was ~0.11 dB. The other problem could be due to the low pump absorption in a 12-cm long laser cavity; to resolve this, a distributed Bragg reflector (DBR) was constructed in the following section.

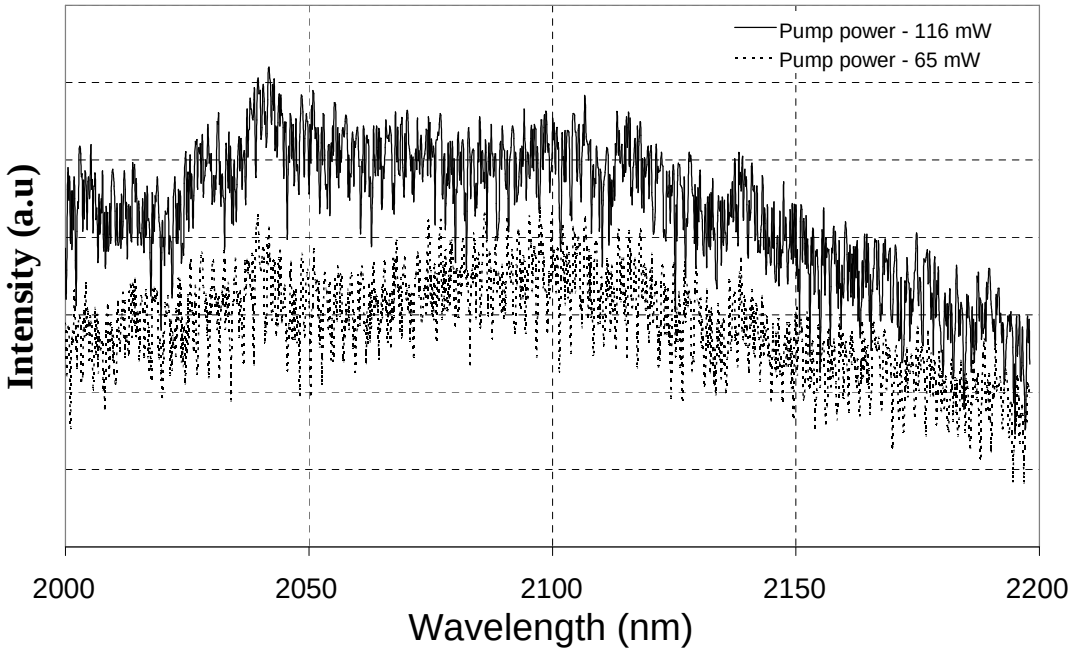

Figure 6.9: *The output spectrum of the Ho^{3+}-doped DFB laser pumped at $^5I_7$ band.*

6.5 DBR laser: Experimental set-up and result

This section describes the realisation of a distributed Bragg reflector (DBR) for increasing the pump absorption by using a longer cavity length. In [11, 12], the DBR fibre laser was formed with two Bragg gratings that were written into the core of the Er^{3+}-doped fibre by using a two beam interference pattern. The two reflector gratings were written on opposite ends of the fibre. In this work, a DBR Ho^{3+}-doped fibre laser was constructed, by fusion-splicing two reflector gratings on opposite ends of a

length (L) of Ho^{3+}-doped fibre, to form a cavity. By splicing the gratings on both ends of the fibre additional splice loss will be introduced; however, it was the initial trial for this set-up. The gratings were cut from both ends of the DFB laser and spliced to both ends of the Ho^{3+}-doped fibre. The gratings were 4 cm long so that the Bragg wavelength of the two reflectors was the same. The reflectivities of the 4 cm long gratings were 96.4%, i.e. 0.16 dB loss at the reflectivity of the gratings. The cavity lengths of the laser used were 31 and 85 cm long. The laser was end pumped with the Yb^{3+}-doped fibre laser with 230 mW at 1119 nm. Figure 6.10 shows the schematic diagram of the DBR fibre laser configuration together with the pump source.

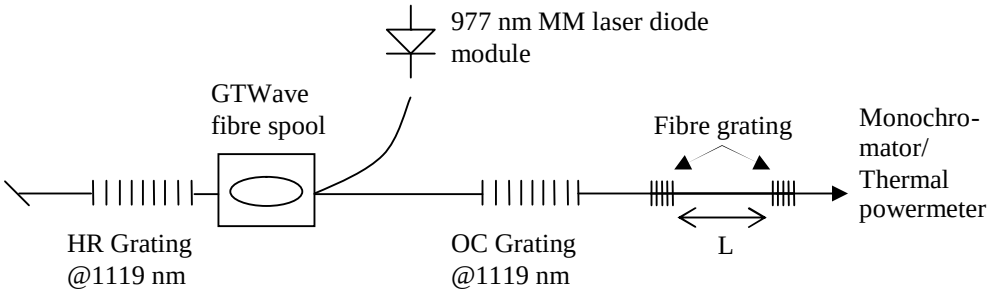

Figure 6.10: *Ho^{3+}-doped DBR fibre laser configuration.*

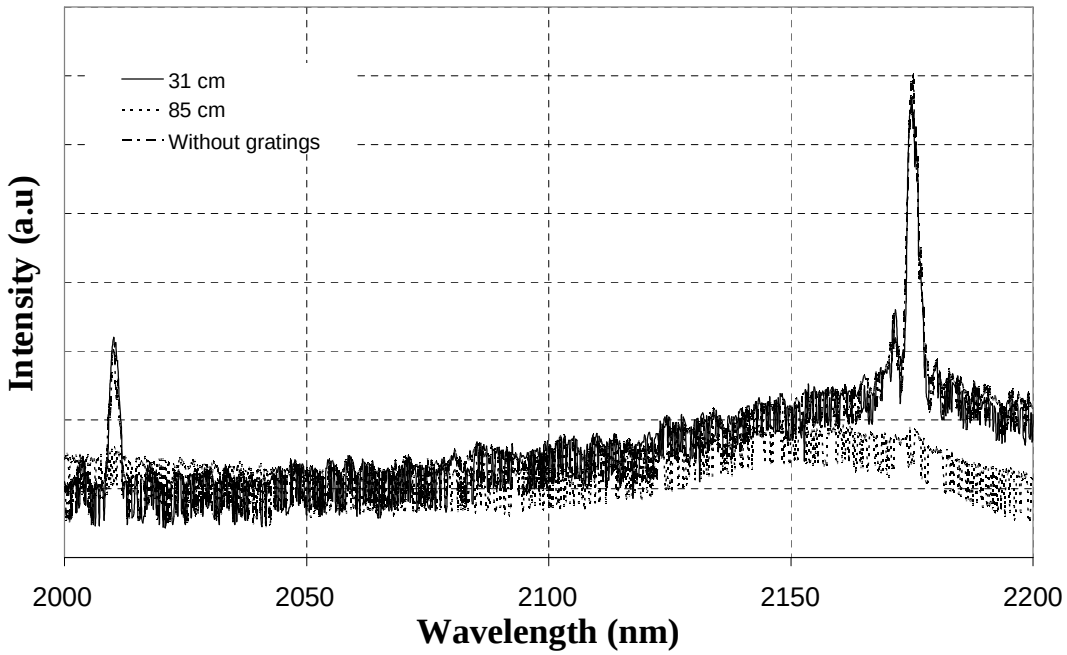

Figure 6.11: *Spectrum of DBR for a cavity length of 31 and 85 cm; and without reflector gratings for 31 cm of Ho^{3+}-doped fibre pumped at 230 mW.*

The power measured at the output of the DBR laser was 50 and 2 mW for a cavity length of 31 and 85 cm respectively. The output of the laser was investigated with the scanning monochromator and the spectrum is shown in Figure 6.11. With the 31 cm cavity length, peaks were observed at ~2010 and 2175 nm which is corresponded to the emission spectrum of Ho^{3+}. However, neither of these wavelengths was corresponded to the designed operating wavelength. Accordingly, the gratings at the ends of the fibre were then un-spliced and the 31 cm long Ho^{3+}-doped fibre was spliced directly to the output of the Yb^{3+}-doped fibre laser. Again, the peaks coincided exactly with the DBR laser wavelength and lasing occurred as explained in section 6.4. For a cavity length of 85 cm, only the ASE was observed and no peak. This might be because the cavity length was too long and signal reabsorption can occur.

6.6 Conclusion

This chapter describes the preliminary work involved to implement a Ho^{3+}-doped DFB fibre laser and assess the performance of the laser. The DFB laser was designed to operate at 2140 nm, the peak emission of Ho^{3+}. It was pumped at 1119 nm by an Yb^{3+}-doped fibre laser and at 1836 nm by a Tm^{3+} DFB laser. The quantum efficiency limit at pump wavelengths 1119 nm and 1836 nm was 52% and 86% respectively. However, neither pump wavelength managed to get the DFB laser to lase. This could be because the losses in the cavity were high and the gain of the fibre was insufficient to overcome it. The other possibility was due to the pump absorption for a 12 cm Ho^{3+}-doped fibre, that was low at both pump wavelengths ~0.2 - 0.3 dB/cm. Since the absorption of the DFB is low, a pump source with much higher power, perhaps, could reach the threshold of the laser. Then, a DBR fibre laser was constructed to increase the pump absorption by using a much longer cavity length. The cavity lengths of 31 and 85 cm were used, but still no lasing was observed. Concentration quenching effects could be one of the problems as our fibre was doped with a huge Ho^{3+} concentration. Other possible problems were due to the dominant non-radiative transition in the 2 μm region and the large intrinsic losses of the silica fibre associated with the 2.1 μm wavelength.

6.7 References

[1] D. C. Hanna, R. M. Percival, R. G. Smart, J. E. Townsend, and A. C. Tropper, "Continuous-wave oscillation of holmium-doped silica fibre laser," *Electronics Letters*, vol. 25, pp. 593-594, 1989.

[2] K. Oh, T.F. Morse, A. Kilian, and L. Reinhart, "Continuous-wave oscillation of thulium-sensitized holmium-doped silica fiber laser," *Optics Letters*, vol. 19, pp. 278-280, 1994.

[3] A. S. Kurkov, E. M. Dianov, O. I. Medvedkov, G. A. Ivanov, V. A. Aksenov, V. M. Paramonov, S. A. Vasiliev, and E. V. Pershina, "Efficient silica-based Ho^{3+} fibre laser for 2 μm spectral region pumped at 1.15 μm," *Electronics Letters*, vol. 36, pp. 1015-1016, 2000.

[4] S. D. Jackson and S. Mossman, "Diode-cladding-pumped Yb^{3+}, Ho^{3+}-doped silica fiber laser operating at 2.1-μm," *Applied Optics*, vol. 42, pp. 3546-3549, 2003.

[5] S. D. Jackson, "2.7-W Ho^{3+}-doped silica fibre laser pumped at 1100 nm and operating at 2.1 μm," *Applied Physics B: Lasers and Optics*, vol. 76, pp. 793-795, 2003.

[6] A. Taniguchi, T. Kuwayama, A. Shirakawa, M. Musha, and K. Ueda, "1212 nm pumping of 2 μm Tm-Ho-codoped silica fiber laser," *Applied Physics Letters*, vol. 81, pp. 3723-3725, 2002.

[7] S. D. Jackson and A. A. King, "High-power diode-cladding-pumped Tm-doped silica fiber laser," *Optics Letters*, vol. 23, pp. 1462-1464, 1998.

[8] J. Y. Allain, M. Monerie, and H. Poignant, "High-efficiency CW thulium-sensitised holmium-doped fluoride fibre laser operating at 2.04 μm," *Electronics Letters*, vol. 27, pp. 1513-1515, 1991.

[9] R. M. Percival, D. Szebesta, S. T. Davey, N. A. Swain, and T. A. King, "Thulium sensitised holmium-doped CW fluoride fibre laser of high efficiency," *Electronics Letters*, vol. 28, pp. 2231-2232, 1992.

[10] S.D. Jackson and Y. Li, "High-power broadly tunable Ho^{3+}-doped silica fibre laser," *Electronics Letters*, vol. 40, pp. 1474-1475, 2004.

[11] G. A. Ball, W. W. Morey, and W. H. Glenn, "Standing-wave monomode erbium fiber laser," *IEEE Photonics Technology Letters*, vol. 3, pp. 613-615, 1991.

[12] J. L. Zyskind, V. Mizrahi, D. J. DiGiovanni, and J. W. Sulhoff, "Short single frequency erbium-doped fibre laser," *Electronics Letters*, vol. 28, pp. 1385-1387, 1992.

Chapter 7

Conclusions

7.1 Subject of this research

Short-cavity single-frequency fibre lasers have been a topic of continued interest since the early work of Ball et al. on Er^{3+}-doped distributed Bragg reflector fibre lasers. These fibre lasers have shown kilohertz linewidths, direct compatibility with fibre networks, wavelength tunability and are also simple to fabricate. The above characteristics have made them attractive for a number of applications; such as in optical coherent communications, wavelength division multiplexing (WDM), optical fibre sensors and high-resolution spectroscopy. A highly stable laser source is required to achieve a high performance coherent radar system for measuring gas concentration whereby the laser wavelength has to be held typically within a few pm from the absorption line centre and the relative intensity noise has to be typically less than -110 dB/Hz [1]. Also mentioned by [2], the optical based gas sensing required the laser linewidth to be narrower than the absorption line of the gas to be detected for a good spectral overlap so as to lower the minimum detectable gas concentration as well as the cross-sensitivity to other gases. The wavelength stability in the WDM applications becomes an important factor as the channels are increased. Fibre lasers with a wavelength stability of 0.1 pm have been demonstrated in the 8- and 16-

channel systems. The power levels required for these applications were in the milliwatt regime. The objective of this research is to develop a narrow linewidth, low noise, wavelength stable and compact source for high end applications.

There have been a few detailed experimental investigations on the linewidth/phase noise characteristics of these lasers, with much of the work focused on improving the efficiency and output power through optimising the fibre, cavity and grating design. The phase noise properties of these lasers fails to measure up to that achievable in bulk solid-state lasers, even though the linewidth of fibre lasers, based on the well-known Schawlow-Townes formula, indicate values of 60 Hz or less. One common suggestion for the source of this excess phase noise is that it is caused by the environmental perturbations, such as external vibrations and acoustic noise. We experimentally investigated the main cause(s) of the anomalous linewidth behaviour of these fibre lasers and the possible ways of reducing this laser linewidth. In this research, we also aimed to develop single-frequency fibre DFB lasers operating in the 2 μm 'eye safe' wavelength region as it begins to become more important due to a number of possible applications around 2 μm, such as remote gas sensing, LIDAR and medicine.

7.2 This thesis

In this thesis the anomalous behaviour of the laser linewidth of the single-frequency fibre DFB lasers was studied [3, 4] and an analytical model was developed to describe the main cause of the excess noise in the fibre lasers [5, 6]. Then, the laser performance of the step apodised and the double phase shifts designs were compared with the standard design. The effective cavity length of the step apodised DFB laser can be increased without offsetting the optimal cavity confinement. The 2 x $\pi/2$ phase shift design was used to show the intra-cavity effect [7]. A single-frequency fibre DFB laser with improved efficiency operated at 1836 nm was realised with thulium as the gain medium [8, 9]. Then, aiming for a laser operating wavelength longer than 2 μm, this was attempted to be demonstrated with holmium.

The first chapter described the motivation of this study and a brief history of the developments in the single-frequency fibre DFB lasers which included the laser operating wavelength regions that have been covered and the current laser cavity designs as well as the mask-technique used for fabricating the feedback gratings into the core of the fibre.

The feedback mechanism and gain medium, that are essentials for the lasing in DFB lasers, were described in Chapter 2. This covered the definitions of the reflectivity of gratings, the effective length in which the signal circulated in the grating before emerging from the front end, and the rate equations describing the gain medium of the laser.

Chapter 3 presented an experimental investigation and theoretical analysis of the anomalous linewidth behaviour of an Er^{3+}-Yb^{3+} co-doped DFB fibre laser [3, 4]. It was shown that not only does the laser linewidth deviate from the Schawlow-Townes linewidth formula by increasing with pump and laser power but it also varied with the pump configuration. The backward pumping scheme has the lowest threshold and highest efficiency, while the dual-pumping scheme was the worst in these aspects. If maximising efficiency and output power are the over-riding criteria, then backward pumping is clearly the configuration to adopt. The measured 3-dB laser linewidth showed that the lowest linewidth operation was actually obtained with the dual-pumping configuration. This suggested that the designs aimed at maximising the laser efficiency and output power may well impact its phase noise properties in unexpected and undesired ways.

This excess laser linewidth cannot be explained by the environmental noise and fundamental thermal noise floor. The dependence on the pump and output power suggested that the variations in linewidth are a feature of the laser rather than simply being due to environmental perturbations. External perturbation should only contribute to a noise floor independent of pump power. With our pump powers of up to 100 mW and more, the lasing wavelength was increased by ~20 pm for the given pump power and this indicated a temperature increase of no more than 3 ºC. The temperature in the fibre was confirmed with a numerical simulation of heat diffusion

equations. The 3 ºC change incurred in the fibre over the entire laser operating range would seem to be much too small to account for the observed increases in linewidth. However, the thermal noise fluctuations in the laser do comprise a substantive portion of the laser phase noise, particularly at the low operating powers. At higher pump powers, the laser linewidth was insensitive to temperature over the range that we were able to investigate.

The unusual behaviour of the laser linewidth was found to be caused by the fundamental thermal noise at low pump power levels and temperature fluctuations induced by pump intensity at higher powers [5, 6]. The low-frequency intensity noise of the pump laser leads to fibre temperature fluctuations, which in turn lead to refractive index fluctuations and, thus, to the laser frequency jitter. The pump power fluctuation effect is configuration dependent. The difference between the model calculation and the experimental results can be explained by fundamental thermal noise in which a linewidth floor of ~15 kHz was observed.

The potential techniques to overcome these linewidth limitations were discussed. One possible solution was to use a low noise pump which may not be the most cost-effective solution. Another possibility is to use a material with a temperature-insensitive refractive index ($dn/dT \approx 0$), such as special tailored phosphate glasses [10, 11]. The fundamental thermal noise associated with the linewidth floor can be modified by the effective grating length (L_{eff}) and it is scaled as $\Delta f \propto 1/\sqrt{L_{eff}}$. Similarly, the fibre core radius can be enlarged to increase the mode volume and hence decrease the thermal effects. Another technique is to operate the laser at low power, at which the linewidth is much narrower, and subsequently amplify its output power with a MOPA configuration.

Chapter 4 presented the performance of the non-standard and standard DFB laser designs. The laser linewidths of $\kappa \sim 200$ m^{-1}, $\kappa \sim 150$ m^{-1} and $\kappa \sim 100$ m^{-1} and a step apodised grating design as well as showing the laser wavelength shift were measured. The linewidth was found to be configuration dependent. The laser linewidth of $\kappa \sim 100$ m^{-1} followed the Schawlow-Townes linewidth formula, but its

magnitude was a few orders higher. However, the laser output power was the lowest because of weak optical feedback. The laser efficiencies of κ~150 m^{-1} and κ~200 m^{-1} were similar. By increasing the L_{eff}, the fundamental thermal noise contributing to the laser linewidth at low pump level was reduced, as observed in the dual pumping configuration with κ~150 m^{-1} and κ~200 m^{-1}. The linewidth of κ~150 m^{-1} was lower than κ~200 m^{-1} in the forward and backward pumping configurations. In the backward pumping configuration, the linewidth was about the same at high output power. We observed a decrease in the laser wavelength shift as κ reduced. This was because the intensity distribution around the vicinity of the phase shift decreased as the reflectivity of the grating reduced.

The 2 x π/2 phase shift DFB laser with phase shifts located at 5 mm and 10 mm apart were used to show that the laser wavelength shift was not only due to the absorbed pump power but also the signal intensity profile in the laser cavity [7]. We observed a reduction in lasing wavelength shift as compared with the single phase shift design for the similar laser efficiencies. We also observed a decrease in the laser linewidth for the laser with the phase shifts 5 mm apart. However, the slope of the laser wavelength shift change with the pump power was not in a quantitative agreement with the linewidth reduction.

Chapter 5 reported the demonstration of an improved efficiency, thulium doped fibre DFB, laser operating at 1836 nm. Our fibre DFB laser was 8-cm long, with a grating strength (κL) of 9.6, and a π-phase shift located at the 44 % point of the total length of the laser. This is the longest reported operating wavelength of a single-frequency fibre DFB laser [8, 9]. The laser itself shows an output power of 5 mW having a slope efficiency of 1% and, with the aid of a master-oscillator power amplifier (MOPA), the power of the DFB fibre laser was amplified to 345 mW with an amplifier length of 1 m. The laser was in-band pumped at 1565 nm, which was the first reported Tm^{3+} doped fibre DFB laser with in-band pumping. Intracavity pumping of the laser was also conducted with a Raman fibre laser, an output power of 144 mW was observed. However, the laser output was unstable owing to the unstable pump. Some of the possible applications of the laser, operated around 2 μm, were discussed and we believe that this laser could be a practical source for

spectroscopy, LIDAR, and medical applications because the lasing wavelength is in the 'eye-safe' spectral region.

Chapter 6 described the development of a DFB fibre laser, operating at ~2.1 μm, with Ho^{3+}. The laser was pumped at 1119 nm by an Yb^{3+} fibre laser and at 1836 nm by a Tm^{3+} DFB laser. However, with neither of the pump wavelengths was lasing achieved in the DFB. This could be due to the low pump absorption available in a length of 12-cm Ho^{3+} fibre. Then, a DBR fibre laser was constructed to increase the pump absorption by using a much longer cavity length. The cavity lengths of 31 and 85 cm were used, but still no lasing was observed. This might be related to the high concentration of the Ho^{3+} in the fibre that resulted in concentration quenching. Other possible problems were due to the dominant nonradiative transition in the 2 μm region and the large intrinsic losses of the silica fibre associated with the 2.1 μm wavelength.

7.3 Future work

Initial moves towards the 2 μm spectral region have followed a number of important applications in medicine, spectroscopy, and LIDAR. The characteristics of the DFB fibre lasers, such as narrow linewidth, wavelength stability and tunability, are believed to be a viable source for these applications. However, in order for the DFB fibre lasers to be a practical device in medical applications, the laser power needs to be in a few watts regime. This can be solved by using a MOPA configuration in which the DFB fibre laser acts as a seed for the amplifier. Currently, the fibre optic communication networks are operated in the 1550 nm region which is constrained by the gain band of Er^{3+}. Er^{3+}-doped fibre amplifiers are frequently used to amplify the signal so as to increase the transmission distance and as a result the wavebands are limited to 1530 – 1570 nm, i.e. the gain band of Er^{3+}. The technology is now relatively mature, but the demanding is still increasing, therefore it might be a need for expanding the operating region to 2 μm spectral region. Perhaps, the emission spectral of Tm and Ho in the 2 μm could open up a new window for optical telecommunication networks.

However, the Ho^{3+}-doped DFB laser developed is needed to improve through optimise the amount of Ho^{3+} concentration, co-doped with a sensitizer material such as Yb or Tm, and photosensitivity of the fibre. The concentration of holmium in the reported fibre lasers was below 2000 ppm as, for our holmium concentration of 12000 ppm in an aluminosilicate glass host, there could be a possibility of the concentration quenching effect due to limited amount of aluminium to even out the distribution of the dopants by increasing dopant solubility. Co-doping Ho with sensitizer has shown an improvement in laser efficiency. Perhaps, to increase the photosensitivity of the fibre by co-doping with Sb.

So far, the gain of the DFB lasers demonstrated has been based on rare-earth ions in which the operating wavelength was dependent on the ions' transitions. The DFB lasers in the spectral region of 1.08 μm have been demonstrated with Yb^{3+} and Nd^{3+} as the gain medium. In the wavelength region of 1.5 μm, the gain medium used is Er^{3+} ions. Lasers operating in the 2 μm region have been demonstrated with Tm^{3+} and Ho^{3+}. The fibre DFB Raman laser has been proposed by Perlin and Winful [12], in which the gain mechanism of the laser is provided by stimulated Raman scattering (SRS). In the stimulated Raman scattering, light is scattered by optical vibration modes (optical phonons) of the material, resulting in frequency down-shifted Stokes light. With this scattering process, a laser wavelength should be possible from 1 to 2 μm which is not limited by the rare-earth ions' transition. The proposed Raman DFB fibre laser was about 1-m long owing to the fact that the gain provided by SRS is small as compared with the rare-earth dopant. The Raman gain coefficient of a standard single-mode fibre is ~ 10^{-13} m/W. However, the Raman gain bandwidth is quite broad, ~7 THz, which is 1000 times broader than the grating bandwidth of $\kappa \sim 100 m^{-1}$, so the Bragg grating interaction with the Raman gain can be considered constant. The characteristics of this laser include a flat intensity distribution inside the cavity and a lasing frequency linearly dependent on pump power.

7.4 References

[1] P. Laporta, M. Marano, L. Pallaro, and S. Taccheo, "Amplitude and frequency stabilisation of a Tm-Ho:YAG laser for coherent lidar applications at 2.1 μm," *Optics and Lasers in Engineering*, vol. 37, pp. 447-457, 2002.

[2] F. J. McAleavey, J. O'Gorman, J. F. Donegan, B. D. MacCraith, J. Hegarty, and G. Maze, "Narrow linewidth, tunable Tm^{3+}-doped fluoride fiber laser for optical-based hydrocarbon gas sensing," *IEEE Journal of Selected Topics in Quantum Electronics*, vol. 3, pp. 1103-1111, 1997.

[3] N. Y. Voo, P. Horak, M. Ibsen, and W. H. Loh, "Linewidth and phase noise characteristics of DFB fibre lasers," in *SPIE European Symposium on Optics and Photonics in Security and Defence*, vol. 5620. London, 2004, pp. 179-186.

[4] N. Y. Voo, P. Horak, M. Ibsen, and W. H. Loh, "Anomalous linewidth behavior in short-cavity single-frequency fiber lasers," *IEEE Photonics Technology Letters*, vol. 17, pp. 546-548, 2005.

[5] P. Horak, N.Y. Voo, M. Ibsen, and W. H. Loh, "Dominant cause of linewidth in DFB Fiber lasers," in *CLEO/QELS 2005*. Baltimore, USA, 2005, pp. 1566-1568.

[6] P. Horak, N. Y. Voo, M. Ibsen, and W. H. Loh, "Pump-noise induced linewidth contributions in distributed feedback fiber lasers," *IEEE Photonics Technology Letters*, vol. 18, pp. 998-1000, 2006.

[7] N. Y. Voo and M. Ibsen, "Multiple phase-shift all-fibre DFB lasers," in *OFC 2006*. Anaheim, USA, 2006, pp. OWM3.

[8] N. Y. Voo, J. K. Sahu, and M. Ibsen, "345-mW 1836-nm single-frequency DFB fiber laser MOPA," *IEEE Photonics Technology Letters*, vol. 17, pp. 2550-2552, 2005.

[9] N. Y. Voo, J. K. Sahu, and M. Ibsen, "345 mW single-frequency Tm^{3+}-Sb co-doped DFB fibre laser MOPA at 1836 nm," in *OAA*. Budapest, Hungary, 2005, pp. TuD2.

[10] E. T. Y. Lee and E. R. M. Taylor, "Thermo-optic coefficients of potassium alumino-metaphosphate glasses," *Journal of Physics and Chemistry of Solids*, vol. 65, pp. 1187-1192, 2004.

[11] E. T. Y. Lee and E. R. M. Taylor, "Compositional effects on the optical and thermal properties of potassium aluminophosphate glasses," *Optical Materials*, vol. 27, pp. 323-330, 2004.

[12] V. E. Perlin and H. G. Winful, "Distributed feedback fiber Raman laser," *IEEE Journal of Quantum Electronics*, vol. 37, pp. 38-47, 2001.

Appendix I

List of Publications

Publications from results reported in this thesis

Journal articles:

- **N.Y. Voo**, P. Horak, M. Ibsen, and W.H. Loh, Anomalous linewidth behaviour in short-cavity single-frequency fiber lasers, *IEEE Photonics Technology Letters*, Vol. 17, pp. 546-548, 2005.
- **N.Y. Voo**, J.K. Sahu, and M. Ibsen, 345-mW 1836-nm single-frequency DFB fiber laser MOPA, *IEEE Photonics Technology Letters*, Vol. 17, pp. 2550-2552, 2005.
- P. Horak, **N.Y. Voo**, M. Ibsen, and W.H. Loh, Pump-noise induced linewidth contributions in distributed feedback fiber lasers, *IEEE Photonics Technology Letters*, Vol. 18, pp. 998-1000, 2006.

Conferences:

- **N.Y. Voo**, P. Horak, M. Ibsen, and W.H. Loh, Linewidth and phase noise characteristics of DFB fibre lasers, *in Proc. SPIE European Symposium on Optics and Photonics in Security and Defence 2004*, Vol. 5620, pp. 179-186.

- J.K. Sahu, M.R. Mokhtar, **N.Y. Voo**, D.N. Payne, and M. Ibsen, Photosensitivity in germanium-free antimony doped alumino-silicate optical fibre prepared by MCVD, *In Proc. ECOC 2004*, paper Th3.3.5.
- P. Horak, **N.Y. Voo**, M. Ibsen, and W.H. Loh, Dominant cause of linewidth in DFB Fiber lasers, *in Proc. CLEO/QELS 2005*, pp. 1566-1568.
- **N.Y. Voo**, J.K. Sahu, and M. Ibsen, 345 mW single-frequency Tm^{3+}-Sb co-doped DFB fibre laser MOPA at 1836 nm, in Proc. *OAA 2005*, paper TuD2.
- **N.Y. Voo** and M. Ibsen, Multiple phase-shift all-fibre DFB lasers, *in Proc. OFC 2006*, paper OWM3.